Fakulteit Ingenieurswese, Bou-omgewing & IT

Faculty of Engineering, Built Environment & IT

Evaluation of ilmenite as a possible medium in a dry dense medium fluidized bed

by

Kalenda Narcisse Tshibangu

Dissertation submitted in partial fulfilment of the requirements for the degree
Master of Science in Applied Sciences Metallurgy

Supervisor: Prof N Naudé

Co-supervisor: Dr B North

School of Engineering
Department of Materials Science and Metallurgical Engineering

UNIVERSITEIT VAN PRETORIA
UNIVERSITY OF PRETORIA
YUNIBESITHI YA PRETORIA

Denkleiers • Leading Minds • Dikgopolo tša Dihlalefi

ABSTRACT

Dry beneficiation of coal as alternative to water-based methods is in high demand, especially in arid geological environments. Benefits of this dry process include that it eliminates the need for water use, while high separation precision and quick return on investment are also possible.

One of these dry beneficiation methods proposed and developed in China is the dry dense medium fluidized bed of coal. Published work on this method of separation has mainly focused on using magnetite as a medium, but the recovery and reuse of the magnetite were found to be problematic.

This study will extend the possibilities of this method by investigating the use of ilmenite ($FeTiO_3$) as an alternative medium for the dry dense medium fluidization process. Ilmenite is considered due to its clean surface properties, hydrophobicity, and sphericity. It is expected that the ilmenite will not attract contaminants to its surface and will not be lost to the coal due to attachment. The initial investigation considered two types of mediums: a reference medium, which consists of ilmenite and sand; and a medium that resembles the medium used in the current dry dense medium fluidization process, consisting of ilmenite and fine coal. The experiment was conducted on coal sized between – 50+13,2 mm in a laboratory-scale cylindrical fluidized bed, and density tracers were used to determine the écart probable moyen (EPM).

The results revealed that a uniform and stable fluidized bed can be achieved in both scenarios. At optimal conditions, the bed medium mixtures consisting of ilmenite with sand had a separation EPM of 0,045, and a cut density of 1800 kg/m^3. As a result, the sand could not be used to separate coal as lower cut densities are required by the coal industry.

The blend of 60% fine coal and 40% ilmenite as medium at an observed bed split of 1580 kg/m^3 was used as the optimum condition with a separation efficiency (EPM) of 0,05.

The yield of feed to the plant coal sample (AFE) and run of mine coal sample (ROM) were 61,44% and 71,27% respectively at the optimal condition of a binary medium of fine coal with ilmenite.

It was found that the ilmenite does not attach to the surface of dry coal, resulting in the highest recovery of 99,79% when the ilmenite is only used once. The recovery of ilmenite slightly decreased with increase the surface moisture content of coal. The biggest losses of ilmenite on coal were 24,25 kg/t at an external moisture of 4%, which translated into $3,88. However, the experiments did not make use of the high-frequency screen, which will result in better recoveries.

At the end of this study the conclusion can be made that ilmenite can be considered as a viable alternative medium in a dry dense medium fluidized bed process, due to its material properties.

Keywords: Dry beneficiation, Coal, Fluidized bed, Ilmenite, Sand, Fine coal, Medium

PLAGIARISM DECLARATION

Full names	Kalenda Narcisse Tshibangu
Student number	13088565
Topic of work	Master's degree thesis – Evaluation of ilmenite as a possible medium in a dry dense medium fluidized bed.

Declaration

1. I understand what plagiarism is and am aware of the University's policy in this regard.
2. I declare that this dissertation is my own original work. Where other people's work has been used (either from a printed source, internet or any other source), this has been adequately acknowledged and referenced by the requirements as stated in the University's plagiarism prevention policy.
3. I have not used another student's past written work to hand in as my own.
4. I have not allowed, and will not allow, anyone, to copy my work with the intention of passing it off as his or her own work.

Signature: ....

ACKNOWLEDGEMENTS

I would like to give thanks to God Almighty for strength, bravery and abilities through the accomplishment of the project.

My sincere gratitude goes to Prof Natasia Naudé and Dr Brian North for their guidance, valuable advice, expertise, and helpful criticism all the way through the research.

My gratitude goes to Mr Johan de Korte and Dr Andre Englebert for their vital technical assistance and suggestion throughout the research work.

My sincere gratitude and appreciation go to Coaltech Research Association for their financial and vital technical assistance, constructive comments and criticisms; special thanks to CSIR Pretoria for their technical support and equipment and the Department of Material Sciences and Metallurgical Engineering.

I acknowledge with gratitude the support of Tronox Limited with the provision of ilmenite samples.

I would like to extend my truthful thankfulness and appreciation to my parent, brothers and sister for their financial and emotional support.

My gratitude goes to my colleagues in the mineral processing field, and all my friends for their constant backing and words of reinforcement.

Lastly, I would like to give express thanks to all the people that have contributed to this study, without your contribution this project would not have been a success.

TABLE OF CONTENTS

LIST OF FIGURES

LIST OF TABLES

1 INTRODUCTION

1.1 Background

Coal is the main source for generating electricity and metallurgical industries application in South Africa (De Korte, 2010). According to Zhao *et al.* (2015), coal is a complex sedimentary rock that comprises both organic and inorganic matter. However, in general raw coal does require the removal of ash-forming inorganic matter, and this can be achieved through beneficiation processes. In South Africa, water-intensive wet float and sink beneficiation processes are mainly used (De Korte, 2015). Process water requires significant water treatment to comply with environmental policies. Moreover, these wet processes are becoming less viable because much of the remaining coal reserves within South Africa are situated in arid geographical areas; where pipelines must supply water. Consequently, alternative dry coal beneficiation methods are being sought in order to eliminate the need for water, while it may also have the added benefits of higher separation precision and quick return on investment. An example of a dry dense medium fluidization process (Zheng, 2016) which have shown positive results for the upgrading of coal in the size fraction −200+13 mm, is the Bohou process (Figure 1), with a handling capacity of 500 t/h, using a dryer to dry the feed coal.
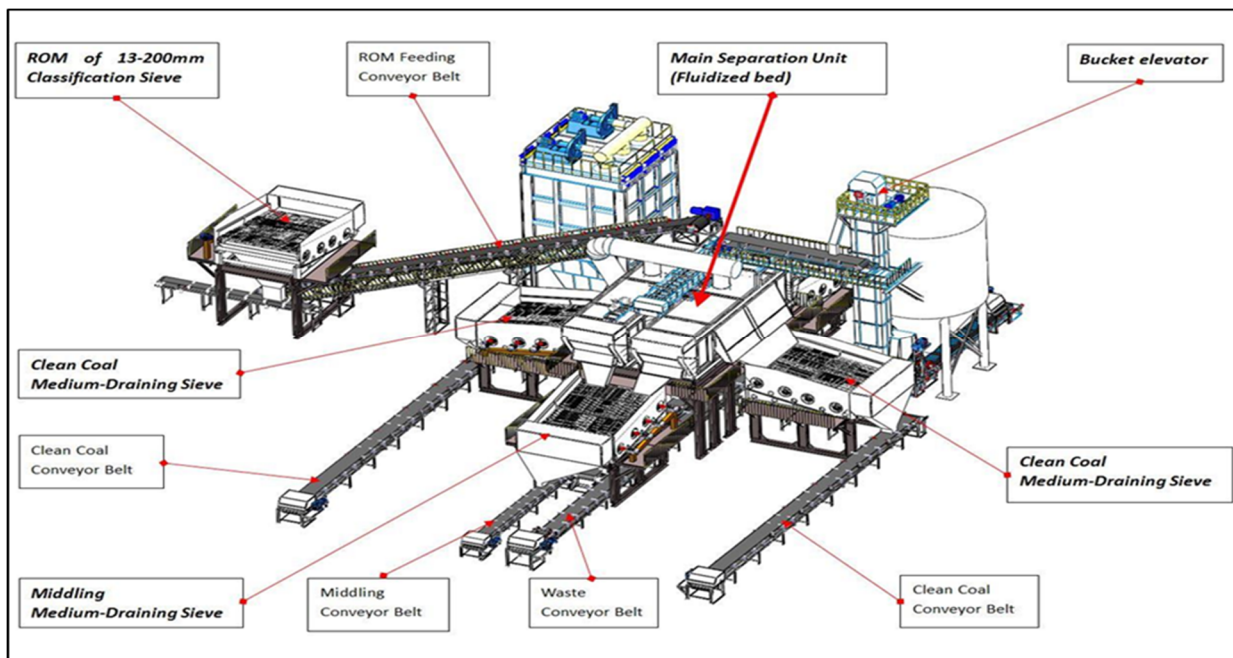
Figure 1 Schematic graph of Air-Dense Medium Fluidized Bed dry coal separation Bohou process (Zheng, 2016)

This process operated with a high-frequency screen to separate the float and sink products from the medium. The Air-Dense Medium Fluidized bed (ADMFB) process was found to be efficient at a cut point of 1580 kg/m^3 with feed coal of less than 5% moisture, Ecart Probable Moyen (EPM) of 0,05–0,08 and clean coal of 9,85% ash content.

Magnetite is currently widely used as a medium during wet dense medium separation (DMS) processes in the coal industry. There is some uncertainty regarding the future availability of magnetite for use in the conventional wet DMS processes, and therefore it is essential for the coal industry to investigate alternative mediums such as ilmenite, not only for wet beneficiation, but also for dry beneficiation. Daris (1987) argues that the loss of media materials can be expensive and plays a critical role in determining the commercial viability side of any process.

Ilmenite ($Fe^{2+}Ti^{4+}O_3$), a titanate ferrous iron mineral, is one of the main TiO_2-bearing minerals and is the primary source for production of titanium metal and titanium dioxide (Song & Tsai, 1989). Ilmenite (nominally $FeTiO_3$) is a naturally occurring heavy mineral associated with mineral sands deposits. It is separate from other minerals in the heavy mineral concentrate, based on magnetic susceptibility properties (Balderson, 1999). Nell and Den Hoed (1997) stated that a crude ilmenite concentrate produced in a Southern African East Coast deposit contains typically 90% ilmenite, 5% Ti-hematite, 3% spinel (including chromite and magnetite) and 2% silicates by weight. Ilmenite is considered due to its specific surface properties and sphericity. These properties give it an advantage compared to magnetite, as it does not attach to the coal particles as much as magnetite does. Additionally, ilmenite also possesses hydrophobicity, which is also desirable in the process.

Approximately two-thirds of coal reserves in China are found in arid areas. China University of Mining and Technology (CUMT) Research Center has remained in charge of the development of dry beneficiation using an air dense medium fluidized bed (Chen & Wei, 2003). The ADMFB separator uses density as a critical parameter and pseudo-fluid characteristic of medium to separate coal from ash-forming mineral matter. The ADMFB process used magnetite powder as a fluidizing medium. Particles with density lower than the bed density report to the float (clean coal), whereas particles heavier (tailings) than

the bed density report to the sink, which is predictable from Archimedes Law (Luo *et al.*, 2010). This technology has faced some challenges when using coal with superficial moisture content of more than 2%. Magnetite as medium easily adhered to wet coal surface and the fluidizing quality was significantly affected because of the increase in its viscosity.

Current published work on dry dense medium separation has mainly focused on using magnetite as a medium, but various complications, such as coal external moisture content that should be controlled to less than 2% and the fact that magnetite readily adhered to wet coal surface, have been encountered. This study will extend the approach by investigating the use of ilmenite as an alternative medium for this dry dense medium fluidization process.

1.2 Problem statement

The dry beneficiation process of coal using an ADMFB has shown great potential to successfully separate coal in China (Zhao *et al.*, 2017). The loss of magnetite during the dry beneficiation of coal process has become costly, therefore necessitating the study of alternative mediums to reduce the cost, since the choice of media type plays a critical role in determining the financial side of dry beneficiation of coal. Luo *et al.* (2010) stated that when using magnetite, the surface moisture must be restrained to below 2%, firstly because moisture transmitted among the magnetite and coal tend to increase the powder viscosity. A part of the magnetite materials becomes agglomerated, decreasing the contact efficiency among particles and gas, therefore causing particle dispersal to depress, increasing local and entire non-uniformity in the bed density (Mohanta & Meikap, 2015). Consequently, the bed fluidization and splitting performance tend to decrease. Secondly, the magnetite has a hydrophilic surface which readily sticks to the wet coal surface and a contaminated medium (magnetite) may become difficult to recover or can only be liberated with very much difficulty. As a result, the coal (floats and sinks) split quality decreases and the operating cost increases.

1.3   Objectives

This study aims to evaluate ilmenite as an alternative medium to be used to replace magnetite in the dry dense medium fluidized bed process. In summary, the itemised objectives of this study are to:

1)   conduct a comprehensive literature study on all the previous work done on ilmenite as medium (Exxaro, Mintek and CSIR), for both wet and dry DMS processes;

2)   identify all potential sources of ilmenite, availability, cost analysis and projected availability in SA;

3)   investigate the availability, cost analysis and projected availability of magnetite and ilmenite;

4)   investigate the physical and chemical properties (micro-characteristic) of ilmenite;

5)   determine pressure drop vs superficial gas velocity of ilmenite as medium;

6)   determine the bed density (ilmenite with sand and ilmenite with fine coal);

7)   investigate the recoverability of ilmenite as a medium; and

8)   compare the operating expenses (OPEX) of ilmenite and magnetite recovery processes – wet as well as dry.

1.4   Hypothesis

Ilmenite can be efficiently used and recovered from a dry dense medium fluidized bed process due to its material properties.

1.5   Thesis organisation

The body of this thesis is organised into three informative chapters, while an introductory and a concluding chapter complete the thesis.

Chapter 2: Literature review – The literature review discusses an overview of coal in South Africa and geographic locations of ilmenite minerals in South Africa. The literature review also investigates ilmenite production, properties, hydrophobicity and impurities. An air dense medium fluidized bed mechanism is also considered and discussed.

Chapter 3: Methodology – The methodology defines the steps followed to carry out the test, as well as sampling characterisation, fluidized bed evaluation and ilmenite recovery.

Chapter 4: Results and Discussions – This section discusses the results obtained, as well as the possible recovery and arrangement that can be reached by using an air dense medium fluidized bed.

Chapter 5: Conclusion – This section summarises all results and activities from the experiment.

Chapter 6: Recommendations – This section defines possible further work.

2 LITERATURE REVIEW

2.1 Introduction

The essential locations of coal mining in South Africa are Lephalale in Limpopo, Ermelo and the Witbank-Middelburg and Standerton-Secunda areas in Mpumalanga, and around Sasolburg and Vereening in the Free State and Gauteng. Minor process plants are located in northwestern KwaZulu-Natal (KZN).

Ilmenite is a heavy material found all over the world, though not always found in economic concentrations. The mineral is typically found as a detrital mineral in coastal dune sands, for instance the Namaqualand coast and Richards Bay. The mineral may also be found in ancient sedimentary deposits, notably the Witwatersrand goldfields (Wilson & Anhaeusser, 1998). Ilmenite is typically a mineral which originates from metamorphic and igneous rocks, such as the marbles at KwaZulu-Natal, the Marble Delta, and the Phalaborwa and Glenover carbonatite pipes (Wilson & Anhaeusser, 1998). Ilmenite has not yet been applied in an air dense medium fluidized process as a medium, the literature review of the medium was focused on magnetite as the common medium used in dense medium separation.

2.2 Overview of coal in South Africa

All South African coal always contain water, which is referred to as its moisture. The moisture in coal is defined as inherent, surface and crystal (Falcon & Snyman, 1986). The mineral matter is the inert solid material in coal, such as:

- Inherent mineral matter: quartz, pyrite group minerals, clays and carbonate
- Extraneous mineral matter: shales, sandstones, dirt bands and intermediate rocks
- Other types of mineral matter: pyrite and ankerite or calcite

South Africa possesses 19 coalfields, shown in Figure 2, which are widely located in different provinces throughout the country, namely the Free State, Mpumalanga, Limpopo and KZN, with smaller quantities in the Eastern Cape, North-West and Gauteng (data in Appendix 1). In 1999, the South African coal reserve ranged from 9 billion tons to 59 billion tons. However, the most recent estimation from the Minerals Bureau projected a reserve of 39,1 billion tons in 2000 (Jeffrey, 2005).
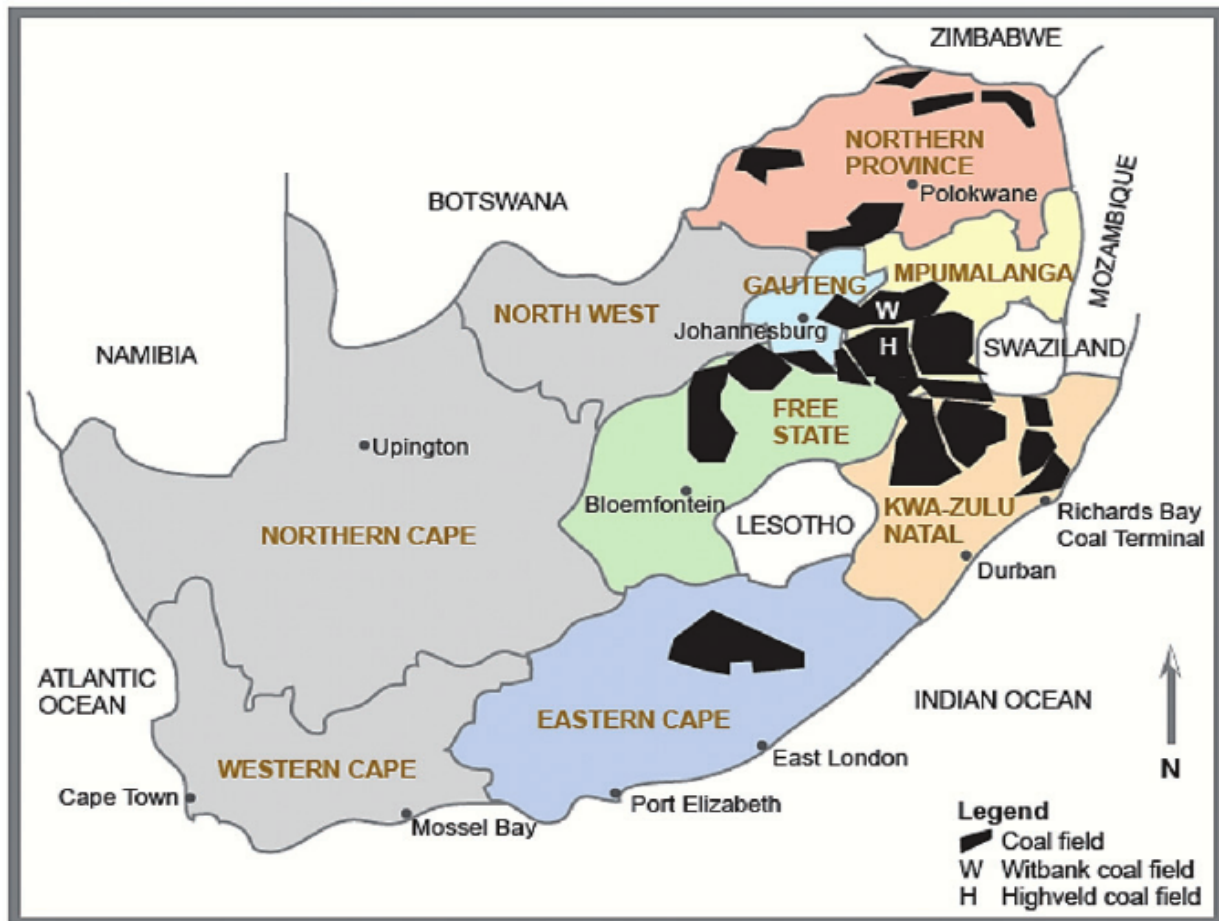
Figure 2 Coalfields of South Africa (Redrawn after Pinetown, Ward, and Van der Westhuizen, 2007)

The Grootegeluk Coal Mine (GGC) is an open-pit colliery owned by Exxaro Resources (Pty) Ltd. GGC is situated in the west of Ellisras/Lephalale in the shallow portion of the coalfield (Jeffrey, 2005b). Jeffrey (2005a) states that GGC's reserve was estimated at 442 Mt in 2005, with complete resource of 3 000 Mt. GGC is the only provider of coal to Eskom's new power station Medupi, which was due for completion in 2015. The characteristic of washed coal for a particular specific gravity (SG) cut point indicate yields 47–53% with ash values of 10–12%, sulphur of 1,1%, volatiles of 35,5–36,5% and swelling indices of 8,0–8,5 (Jeffrey, 2005).

The Witbank coalfield is divided into different seams, based on coal quality. For instance, the No. 1 Seam of the Witbank coalfield is a source of high-grade steam coal most suitable for export after beneficiation (Smith & Whittaker, 1986; Snyman, 1986). Barker (1999) noted that the No. 1 Seam commonly contains low phosphorus content, and is

typically excavated independently as metallurgical raw material. The best quality of coal is found in the No. 2 Seam. It shows a defined region with seven (five in some areas) separate coal regions of various coal quality with three basal regions being mined mostly for both ship steam coal and production of low-ash metallurgical coal. The upper part is unmineable and shaly; however selective mining occurs for the superior quality found in the lower part of the seam (Smith & Whittaker, 1986). The No. 4 Seam consists predominantly of dull to dull lustrous coal with the upper portion typical of poor quality. As a result, digging is limited to the lower 3,5 m portion of the coal seam, which is mostly used as a domestic steam coal and power station feedstock (Smith & Whittaker, 1986). Lastly, the No. 5 Seam has been dug as a source of blend coking coal and for metallurgical procedures, particularly in areas where it is of higher quality, for instance in the central Witbank area (Smith & Whittaker, 1986).

The mining conditions or quality of coal are significant barriers to instant conventional exploitation in the Waterberg, Springbok and Free State Flats coalfields (Jeffrey, 2005). De Korte (2015) notes that the remaining reserves of coal in coalfields such as Witbank, Highveld, and Ermelo would, in the long run, become exhausted, and predicted this to happen by about 2040. The coalfields of Witbank and Highveld are approaching exhaustion with remaining recoverable coal estimated at 9 billion tons in each area respectively. Moreover, in Limpopo province, some coalfields present challenges for exploiting, the most significant of which are insufficiently developed infrastructure, severe water shortages, brittle areas and inadequate roof circumstances due to the penetration and multifaceted geology.

2.2.1 History of coal beneficiation in South Africa

In South Africa, the first coal beneficiation process was a jig plant built in the Witbank region in the year 1909 (Coulter, 1957). The increasing request for coal and the growing pressure to deliver good-quality coal caused the instalment of several jig washers in many coal mines around South Africa. However, these jigs were slowly substituted with the more efficient dense medium process during the 1950s, using magnetite as a medium.

Currently, the majority of the processes produce the export thermal coal, as well as the local process, produce coal with the use of DMS cyclones and drums for beneficiation of

coarse coal, while the fine coal is separated using spirals process (De Korte, 2015). However, South Africa has recently implemented some new technologies for coal processing, consisting of the three-product DMS cyclone and dry process. South Africa is an arid country and coal production is consequently often under pressure of reducing the quantity of water used for coal beneficiation. In this regard, many coal beneficiations industries have implemented filter presses to close their water circuits.

Dry processing of coal does not require water usage. Therefore dry beneficiation methods appear to be very attractive, considering the country's water scarcity. Two dry beneficiation process technologies have been assessed and applied in South Africa, namely the fluidization gas separation (FGX) and X-Ray sorting (XRT) dry coal beneficiation. Unfortunately, the separation efficiency of the accessible dry beneficiation technologies is less than the wet processing. In general, these dry technologies are not appropriate to all raw coals (De Korte, 2013).

These processes' low separation efficiency make them inefficient over an extended period, thus more research is needed to improve the dry ADMFB process. It is said that dry DMS offers good efficiency, but in practice this remains unproven (De Korte, 2013). Currently, in China, a pilot-scale dry ADMFB is available for testwork and has shown better separation efficiency (Zhao *et al.*, 2017). The South African coal industry, through the Coaltech research programme, is assessing this technology through various projects.

2.3   Geographic locations of ilmenite minerals in South Africa

South Africa is the second most prominent producer of ilmenite globally, providing 23% to 30% of global ilmenite production. In 2016, South Africa produced an average of 1,3 million metric tonnes of ilmenite (USGS, 2017). The critical minerals produced from the extensive beach placer deposits located along the eastern, southern and northeastern coasts of South Africa are mainly ilmenite, zircon and rutile (Motsie, 2008). Smaller deposits are situated in the Northern Cape and the west coast of South Africa (Figure 3). Ilmenite minerals are recovered in three significant mines, namely Namakwa Sands mines (Tronox), Richard's Bay Minerals and KwaZulu-Natal Sands (Tronox). Kenmare Resources (Moma) is also a potential producer of ilmenite in Mozambique.
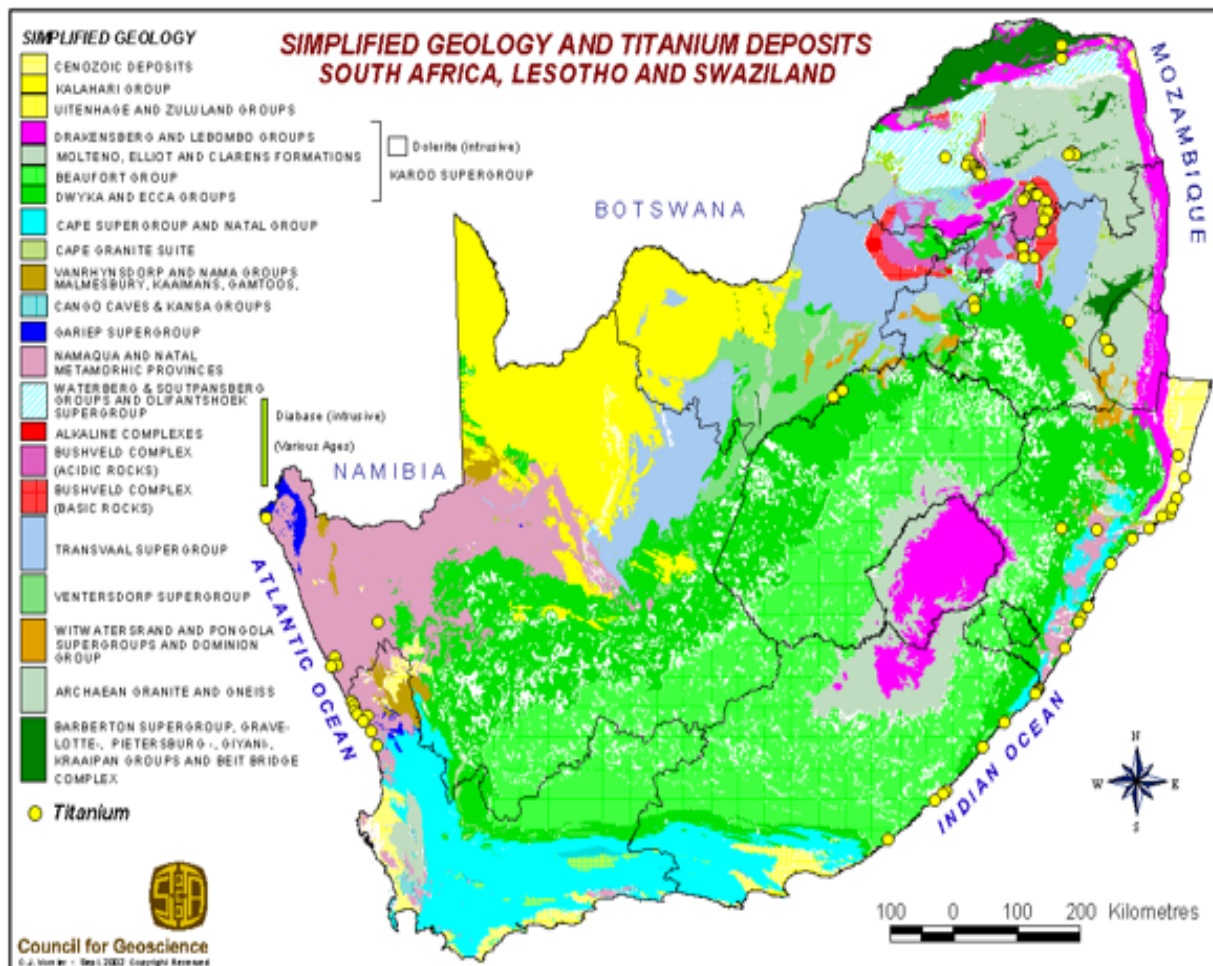
Figure 3 Simplified geology and titanium deposits South Africa, Lesotho and Swaziland (Council for Geoscience, 2002)

The mineral resources deposit of the Tronox Namakwa Sands are estimated at 1,17 billion tons (Bt), with an in-situ grade of 7,9 weight percentage (92,6 Mt) total heavy minerals, of which the valuable mineral fraction consists of 2,98 weight percentage (34,9 Mt) ilmenite, 0,80 weight percentage (9,4 Mt) zircon, 0,42 weight percentage (4,9 Mt) leucoxene, and 0,19 weight percentage (2,3 Mt) rutile (Philander & Rozendaal, 2015).

The Southern Mining Corporation holds the privileges to the Bothaville heavy mineral (HM) occurrence, with reserves assessed to be 90 Mt (Motsie, 2008). The entire inferred resource is valued to more than 185 Mt, with possible in-situ HM reserves of more than 50 Mt, based on an assessed HM grade of 30%. Of this, a projected 40 Mt contains the in-situ valuable HM which, at a 75% recovery, have to yield of 30 Mt of valuable heavy

minerals. The composition of these heavy minerals is estimated to constitute 68% of ilmenite, 9% of zircon, 23% of other titaniferous minerals, and <1% monazite. The Xolobeni project is located on the East Coast of South Africa, with tenements covering 2,867 hectares. Xolobeni has an expected resource of 346 million tonnes grading 5,14% heavy minerals, containing 16,9 million tonnes heavy minerals and 9,1 million tonnes ilmenite (data in Appendix 2).

2.4   Ilmenite production

The United States Geological Survey (USGS) noted in its mineral commodity summaries of 2017 that ilmenite can be used as feedstock for bulk TiO_2 production. There is ample ilmenite deposits in most of the continents around the globe with a current estimated reserve surpassing 770 million tonnes.

Ilmenite ($FeTiO_3$) represents the primary product of heavy mineral sand processing, along with zircon ($ZrSiO_4$) and rutile (TiO_2) as by-products. It is important to note that rutile, ilmenite and 'synthetic rutile' (upgraded ilmenite) are essential sources of titanium dioxide (Ti-dioxide) and are a subsidiary source of titanium metal. Based on reported data of the world production of ilmenite in 2017, South Africa stands as the most significant mine production of ilmenite, and it was estimated to increase in 2017 (Table 1).

Table 1 Ilmenite production in the world (USGS, 2017)

(Data in thousand metric tonnes of contained TiO_2)

Countries	Mine production		Reserves[2]
	2015	2016[e]	
Ilmenite:			
United States[1,3]	200	100	2 000
Australia	720	720	150 000
Brazil	48	50	43 000
Canada[4]	595	475	31 000
China	850	800	220 000
India	180	200	85 000
Kenya	267	280	54 000
Madagascar	140	140	40 000
Mozambique	460	490	14 000
Norway	258	260	37 000
Russia	116	40	NA
Senegal	257	260	NA
South Africa[4]	**1 280**	**1 300**	**63 000**
Ukraine	375	350	5 900
Vietnam	360	300	1 600
Other countries	77	90	26 000
World total (ilmenite rounded)	**6 190**	**5 860**	**770 000**

[e]Estimated. NA not available.

[1]Rounded to one significant digit to avoid disclosing company proprietary data.

[2]Resource/reserve definitions and information concerning data sources.

[3]Includes rutile.

[4]Mine production is primarily used to produce titaniferous slag.

The current market price of ilmenite varies from 130 to 160 USD/ton freight on board (FOB) as shown in Figure 4.
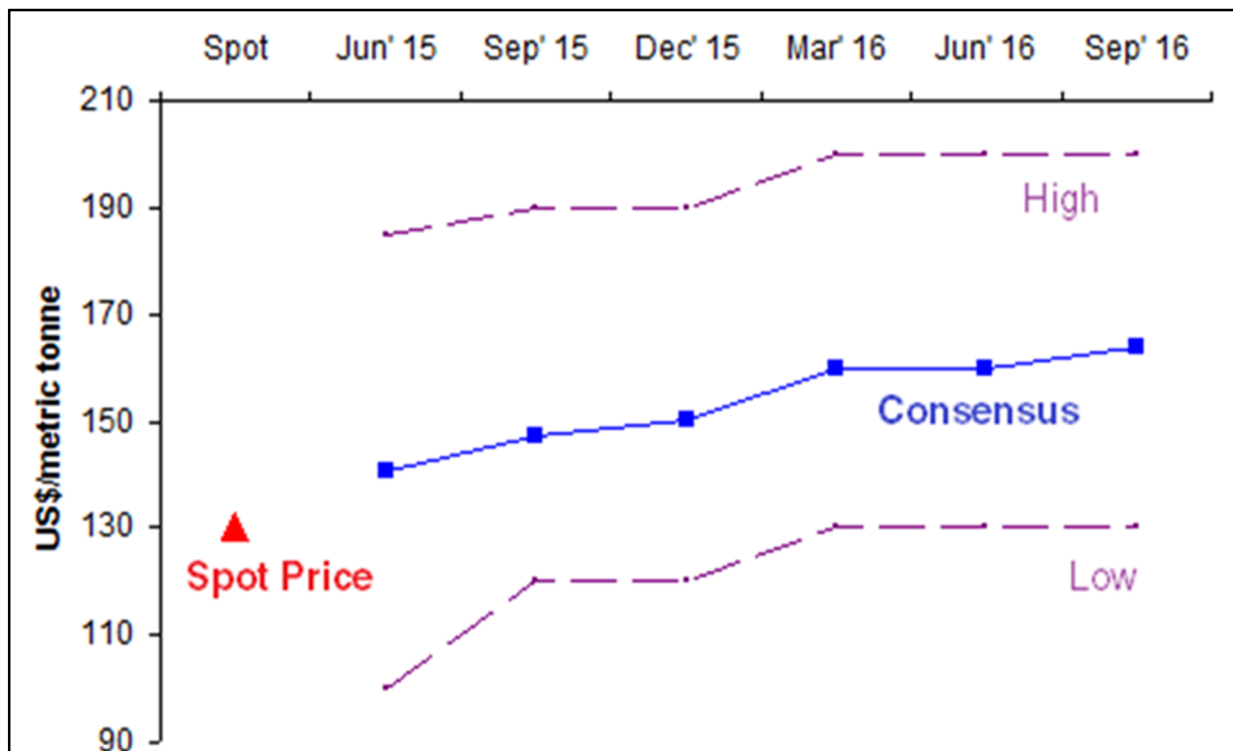
Figure 4 Sample graph of ilmenite forecasts for the next six quarters (Energy & Metals Consensus Forecasts, June 2015)

The process applied to recover the heavy minerals is known as primary wet plant beneficiation process (PWP). A hydraulic monitor gun is used to turn the in-situ sand into slurry or run of mine (ROM), after which the slurry is pumped to the PWP. The slurry of heavy mineral sand is screened through a trommel screen. The product from the trommel screen is then deslimed using cyclones before it goes into spirals. The spiral concentration is divided into three different streams, namely heavy minerals, remaining fine sand and remaining coarse sand. This process utilises water with a flocculant to get rid of the ultrafine particles. The heavy minerals concentrate (HMC) magnetite stream is then separated using a low-intensity wet magnetic separator. Magnetic magnetite and non-magnetic heavy mineral concentrate, holding rutile, ilmenite, and zircon is conveyed to the mineral separation plant where zircon and rutile are produced as final products and raw ilmenite as a transitional product. The fine sand is essentially pumped to a residue dam, while the coarse sand is pumped back to the mining void as backfill material.
The primary wet plant (PWP) at Hillendale Mine is shown in Figure 5.
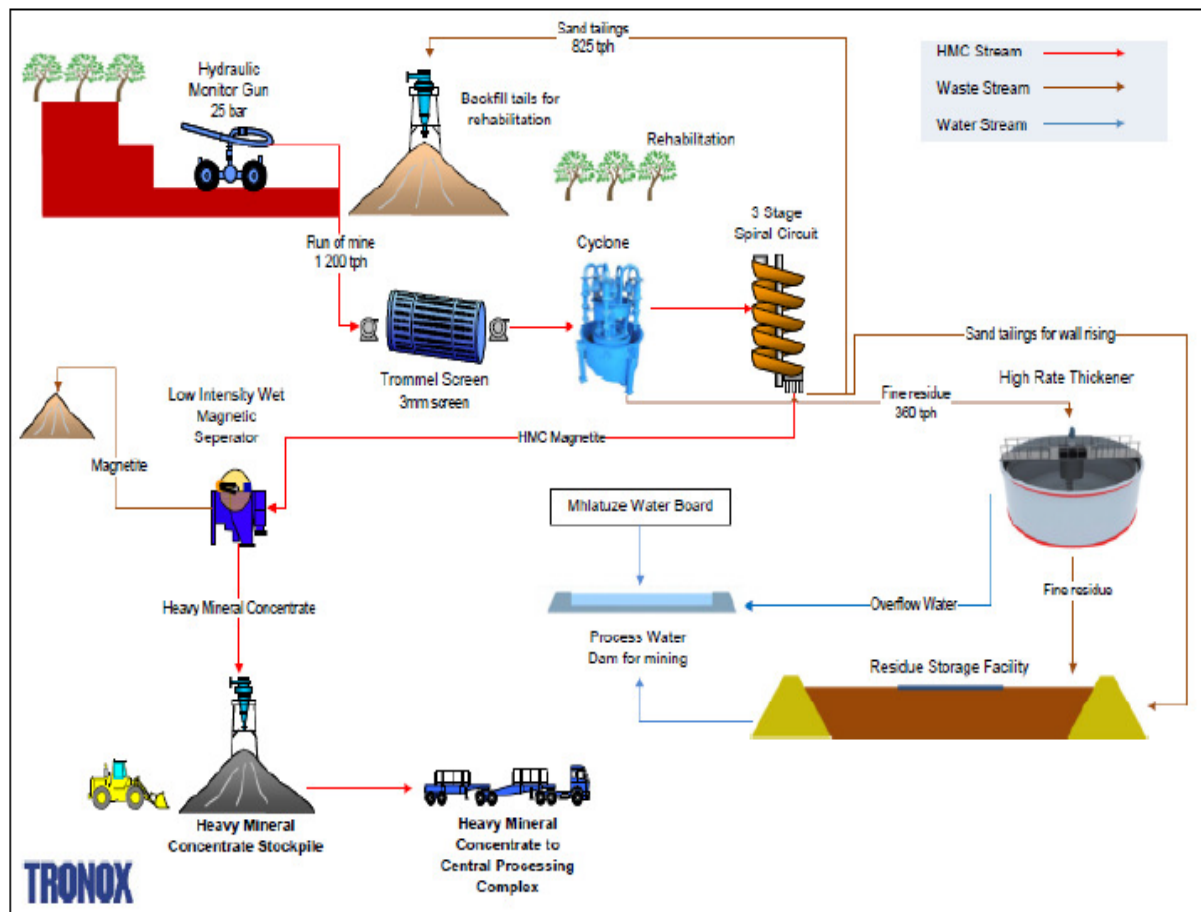
Figure 5 Primary wet plant beneficiation process (Dhanraj, 2016)

Rio Tinto is the world's leading producer of titanium feedstock with operations in Fer et Titane in Canada, QMM Madagascar and Richards Bay Minerals (RBM) in South Africa. The world's second-largest feedstock producer is Tronox Limited. In South Africa, Tronox operates KZN Sands and Namakwa Sands.

Namakwa Sands achieves a yearly production capability of 21 million tons ROM, 25 kt rutile, 350 kt ilmenite and 130 kt zircon with a life-span of mining being more than 30 years (Rozendaal, Philander & Carelse, 2009). In South Africa, Namakwa is named as the second-leading producer of HM afterwards RBM.

Carvill (2017) emphasises that Moma realised a record in ilmenite production in the three months to 30 September, which is the company's highest production in a year that falls within Kenmare's guidance ranging between 950 000 t and 1,05 million tons.

2.5   Properties

Ilmenite is a natural mineral ore made up of titanium and iron oxide, a small portion of magnesium as well as manganese. Lee *et al.* (2017) also indicated that ilmenite minerals can be both natural and synthetic.

Ilmenite represents the world's most valuable titanium-bearing ore. The advantage it holds for coal beneficiation lies in its reasonably high reported specific gravity (SG) of 4500–5000 kg/m^3 (Wills, 2016). The high SG, together with the typically smooth pebble-like structures of beach sand, makes ilmenite a very suitable material for a fluidized bed.

Izvorni (2014) determined the morphology of ilmenite grains. Figure 6 confirms that the morphology of the ilmenite grains is significantly constant. The individual grains of ilmenite are often an asymmetrical shape of the polyhedrons, free of the significant sharp edges. They are present as grains with the form of the quadrangle or pentagon. The particle shape of the grains is usually within the range of 0,7 to 0,8.
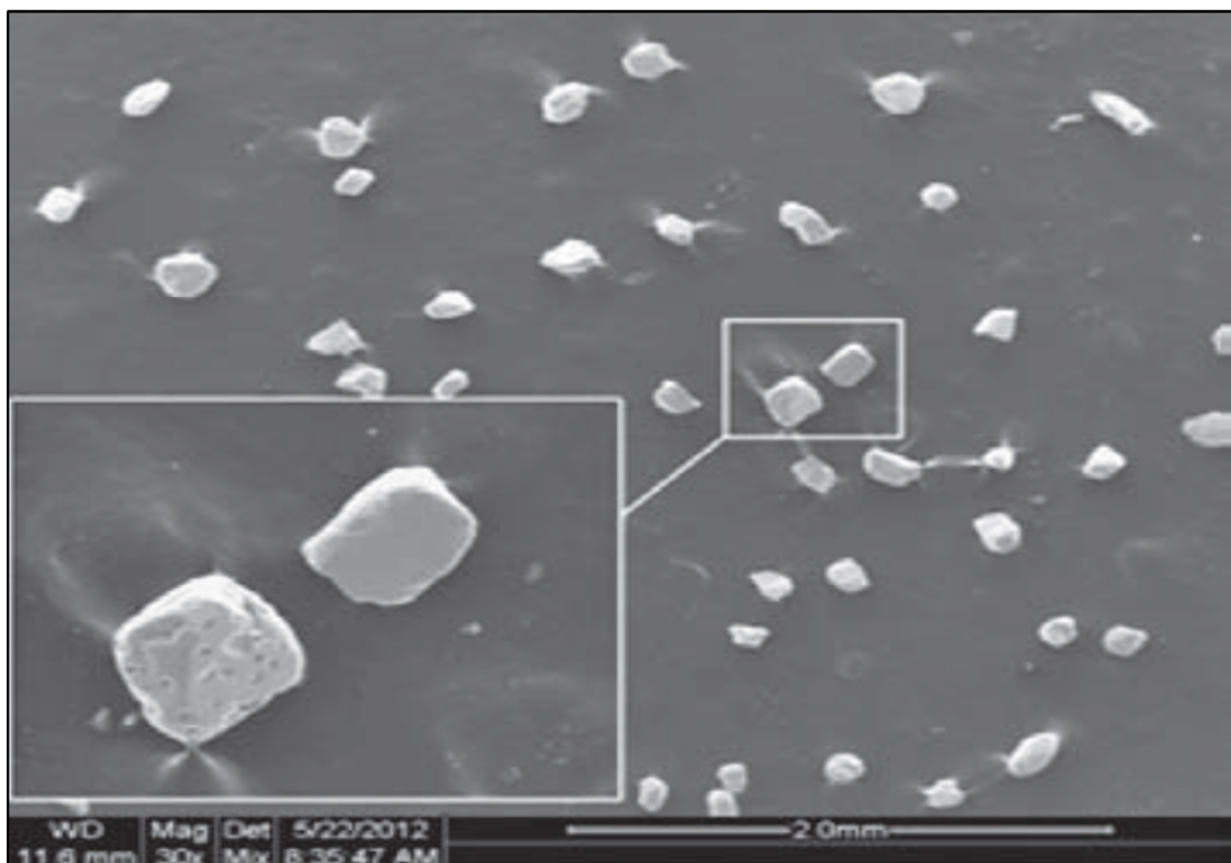
Figure 6 Detail of the ilmenite sand grains (Izvorni, 2014)

2.5.1 Synthetic ilmenite

Synthetic ilmenite has high potential in the fields of materials science and engineering, especially in heterogeneous photocatalysis, solar cells, electronic circuits and gas sensors (Tang & Hu, 2006; Fujii *et al.*, 2011; Zarazúa *et al.*, 2011; Zhou *et al.,* 2003). As a result, ilmenite can be synthesised via hydrothermal emulsion, solid-state reaction and sol-gel techniques (Crişan *et al.*, 2015; Adán *et al.*, 2014; Ctibor, 2014). Kim's (2009) work indicated hetero-junction of $FeTiO_3$ nanodisc, and TiO_2 nanoparticle demonstrated significant photocatalytic activity in mineralisation of 2-propanol under visible light irradiation. Truong *et al.* (2012) demonstrated CO_2 reduction to CH_3OH by using $FeTiO_3/TiO_2$ composite under both visible and UV-vis light irradiation.

Although synthetic ilmenite ($FeTiO_3$) has been studied in the past years, only a handful of researchers has indicated the potential ability of natural ilmenite. Tao *et al.* (2011) showed that natural ilmenite nanoflower has distinct and stable pseudo-capacitance. Hence, it presented functionality as an electrode material for supercapacitors. Moctezuma *et al.* (2011) demonstrated photodegradation of phenol to carboxylic acid by using ilmenite as a catalyst.

2.5.2 Magnetic properties of ilmenite

The natural ilmenite ($FeTiO_3$) is formed in magma, with moderate titanium content, typically 45% to 60%. The structure of natural ilmenite is rhombohedral crystal in space group R-3H with hexagonal packing. The oxygen atoms occupy 2/3 of the octahedral positions, whereas Fe and Ti together occupy alternating layers (Navrotsky, 1998; Liferovich *et al.*, 2006; Giaquinta & Loye, 1994). Tang and Hu (2006) state that ilmenite is a semiconductor with a wide bandgap (2,5–2,7 eV) and possesses antiferromagnetic property. It is an antiferromagnetic only below the Néel temperature of 55 K (Svoboda, 2004). Antiferromagnetic above the Néel temperature is paramagnetic, as shown in Figure 7 (Nagata,1961). The paramagnetic material has a magnetic susceptibility of approximately 5×10^{-3} (Tarling & Hrouda, 1993; Dahlin & Rule, 1993).
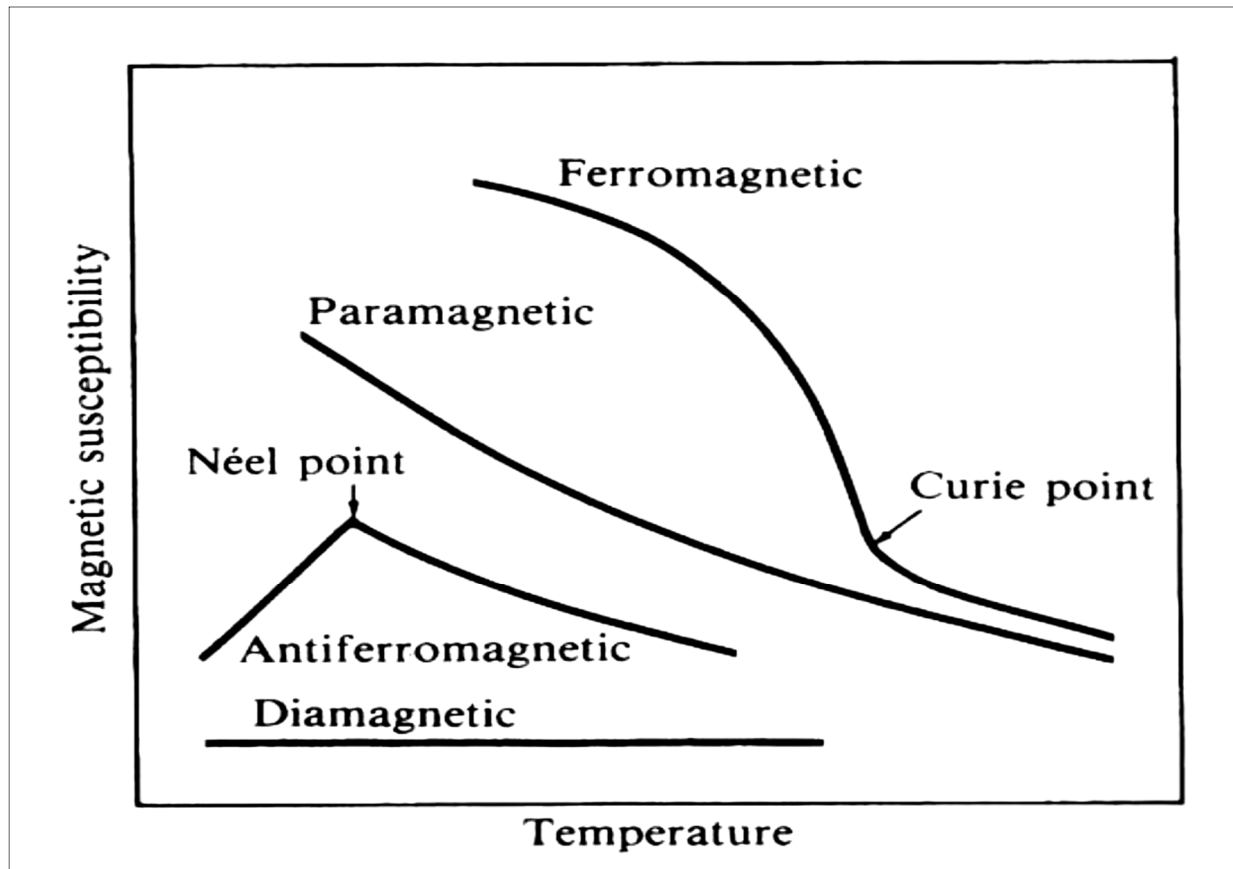
Figure 7 Temperature behaviour of various classes of magnetic materials (Svoboda, 2004)

Dahlin & Rule (1993) found that the paramagnetic material was found to be substantially independent of the magnetic induction (flux density) in the range from 0,1 to 9 Tesla. It is important to note that ilmenite is one of the magnetically weakest members with saturation polarisation of about 0,012 Tesla (Svoboda, 2004).

2.5.3 Magnetic separator

Previous studies propose that weak magnetic solids can be recovered through a magnetic separator, which can generate magnetic induction capable of 1,0 Tesla, and the field gradient in the range of 50 to 500 T/m (Svoboda, 2004). This panel group of substances includes some ferrimagnetic, antiferromagnetic and paramagnetic minerals (Svoboda, 2004). The group includes iron and manganese oxides and carbonates, ilmenite, wolframite and other materials. The mass (specific) magnetic susceptibility of these materials ranges between 10^{-7} to 5×10^{-6} m^3/kg (Svoboda, 2004).

Wills (2016) supports that ilmenite ($FeTiO_3$), alongside rutile (TiO_2), wolframite ((Fe, $Mn)WO_4$), monazite ((Ce, La, Nd, $Th) PO_4$), xenotime (YPO_4), siderite ($FeCO_3$), chromite ($FeCr_2O_4$) and manganese minerals are paramagnetic minerals, which are separated by high industrial intensity magnetic separators.

Paramagnetic materials are attracted along magnetic lines of force to points of higher field strength, and paramagnetic materials report to the magnetic product ("mags") of a magnetic separator due to magnetic attraction forces (Wills, 2016). Figure 8 displays the schematic diagram of the alignment of magnetic moments. Paramagnetism is a form of magnetism whereby material originates due to the presence of unpaired electrons that generate magnetic dipoles. When these magnetic dipoles are aligned by an outwardly applied magnetic field, the resultant magnetic moment causes the material to become magnetised and experience a magnetic force along the lines of the applied magnetic field. Individual elements have electron configurations with many unpaired electrons, but the magnetic response of a given mineral depends on the structure of the mineral, as well as its constituent atoms (Wills, 2016). For instance, pyrite (FeS_2) is very marginally paramagnetic. However, the chemical comparable to pyrrhotite ($Fe_{1-x}S$) in the monoclinic structural form is powerfully magnetic, referred to as ferromagnetic (Tarling & Hrouda, 1993).
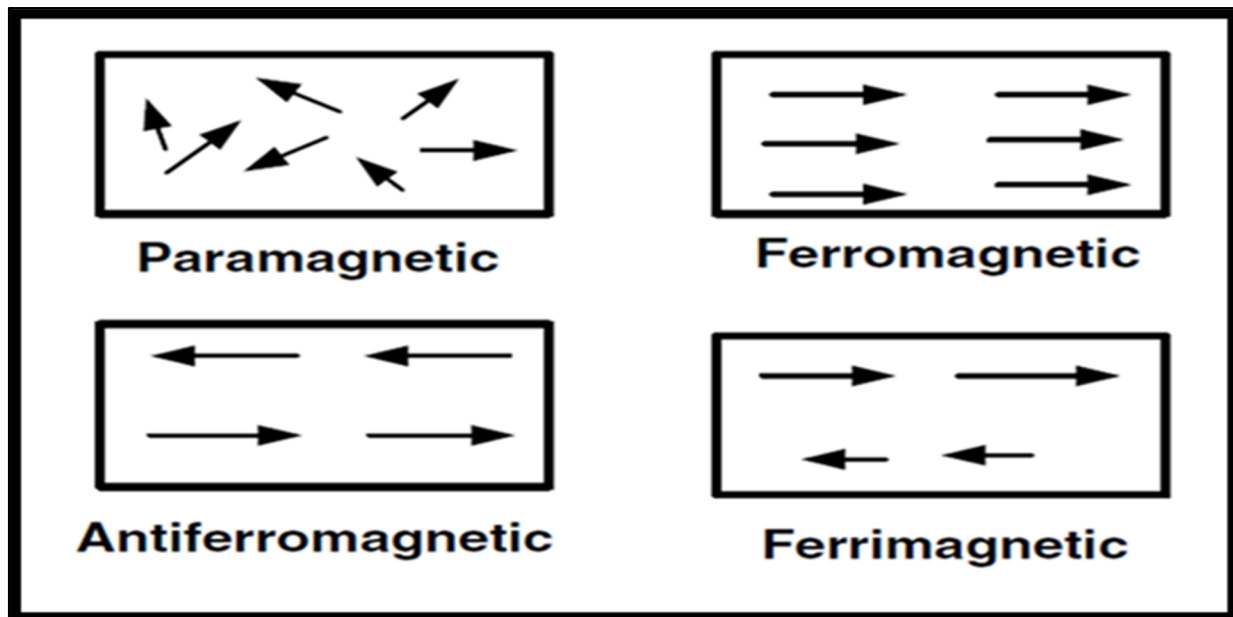
Figure 8 Schematic diagram of the alignment of magnetic moments (Wills, 2016)

2.5.3.1 Equations of magnetism

The magnetic induction or magnetic flux density is the number of lines of force transient through a unit area of the material (Bennett *et al.,* 1978). The magnetic flux density is measured by the unit tesla (T). The magnetising strength that induces the lines of force through a material is called the field intensity represented by H (or H-field), and by International Standard (SI) has the unit's ampere per meter (A/m).

The magnetisation (M, Am^{-1}) or the intensity of magnetisation of a material relates to the magnetisation induced in the material and can also be referred to as the volumetric density of induced magnetic dipoles in the material. The magnetisation is related by Equation 1 (Wills, 2016):

$$B = \mu_0 \, (H + M) \hspace{4cm} 1$$

Where:

μ_0 : permeability of free space and $\mu_0 = 4\pi \times 10^{-7}$ NA^{-2}

B : magnetic induction

H : field intensity

M : magnetisation

In the existence of the external magnetic field, and under standard practical conditions. The magnetisation of paramagnetic material is stated by Equation 2:

$$M \cong \frac{c\mu_0 \, n\mu_M^2 H}{kT} \hspace{4cm} 2$$

i.e. when $\mu_M \, H/kT \ll 1$.

Where:

μ_M : magnetic moment

k : Boltzmann constant

T : absolute temperature

n : number of magnetic dipoles

c : constant

The susceptibility of paramagnetic materials is stated by Equation 3:

$$M \cong \frac{c\mu_0\, n\mu_M^2}{kT} = \frac{C}{T} \qquad\qquad 3$$

Where:

C : Curie constant

Equation 3 is regularly called the Curie law, which indicates that the magnetic susceptibility of the paramagnetic solid is inversely proportional to the temperature. The paramagnetic susceptibility is always small ($k \approx 10^{-5}\ to\ 10^{-3}$ (SI)), though the paramagnetism can be several orders of magnitude larger than diamagnetism (Svoboda, 2004).

An illustration of diamagnetic and paramagnetic behaviour is shown in Figure 9, represented as magnetisation (density of magnetic dipoles) as a function of the applied magnetic field strength. The slope of these curves represents the dimensionless magnetic susceptibility of the material. Figure 9 displays the paramagnetic susceptibility (represented by a positive linear slope) of chromite and the diamagnetic susceptibility (negative linear slope) of quartz.
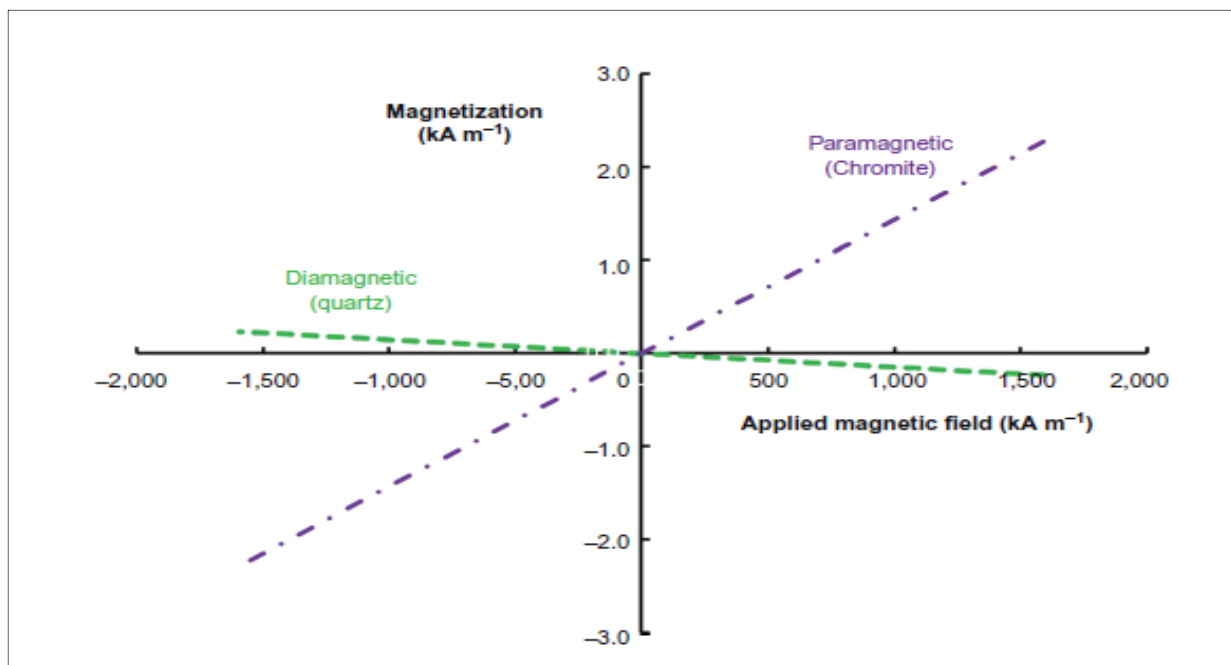
Figure 9 Magnetisation versus applied magnetic field strength for idealised paramagnetic and diamagnetic minerals (Wills, 2016)

2.5.3.2   Types of magnetic separators

Magnetic separators are categorised into two types of separators, namely low- and high-intensity magnetic separators.

2.5.3.2.1 Low-intensity magnetic separators

Low-intensity magnetic separators (LIMS) are widely used for the manipulation of ferromagnetic or paramagnetic minerals of high magnetic susceptibility, and sufficiently large particle size (Wills, 2016). Such separators can operate in both dry and wet modes. For example, the dominant ferromagnetic material concentrated in mineral processing is magnetite (Fe_3O_4), even though siderite ($FeCO_3$) and hematite (Fe_2O_3) can be heated to produce magnetite and therefore provide a better separation in LIMS.

Dry LIMS are mostly restricted to the coarse sands concentration that is strongly magnetic. The process is referred to as "cobbing" and is frequently performed with drum separators. For particles > 5 mm, dry separation is substituted by wet methods, which generate a lower amount of dust and produce a cleaner product. LIMS are often used for the processing of ferromagnetic sands, and in DMS the process is used for the cleaning and recycling of the magnetite media (Figure 10).

In the coal preparation operation, wet drum magnetic separators are mainly used to recover magnetite from the heavy medium circuit. For instance, when the process is correctly executed, the magnetic loss is reduced to less than 0,25 g magnetite/litre in the waste. The wet high-intensity magnetic separator (WHIMS) equates to a magnetite recovery in the range of 99,8 to 99,9%. This performance needs to meet some conditions, such as volumetric flow rate, magnetic loading, percent solids in feed slurry, and magnetic concentration, while the ratio of non-magnetics to magnetics in feed solids must also be satisfied, together with magnetic field strength, tank design and various feed slurry parameters (Norrgran, 2010).

Historically, the losses of medium have often been the primary aspect for the operating costs of DMS plants (Hand *et al.*, 2002). Magnetite losses in coal washing plants vary from 0,4 kg to 2 kg per ton of raw coal. In the modern large cyclone plants operating at − 45 + 0,5 mm of raw coal, the average losses of magnetite amount to 0,45 kg/t.

Figure 10 Wet drum magnetic separators for heavy media application. Self-levelling counter-rotation tank style (Norrgran, 2010).

2.5.3.2.2 High-intensity magnetic separators

High-intensity magnetic separators are employed for the treatment of weakly magnetic materials, coarse or fine, in wet or dry modes. For instance, weakly paramagnetic material can only efficiently be recovered using high-intensity (B-fields of 2 T or greater) magnetic separators (Svoboda, 1994).

Even though dry high-intensity magnetic separators have been efficiently used for the beneficiation of minerals in a vast spectrum, numerous drawbacks exist. Successful dry magnetic separation requires the ore to be completely dry and sized into various fractions (Svoboda, 2004). Accordingly, each fraction must be spread over the separators in a monolayer. Dry magnetic separators require much care to be able to control dust hazards, an expensive preventive measure in both operating and capital costs. Dry magnetic separators also have a significantly lower capacity than wet magnetic separators.

Dry high-intensity separation is mostly restricted to ores containing little, if any, material finer than 75 microns. The effectiveness of separation on such fine material is severely reduced by the effects of air currents, particle-particle adhesion, and particle-rotor adhesion (Wills, 2016).

The weak magnetic and very fine materials can be treated with high-gradient magnetic separators (HGMS). The Eriez separator has been effectively used to concentrate minerals containing Fe (hematite, limonite, siderite, chromite), clean non-ferrous ores (quartz, cassiterite, garnet), recover rare earth minerals, and purify non-metallic ores such as quartz, feldspar, kaolin, alusite and kyanite (Eriez & Gzrinm, 2014).

Forthcoming developments and applications of magnetic separation in the mineral plant lie in the conception and usage of the increasingly superior product of field and field gradient, which is the "force factor" (Wills, 2016). Multiple small working gaps and matrix separators with very high field gradients may derive little benefit from field strengths more significant than the saturation levels of the secondary poles (B-fields of 2 T or higher for an iron/steel matrix material). A one-stage extraction of ilmenite from highly magnetic gangue minerals was developed using a superconducting HGMS technology. The difference in magnetic susceptibility between ilmenite and gangue is only substantial at very high magnetic field strength.

RBM located in the province of KZN is the world leading producer of zircon, rutile raw minerals and titanium, which is made from ilmenite by the on-site smelter. RBM uses a wet high-intensity magnetic separation (WHIMS) process to produce ilmenite.

The mineral separation plant at Namakwa Sands uses an electrostatic separator to produce ilmenite concentrate (Svoboda, 2004).

Reading WHIMS were industrialised by Reading of Lismore (Pty.) Ltd., Australia. They successfully operate in beach sand processes. Chromite, ilmenite, and monazite concentration are standard applications. The units are also used for the concentration of fine weakly magnetic iron ores, as well as the purification of several industrial minerals, for example glass sand.

Figure 11 shows the assembly of Reading WHIMS for application in the beach sand industry.
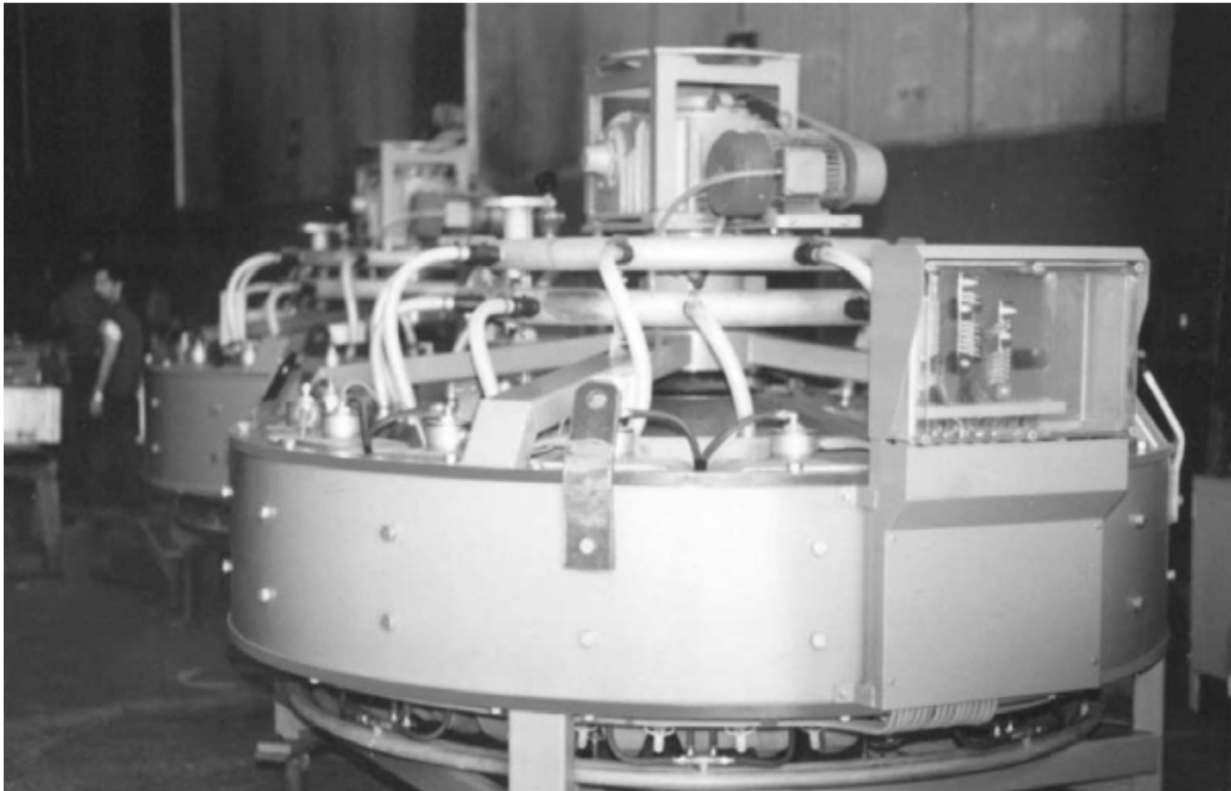
Figure 11 Assembly of banks of Reading wet high-intensity magnetic separation (Svoboda, 2004)

The SLon magnetic separator was developed in 1988. However, it was successfully industrialised in recent years (Zeng *et al.*, 2003). For instance, in 2003 the SLon separator was operated in more than 30 concentrators plants in China (Figure 12). This magnetic separator is used to recover magnetic minerals less than −212 microns, such as ilmenite and hematite, and for dephosphorisation and desulfurisation of iron ore feeds (Xiong, 1994, 2004). The SLon separator applies a high magnetic field of 10 000 Gauss to interact with paramagnetic materials' magnetic matrix (Dworzanowski, 2014).

The SLon vertically pulsating high-gradient magnetic separator (VPHGMS) works with a unique matrix of steel rods oriented perpendicularly to the applied magnetic field, along with flushing of locked-in magnetic particles in the opposite route to the feed, so as to reduce particle momentum, increase separation and maximise particle trapping (Outotec, 2013).
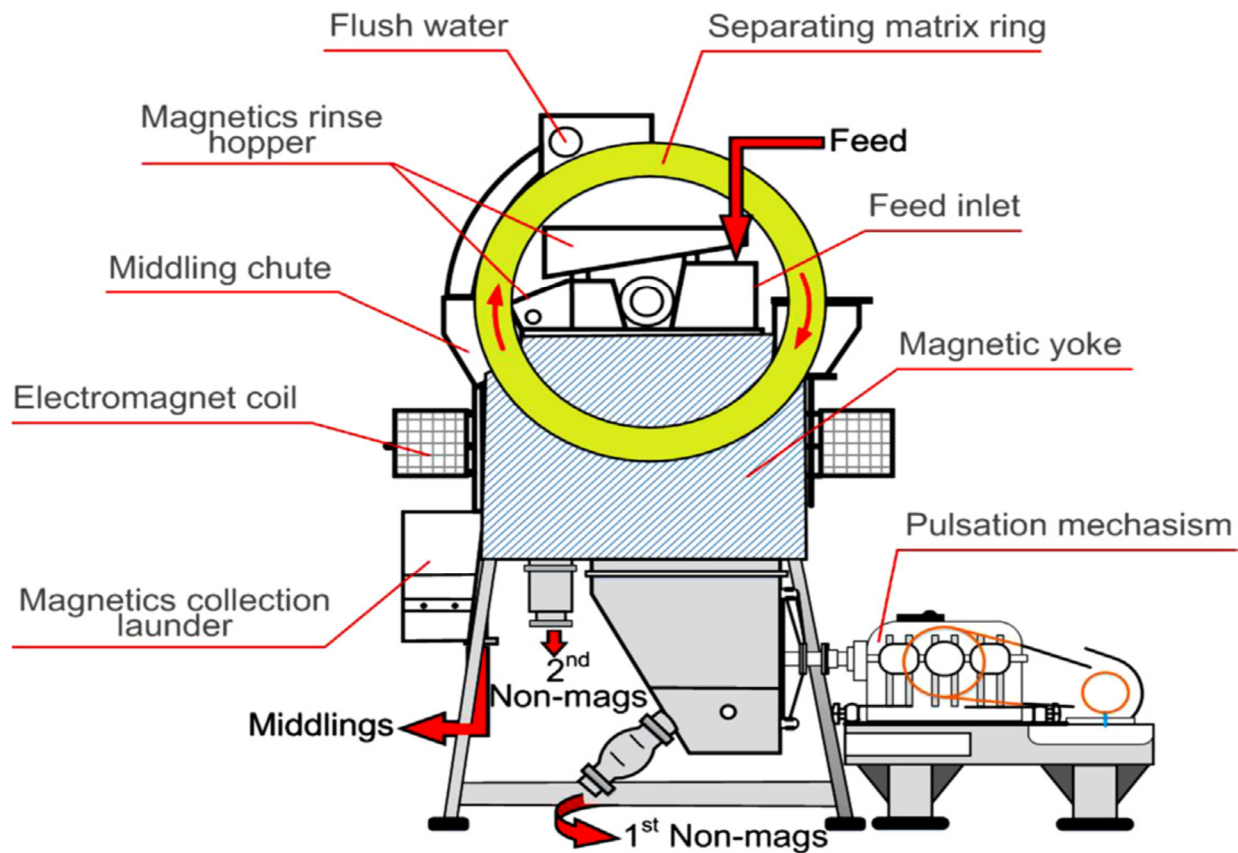
Figure 12 SLon vertically pulsating high-gradient magnetic separator (Outotec, 2013)

2.6   Hydrophobicity of ilmenite

The surface properties character of materials arises from the physicochemical properties of the materials. More precisely, the hydrophilic-hydrophobic character of materials results from a balance of forces, which operate at the three solid-water, water-gas and solid-gas interfaces (Drzymala, 2007). These forces cause the bubble to assume its shape and angle with the solid surface, leading to minimisation of the total energy of the system. That angle is known as the contact angle and can be seen in Figure 13.

The contact angle is measured as the angle between the gas and solid phases, via the water phase. Drzymala (2007) defines the contact angle as the angle existing between solid and liquid phases, via the gas phase. Both ways of defining the contact angle remain equally acceptable, since the sum of the contact angle measured over the water phase, as well as the angle defined through a gas phase, is 180°. Drzymala (2007) notes that it is essential to highlight if the phase of the contact angle was measured clearly.

Mehdilo *et al.* (2013) shows that ilmenite is a hydrophobic material, which does not readily adhere to water.
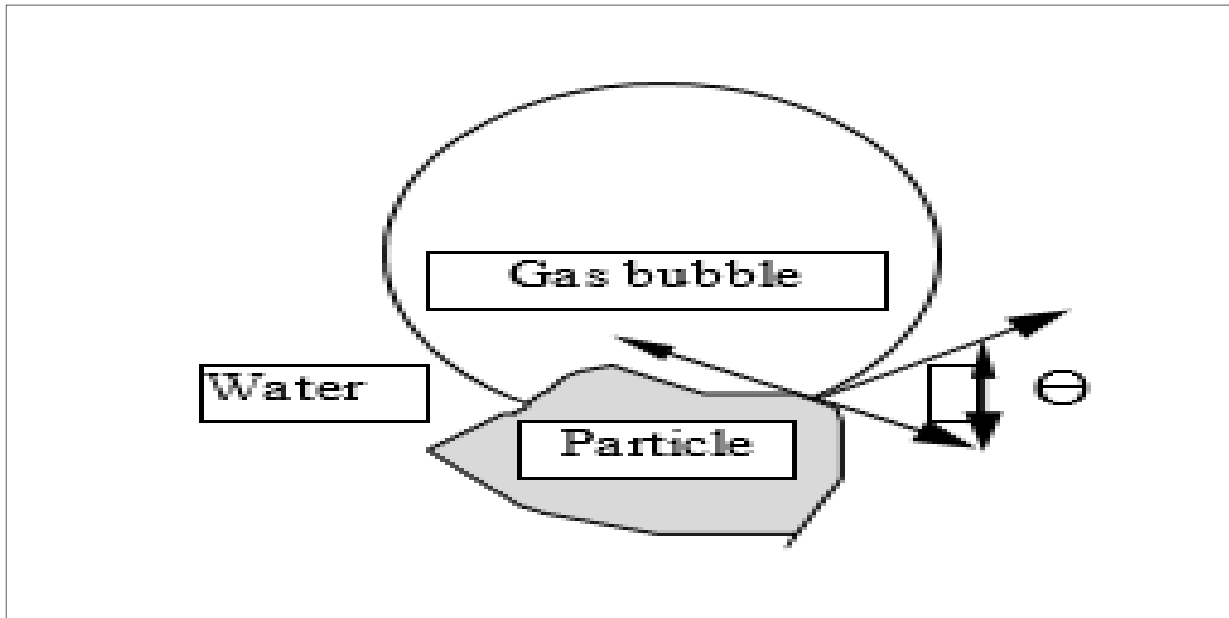
Figure 13 Contact angle (Drzymala, 2007)

For all strongly hydrophilic materials, the contact angle is equal to 0°, whereas for strongly hydrophobic materials (non-wetting), the contact is 180°. When the contact is less than 90° the system is regarded as wetting (hydrophilic). The maximum value of contact angle for materials in contact with water and air is about 110° (paraffin, Teflon). Table 2 shows the contact angles for selected materials measured by flotometry (Drzymala & Lekki, 1989a, 1989b).

The contact angle is covered by Young Equation 4:

$$\gamma_{sg} = \gamma_{sl} + \gamma_{lg} cos\theta \hspace{4cm} 4$$

Where:

γ_{sg} : solid-gas interfacial tension (in mN/m or mJ/m^2)

γ_{sl} : solid-liquid interfacial tension

γ_{lg} : liquid-gas interfacial tension

ɵ   : equilibrium contact angle (degree)

Usually, the contact angle is extensively used for flotation.

Based on reported data of the hydrophobicity of materials, ilmenite material has a hydrophobic surface with a contact angle of 14°, which does not readily adhere to the wet surface. The magnetite material has a hydrophilic surface with a contact angle of 0°, which readily adheres to wet surface.

Table 2 Hydrophobicity of materials (Drzymala, 2007)

(Data in degree)

Strongly hydrophobic*		Hydrophobic		Weakly Hydrophobic		Hydrophilic** = 0
Material		Material		Material		Material
1	2	3	4	5	6	7
Paraffin C_nH_{2n+2}	90+	Sulfides	44–0	Fluorite, CaF_2	10–13	Gypsum $CaSO_4 \cdot 2H_2O$
Teflon, C_2F_4	90+	Silicon carbide SiC	27,6	Arsenic, As_2O_3	9,3	Ferrosilicon
Sulfur, S	63,2	Coal	26–0	Perovskite, $CaTiO_3$	9	Dolomite $CaMg(CO_3)_2$
Mercury, Hg	45,6	Indium, In	25	Scheelite, $CaWO_4$	9	**Magnetite Fe_3O_4**
Ge	39,7	Jodargyrite, AgI	23,5	Diamond, C	7,9	Halite, NaCl
Si	35,4	Cassiterite, SnO_2	22–	Tin, Sn	7,5	Brawn coal
Talc	35,2	Silver, Ag	14	Boric acid, H_3BO_3	6,4	Kaolinite
		Ilmenite, $FeTiO_3$	**14**	Graphite, C	6,2+	Hematite, Fe_2O_3
		Molybdenite, MoS_2	5,9+	PbJ_2	6	Quartz, SiO_2
				Gold, Au	5	Calcite, $CaCO_3$
				Barite, $BaSO_4$	5	Anhydrite, $CaSO_4$
				Corundum, Al_2O_3	4	Bones
				HgO	3,3	Tourmaline
				HgJ_2	3	Vegetables
				Copper, Cu	3	Iron, Fe
						Amber
						Ice, D_2O

 * Flotometric method can measure contact angles in degree smaller than 90º.

** Other hydrophilic materials: chromite, malachite, smithsonite, azurite, rutile, zircon, mica.

2.7   Ilmenite impurities

The practical value of ilmenite concentrates is naturally related to the presence of other phases in the deposit, plus the nature and level of impurities in the ilmenite. The most significant impurity found in the ilmenite structure is magnesium (Mg), which varies from 5,3 to 5,53%, present as a geikielite component (Mehdilo *et al*., 2015).

In addition to magnesium, vanadium (III) oxide (V_2O_3) is another impurity which is essentially substituted for titanium in the ilmenite structure with up to 1,9%.

For instance, the Nataka ilmenite concentrate encompasses chromite (Cr-spinel), and intra-porous Cr, aluminium (Al) and silicon (Si) impurities. The Al and Si impurities arise in two modalities, notably intra-porous and filling/coating amorphous clays. The research findings on ilmenite's impurity state that the intra-porous impurities of Al and Si are associated with diagenetic alteration of ilmenite (Elias, 2016). As a result, their removal necessitates laborious and expensive technologies, such as sodium hydroxide leaching. On the other hand, the amorphous coatings of clay formed by superficial precipitation of iron in Al- and Si-rich environments can effortlessly be washed out using light attrition or through the practice of an acid solution.

Ilmenite grains with intra-porous Cr impurities concentrations above 0,3 weight percentage tend to reduce its market value as a potential feedstock for TiO_2 production (Pownceby, 2005). When the impurity level of the intra-porous Cr (Elias, 2016) appears to be negligible, the chromite modal abundance of the ore occurs as discrete grains, consequently facilitating easy separation from the concentrate using a low magnetising roast treatment (Fisher-White *et al*., 2007).

2.8   Application of ilmenite

Ilmenite mineral deposits account approximately 90% of the world's consumption of titanium mineral (USGS, 2017). The consumption of titanium mineral concentrates is tied to the production of TiO_2 pigments, which is not consumed in its metal form but as titanium dioxide (TiO_2), a white pigment primarily used in paper, paint and plastics. TiO_2 is mostly used as a pigment because of its whiteness, brightness, and opacity. The remaining 10% is used in chemicals, welding-rod coatings and for manufacturing carbides, and metal.

Between the years 2009 and 2015, the USA has imported 34% of South African produced ilmenite (USGS, 2017).

Mlinar and Petersen (2017) states that ilmenite is a titanium-iron oxide mineral and is a principal source of TiO_2. At present, Rio Tinto, Iluka Resources, Tronox Limited, and Kenmare Resources (Moma-Mozambique) offer about 60% of all the ilmenite supplied worldwide.

2.9   Air-dense medium fluidized bed

Coal cleaning aims to separate its ash-forming mineral matters from solid fuel hydrocarbons, increasing combustion efficiency and decreasing materials handling and boiler maintenance and linked downtime production loss (Prashant *et al.*, 1997).

Dry beneficiation of coal with an air dense medium fluidized bed (ADMFB) is proven to be an efficient method of coal separation, which is performed with a gas-solid fluidized bed as the separating medium (Dwari & Rao, 2007).

Wet processes are becoming less viable because much of the remaining coal reserves within South Africa are situated in environments that are arid. The wet process necessitates the installation of pipelines to supply water. Therefore, alternative dry coal beneficiation methods are being sought, especially in the arid geographical environment. This dry beneficiation process eliminates the need for water, and there are claims that it has the benefits of higher separation precision and quick return on investment, which must still be proved.

The ADMFB separator uses density as a critical parameter and pseudo-fluid characteristic of medium to separate coal from ash-forming mineral matter. There is no in-depth information available on the operation mechanism of the ADFMB from China.

De Korte (2013) notes that dry processing technologies are being evaluated for implementation in South African regions and its neighbouring countries, based on the fact that these techniques are perceived to be less expensive than wet beneficiation processes regarding both capital and operating cost. Dry processing appears to be very attractive from an economic point of view, based on the fact that no water is required

during this process, therefore lowering the environmental impact of coal processing significantly.

The world's first industry ADMFB modularised dry coal beneficiation plant was developed by Shenhua Xinjiang Energy Co. Ltd with a handling capacity of 40–60 t/h (Zhao *et al.*, 2017). The raw coal was screened, crushed, and –100 mm coal was loaded in a dryer to remove the surface moisture, which increased the screen efficiency. The dried coal was then screened at a screen aperture of 10 mm, the undersize –10 mm was considered as a clean product. Meanwhile, the coal (–100+10 mm) was used as the feed to the ADMFB. A binary of magnetic powder (–3+0,06 mm) with fine coal (–1 mm) was used as a medium. This process holds an automatic control of bed density that can control the bed density. The float and sink products were screened at 1 mm screen size. The ADMFB modularised coal processing plant confirmed that coal could be efficiently separated in the ADMFB at a cut point 1460 kg/m^3 with clean coal of 3,46% ash content, EPM of 0,055, medium loss of 0,42 kg and less than \$2 was used for separating one ton of raw coal.

2.9.1 Fundamental mechanism of separation in an air dense medium fluidized bed separator

Dry beneficiation of coal has a vital future in South Africa, principally in the arid regions. Dwari and Rao (2007) stated that the bed behaves like a liquid in an ADMFB process. Particles with density below the bed density report to the float, meaning the top surface of the bed, whereas particles heavier than the bed density report to the sink (the bottom of the container). In ADMFB, a stable dispersion fluidization and micro-bubbles must be achieved to obtain an efficient dry separation condition. Desirable physical properties of the ADMFB include a bed media of low viscosity and high fluidity and a bed density that is well distributed in three-dimensional space and remains stable over time. The criteria to determine the optimal operating velocity depends on various parameters, including the pressure drop through the fluidized bed and gas distributor, weeping through grids, bed expansion and gas channelling, maximum bubble size, intensity of back-mixing and particle attrition or agglomeration (Mohanta *et al.*,2013).

The fluidized bed density is equal to the beneficiation density and can be shown by Equation 5 (Chen & Wei, 2003):

$$\rho_b = (1 - \varepsilon)\rho_P + \varepsilon\rho_g = \rho_{50} \hspace{4cm} 5$$

Where:

ρ_P : density of the solid particles, kg/m^3

ρ_g : density of the air, kg/m^3

ρ_b : average density of the fluidized bed, kg/m^3

ρ_{50} : separation density of the fluidized bed, kg/m^3

ε : bed porosity

Zhenfu and Qingru (2001) argues that the coal beneficiation using an ADMFB use the pseudo-fluid properties of the gas-solids fluidized bed to procedure a steady and uniform gas-solids holdup of a specific density. The average density of the bed is calculated by Equation 6:

$$\rho = (1 - \varepsilon)\rho_s = W/(LAg) \hspace{4cm} 6$$

Where:

ε : bed void fraction

ρ_s : density of the medium solid, kg/m^3

W   : total weight of medium solids, kg

L   : depth of bed, m

A   : cross-section area of bed, m^2

g   : gravitational acceleration, m/s^2

In the fluidized bed, the buoyancy of beneficiation materials plays a critical role, and the displaced distribution effect should be controlled. Mohanta *et al*., (2013) and Wei *et al*., (1996) describes the displaced distribution effects, which contain the viscosity displaced distribution effect and movement-displaced distribution effect. This is produced by the viscosity of the fluidized bed. The viscosity declines with accumulative air flow velocity. The movement displaced distribution effect is more substantial when the air flow rate is either too low or too high. However, if the medium particle size distribution and air flow are efficiently controlled, both displaced distribution effects could be controlled successfully. The various forces which act on a particle in a fluidized bed as shown in Figure 14 are:

- Gravity force (F_{gr})

- Effective buoyancy force due to hydrostatic pressure distribution (F_b)

- Drag forces contributed by the relative motion of the coal particle and gas (F_g)

- Force between the coal particle and fluidized particles (F_d)
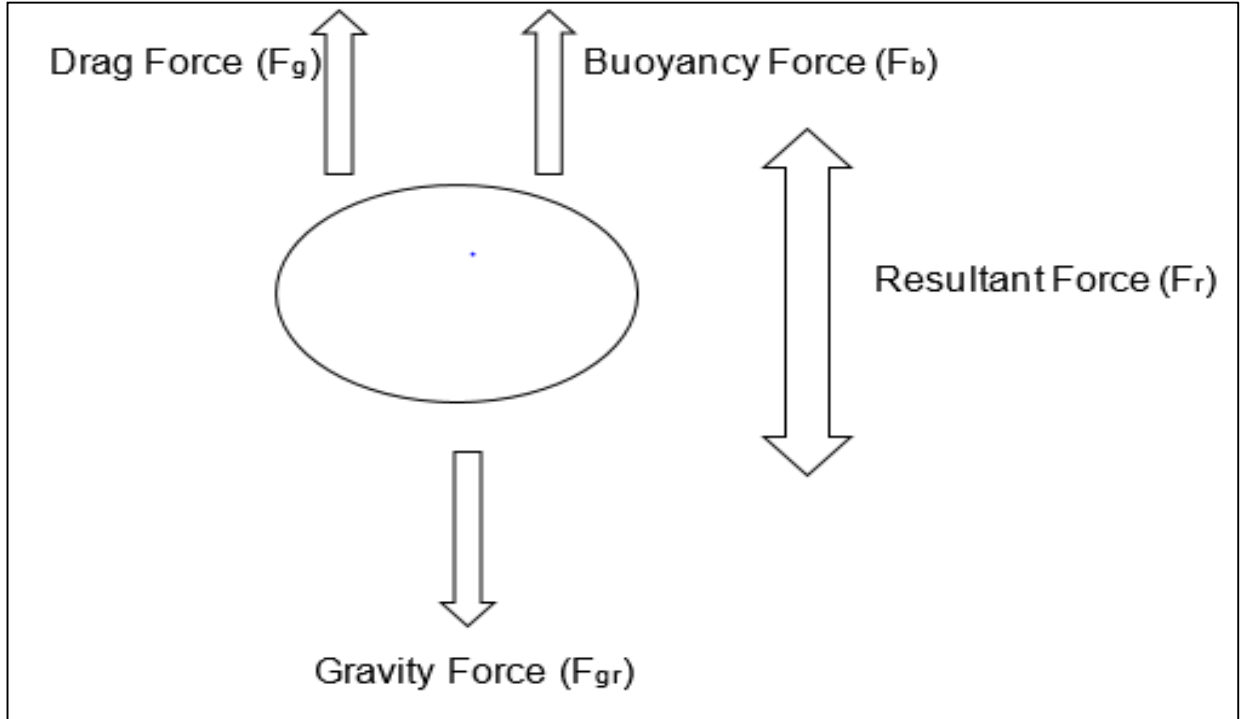
Figure 14 Forces acting on the particle in Air-Dense Medium Fluidized Bed (adapted from Mohanta _et al.,_ 2013)

The drag forces contributed by the relative motion of the coal particle and gas (F_g) can be neglected (Nguyen & Grace, 1978). Consequently, the resultant force (F_r) acting on the coal particle can be stated as Equation 7:

$$F_r = F_{gr} - F_b - F_d \qquad\qquad 7$$

However, these forces can be defined as Equation 8, 9, 10 and 11 (Nguyen & Grace, 1978):

$$F_r = \left(\frac{\pi}{6}\right) d_c^3 \rho_c a \qquad\qquad 8$$

$$F_{gr} = \left(\frac{\pi}{6}\right) d_c^3 \rho_c g \qquad\qquad 9$$

$$F_b = \left(\frac{\pi}{6}\right) d_c^3 \rho_b g \qquad\qquad 10$$

$$F_d = C_d \left(\frac{\pi}{4}\right) d_c^2 \frac{\rho_b u_r^2}{2} \qquad\qquad 11$$

Where:

d_c : equivalent diameter of the coal particle

ρ_c : density of the coal particle

ρ_b : bulk density of the fluidized bed

a   : acceleration of the coal particle

g   : gravitational acceleration

C_d : drag coefficient

u_r : relative velocity between coal particle and fluidized particles

The calculation of drag on the separated materials is important for processing with dense media. The drag coefficient can be calculated by Equations 12,13, 14 (Chen & Wei, 2003):

$$C_D = \frac{24}{Re_m}\left(1 + 0{,}15 Re_m^{0{,}687}\right), \hspace{4cm} 12$$

$$Re_m = \frac{d_o u_r \rho_b}{\mu_e}, \hspace{5cm} 13$$

$$\mu_e = \mu + \frac{\tau_o d_o}{3\mu_r}, \hspace{5cm} 14$$

Where:

C_D : drag coefficient

Re_m : Reynolds number

d_o : diameter of the falling object

μ_r : relative velocity between the object and fluidized particles

μ_c : effective viscosity

μ : viscosity of gas phase

τ_o : yield stress

2.9.2 Geldart's classic classification of powders

After careful observation of all sorts and sizes of solids in the fluidization, Geldart (1973) established four clear and identifiable types of particle behaviour, as shown in Figure 15. From the smallest to the largest particle, they are as follows:

- Group C: Cohesive, or ultrafine powders. Normal fluidization is extremely difficult for these solids, because interparticle forces are more significant than those

resulting from the action of the gas. Face powder, flour, and starch are typical of these solids.

- Group A: Aeratable, or materials having a small mean particle size and low particle density (< ~ 1,4 g/cm^3). These solids fluidize without difficulty, with smooth fluidization at low gas velocities and controlled bubbling with small bubbles at higher gas velocities. Fluidized cracking catalyst (FCC) catalyst is representative of these solids.

- Group B: Sand-like, or most particles of size 40 $\mu m < d_p < 500\,\mu m$ and density 1,4<ρ_s<4 g/cm^3. These solids fluidize well with vigorous bubbling action and bubbles that grow large.

- Group D: Spoutable, or large and dense particles. Deep beds of these solids are challenging to fluidize. They behave erratically, giving large exploding bubbles or severe channelling, or spouting behaviour if the gas distribution is very uneven.
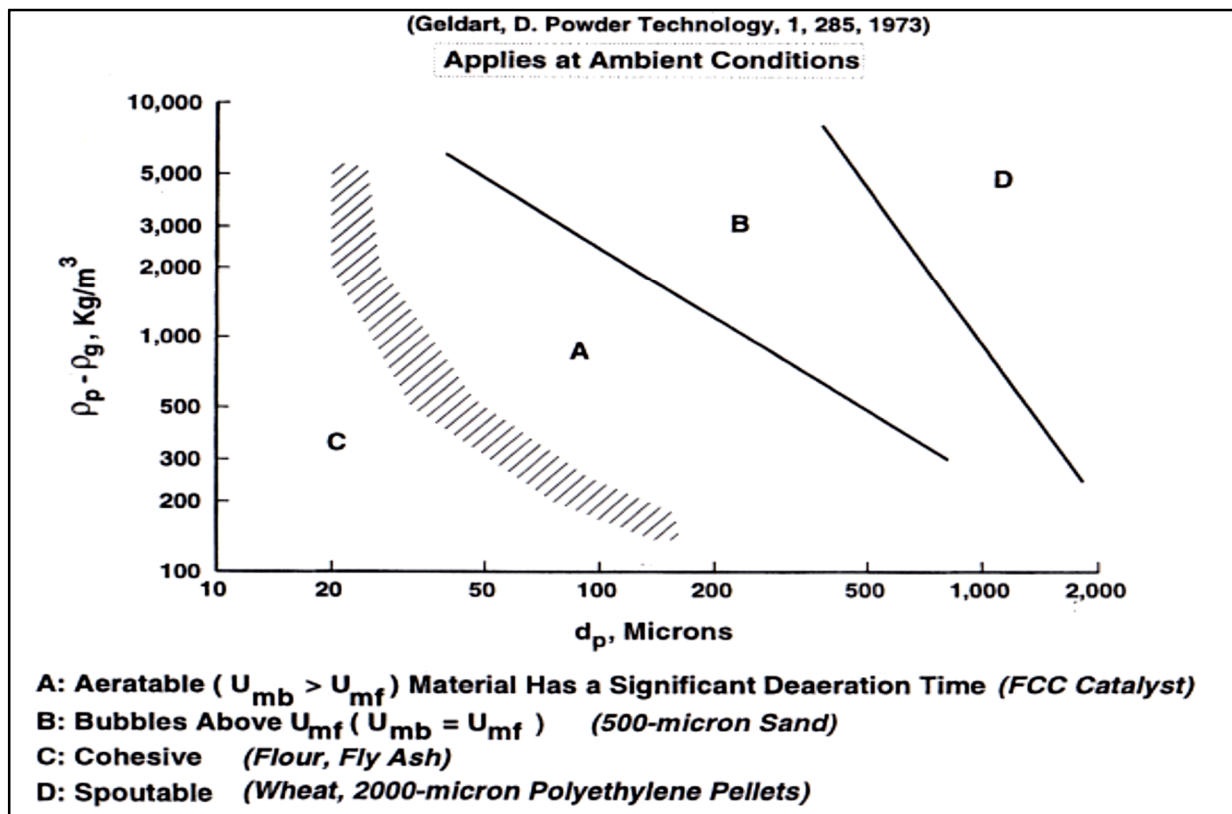
Figure 15 Geldart powder classification (Kunii and Levenspiel, 2005)

The experimental work was carried out using Geldart Group B particles, which is the most suitable group to conduct normal fluidization.

2.9.2.1   Minimum fluidization velocity

The U_{mf} in group B particles represent the point of transition between a fixed bed regime and a bubbling regime in a fluidized bed (Knowlton, 1977; Chiba *et al.*, 1979). The determination and definition of the U_{mf} are not straightforward concerning the mixtures of particles of a different size or density.

Ramos *et al.* (2002) states that U_{mf} is one of the essential normalised parameters when characterising the hydrodynamics in a fluidized bed. The minimum fluidization velocity can be experimentally determined, as shown in Figure 16.
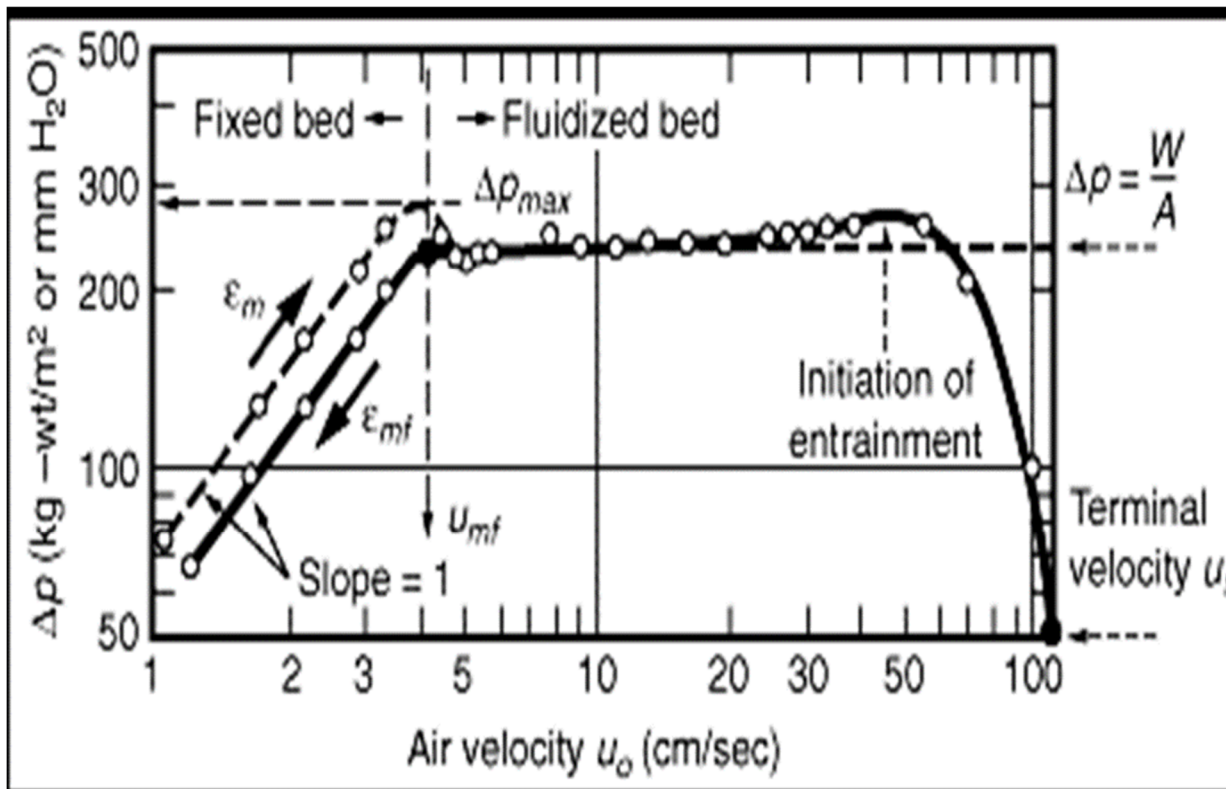
Figure 16 Pressure drop versus velocity diagram (Kunii & Levenspiel, 2005)

During an experiment, Kunii and Levenspiel (2005) found that the most common method of measurement requires that pressure drop across the bed recorded as the superficial velocity is increased stepwise through U_{mf} and beyond. U_{mf} is taken at the intersection of the straight lines corresponding to a fixed bed, and fluidized bed portions of the graph gained when ΔP_{bed} is plotted against U on log-log coordinates.

The U_{mf} is the superficial gas velocity at which the bed pressure drop becomes nearly constant, which is equal to the weight of the bed. The superficial gas velocity at which point the bed powder is just fluidized is known as the minimum fluidization velocity. This state of incipient fluidization can be defined by the Ergun (1952) Equation 15, which was derived from the force balance in Figure 14.

$$\frac{1,75}{\phi_s \varepsilon_{mf}^3}\left(\frac{d_p u_{mf\,g}}{\mu}\right)^2 + \frac{150(1-\varepsilon_{mf})}{\phi_s^2 \varepsilon_{mf}^3}\left(\frac{d_p u_{mf}\rho_g}{\mu}\right) = \frac{d_p^3 \rho_g(\rho_s - \rho_g)g}{\mu^2} \qquad 15$$

Where:

d_p : particle diameter d50, m

U_{mf} : superficial gas velocity at minimum fluidizing velocity, m/s

ρ_g : gas density, kg/m^3

μ : viscosity of gas, kg/ms

$\emptyset_s$: sphericity of a particle, dimensionless

ε_{mf} : void fraction in a bed at minimum fluidizing conditions

ρ_s : density of solids, kg/m^3

In ADMFB, the ideal operating gas velocity can be considered as the velocity at which the best hydrodynamic condition is obtained (Mohanta *et al.*, 2013). There is a criterion for determining an optimal operating velocity which depends on various parameters, for instance the pressure drop through fluidized bed and gas distributor, the intensity of back-mixing, particle attrition or agglomeration, maximum bubble size, weeping through grids, bed expansion, gas channelling, etc. Thus, it is a multifaceted parameter which requires to be selected correctly.

Mohanta *et al.* (2013) states that the optimal operating velocity is typically specified as a ratio to U_{mf} of medium particles which is relatively a fundamental velocity and has a unique value. The minimum fluidization velocity is regarded as an essential design variable and required to be predicted with confidence. Mohanta *et al.* (2013) notes that in current practice, the bed might bubble at a lower gas velocity than the theoretical minimum, due to the bypassing of gas through a small portion of the fluidized bed. However, the bed may remain stationary at gas rates above the theoretical minimum, owing to the extra force required to overcome the inertia force.

Previous studies proposed some correlations for the theoretical prediction of minimum fluidization velocity for various materials (Frantz, 1966; Bourgeis & Grenier, 1968; Babu *et al.*, 1978; Lippens & Mulder, 1993; Bin, 1994; Reina *et al.*, 2000). These correlations derived from dimensional analysis, force balance, pressure drop relations and a relative measure concerning the terminal particle velocity (Coltters & Rivas, 2004). However, significant disagreement exists among these correlations. In ADMFB, it is proposed that the optimum operating velocity is around two times the minimum fluidization velocity to achieve a uniform, smooth, stable fluidization by using group B particles (Chan & Beeckmans, 1982; Dong & Beeckmans, 1990; Kozanoglu *et al.*, 1993; Sahan & Kozanoglu, 1997).

2.9.2.2   Fluidization regimes

Gupta and Sathiyamoorthy (1999) describe fluidization as the phenomenon of imparting the properties of a fluid to a bed of particulate solids by passing a fluid (liquid or gas) through the latter at a velocity which brings the fixed or stationary bed to its loosest possible state just before its transformation into a fluid-like bed. A fluid-like behaviour is accomplished when the drag and buoyant forces exceed the gravitational forces of the solid particles, thus allowing relative motion between them. Fluidization can be achieved by using either gas, liquid, or a combination of both liquid and gas, as the fluid passes through the solid material. Both gas-liquid-solid and liquid-solid systems are significant for numerous industries. Nonetheless, they are not of interest in this research, which is primarily focused on gas-solid systems.

Yang (2003) reflects on six different regimes of fluidization for gas-solid fluidized beds: fixed bed, bubbling fluidization, slugging fluidization, turbulent fluidization, fast fluidization, and pneumatic conveying. Van Ommen and Ellis (2015) schematically illustrate the existent fluidization regimes in a gas-solid fluidized bed, which is shown in Figure 17. It is also stated in this research that in the fixed bed regime, the air flowing across the particle does not have enough velocity to move the particles. As the superficial gas velocity (U_g) rises, the bubbling fluidization regime is achieved in the bed. It is in this same regime that bubbles formation begin and coalesce, causing substantial mixing, and the velocity at which bubbles appear is well-known as the U_{mb}.

Additionally, Crowe (2006) notes that turbulent fluidization usually occurs when, as U_g is increased, it reaches a point where the bubbles or slugs begin to break down instead of continuing to grow. The "critical velocity" U_c, which is responsible for determining the onset of the turbulent fluidization flow regime, is frequently determined experimentally as the superficial gas velocity at which the standard deviation of pressure fluctuations reaches a maximum.
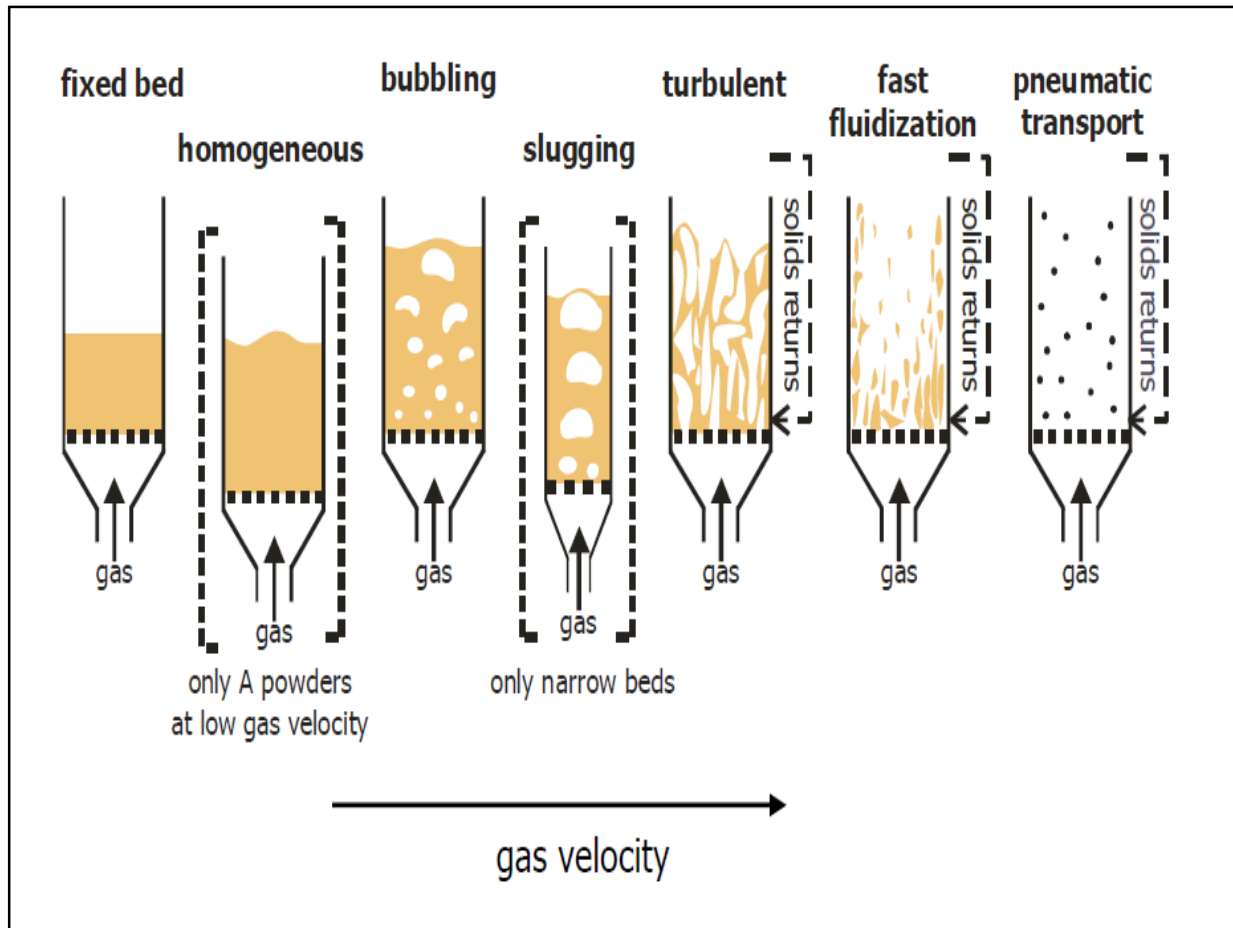
Figure 17 Flow regimes (Van Ommen & Ellis, 2015)

A fast fluidization regime is achieved whenever U_g is increased beyond a velocity known as the "transport velocity" U_{tr}. In the fast fluidization regime, solid particles are thrown outside of the bed, which causes the bed surface to appear indistinguishable. Lastly, the pneumatic conveying regime is achieved when the superficial gas velocity is much higher than the transport velocity; this regime is described by the particle being transported out of bed in a dilute phase. A summary of flow regimes can be seen in Table 3.

Table 3 Summary of flow regimes (Van Ommen & Ellis, 2015)

U range	Regime	Appearance and Principal Features
$0 \leq U < U_{mf}$	Fixed Bed	Particles are quiescent; gas flows through interstices
$U_{mf} \leq U < U_{mb}$	Particulate regime	Bed expands smoothly in a homogeneous manner; top surface well defined, small-scale particle motion
$U_{mb} \leq U < U_{ms}$	Bubbling regime	Gas voids form near distributor, coalesce and grow; rise to surface and break through
$U_{ms} \leq U < U_c$	Slug flow regime	Bubble size approaches column cross-section. Top surface rises and collapses with regular frequency.
$U_c \leq U < U_k$	Turbulent fluidization flow regime	Pressure fluctuations gradually decrease until turbulent fluidization flow regime is reached.
$U_k \leq U < U_{tr}$	(Turbulent Regime)	Small gas voids and particle clusters dart to and fro. Top surface is difficult to distinguish.
$U \geq U_{tr}$	Fast Fluidization	No upper surface to bed, particles transported out the top in clusters and must be replaced.
$U \gg U_{tr}$	Pneumatic conveying	No bed. All particles fed in are transported out the top as a lean phase.

2.10 Medium parameters

2.10.1 Characteristics of medium solids and segregation in ADMFB

Chikerema and Moys (2012) substantiate the effect of coal particle size, shape and density on the performance in an ADMFB using a binary medium of magnetite and silica. The experiment was conducted at the bed height of 0,32 m; the fluidization time was 30 seconds and four coal particles size ranges of −16+9,5 mm, −22+16 mm, −31,5+22 mm and −53+37 mm were used. It was found that the lower EPM of 0.05 was achieved in size range of−53+37 mm. However, the EPM of 0,07–0,11 was obtained at the size range of −16+9,5 mm, −22+16 mm, −31,5+22 mm, as indicating poor separation efficiency. Also, large coal particle (blockish) with the smaller surface area to volume ratio presented lower EPM of 0,08, related to the two categories of coal namely flat and sharp-pointed particles. It was also found that increasing the fluidization time (stratification time) negatively affected the écart probable moyen.

EPM describes the separation efficiency for the separator of any kind feed and can be used for evaluation of performance (partition curve) and comparison between separators (Tromp, 1937).

Mohanta *et al.* (2013) use different alternative materials as a fluidizing medium in ADMFB for the beneficiation of coal, such as magnetite, sand, magnetic pearls, a mixture of limestone and hematite, and a mixture of magnetite and fine coal. The magnetite powder is perceived as the most appropriate medium. As initially stated by the British coal-mining industry, the general specification of magnetite powder is based on particle-size distribution, relative density and magnetic content (Osborne, 1988). Magnetite relative density varies from 4900 to 5200 kg/m^3 with magnetic content not less than 95% by weight. The density of magnetite available in commercial quantities ranges from 4500 to 6500 kg/m^3, depending on its purity and hardness (Taggart, 1927). The acceptable magnetite particle size for ADMFB can be judged from Geldart fluidization classification in Figure 13. It is essential to mention that to achieve an efficient separation, both magnetite and coal particles should be of different Geldart groups, and magnetite particles must be more readily fluidized than the coal particles. For the sake of convenience, the particle size ranges for magnetite and coal for different Geldart groups are calculated and presented in Table 4.

When the size of magnetite particles are less than 20 microns (Geldart Group C), it is challenging to perform normal fluidization, since the interparticle forces are more significant than those that the air can exert on the particle (Geldart, 1973). Several authors noted that particle size ranging from 20 to 45 microns (Geldart Group A) appears to be inappropriate for ADMFB due to back-mixing of coal particle (Sahan & Kozanoglu, 1997; Choung *et al.*, 2006). Consequently, Luo and Chen, 2001a, 2001b; He *et al.*, 2002; Luo, Chen *et al.*, 2002; He *et al.*, 2003; Luo *et al.*, 2003; Wei *et al.*, 2003; Luo *et al.*, 2004; Mak *et al.*, 2008; Sahu *et al.*, 2009 agreed the range of 45 to 452 microns (Geldart Group B) is the most suitable size range to conduct normal fluidization.

On the other hand, previous studies suggested that, in order to achieve efficient separation of coal, the magnetite powder size must range from 150 to 300 microns (Luo

& Chen, 2001a, 2001b; He *et al.*, 2002; Luo *et al.*, 2002; He *et al.*, 2003; Luo *et al.*, 2003; Luo *et al.*, 2004; Wei *et al.*, 2003; Mak *et al.*, 2008; Sahu *et al.*, 2009).

Table 4 Size ranges for magnetite and coal for different Geldart groups (Geldart, 1973)

Geldart Group	Particle size range (μm)			
	C	A	B	D
Magnetite (ρ=5200 kg/m^3)	< 20	20–43	43–438	>438
Coal (ρ=1200 kg/m^3)	< 23	23–187	187–913	>913
Coal (ρ=1700 kg/m^3)	<21	21–132	132–767	>767

*density of air = 1,2 kg/m^3.

It is also suggested that in separating fine coal, finer magnetite particles (Geldart Group A) can be used in combination with bed stabilisation, employing external energy like vibration or magnetic field.

In today's practice, the moisture content of medium solids affects the separation efficacy of ADMFB. When the moisture content is above 2%, the fluidizing quality of magnetite powder is significantly affected because of the increase in its viscosity. A portion of the magnetite material becomes agglomerated, decreasing the contact efficiency between the particles and gas, thereby causing deterioration in particle dispersal and increasing local and overall non-uniformity in the bed density. Therefore, the bed fluidization and splitting performance tend to decrease. Luo *et al.* (2010) suggest a hydrophobic surface modification of magnetite particles to control the surface moisture content of feed coal.

2.10.2   Effect of coal to medium ratio

The coal to magnetite ratio is an essential operating variable from the equipment performance and economic perspective (Mohanta *et al.*, 2013). There exist two different ways in which increasing the volume concentrations of coal can affect the separation. Firstly, the effect is an interaction between neighbouring particles, which arises from hydrodynamics considerations and tends to diminish the settling velocity of coal, thus

influencing the performance of ADMFB. Secondly, the effect arises from the operation when the feed handling capability of the overflow weir is exceeded, and coal particles begin to compete for the chance to escape in the overflow. This crowding effect can swamp the first interaction.

Yang *et al.* (1985) studied the modification of fluidization behaviour by adding fines, using the bed collapsing technique in extensive experiments. As a result, fluidization enhancement increases monotonically as fines concentration are increased in the bed. Remarkable work was done for binary mixtures of Group B–C powders. The research findings indicated that adding the Group C powder into Group B will improve the fluidization behaviour of Group B powder. In the same way, adding Group B into Group C powder will also improve the fluidization behaviour of a cohesive powder. Some limitations exist regarding the amount of powder to be added to the mixture. The addition of powder exceeding the maximum recommended quantity will undesirably deteriorate both the fluidity and fluidization of the mix, although the author did not disclose the amount of powder which needed to be added to the bed.

Sahan and Kozanoglu (1997) report that for fine coal (0,165 x 0,116 mm), the cleaning performance is relatively insensitive toward coal to magnetite ratio in a shallow bed when compared to the other processing conditions. It is claimed that the best performance could be achieved when the volume ratio of coal to magnetite varies between 1 and 2. For a more profound bed more than 120 mm in height, the cleaning performance significantly improves when this ratio changes from 0,1 to 0,7. Choung, Mak and Xu (2006) also arrive at the same conclusion from their experimental results for 3,35 x 1,0 mm coal and point out that the magnetite bed may collapse on increasing this ratio above 0,66 for a shallow bed in height, which requires low air flow to produce a fluidized bed. This bed collapse is due to the blockage of air distributor by the segregating heavy particles at the bottom of the fluidized bed and prevents the formation of uniform air-magnetite pseudo-fluid. Mak *et al.* (2008) also achieved a better cleaning performance for large coal sizes by taking the coal to magnetite ratio of 1:15.

2.10.3 Minimum bed height

Yang (2003) indicates that a slugging regime takes place only when the bed height (H) over the bed diameter ratio (D) is greater than around 2. Also, great H/D ratios will provide sufficient time for bubbles to coalesce into bigger ones. Once the bubbles rise around 2/3 of the bed diameter, the bed moves into the slugging zone with the periodic passing of large bubbles and regular large fluctuation of bed pressure drop corresponding to the bubble frequency.

Baeyens and Geldart (1974) analysis highlight three separate regions in a deep bed operating with a surplus velocity. A freely bubbling bed is found in Region 1, while there is a slugging bed in Region 2. However, the slug increases with ongoing coalescence. Region 3 is the only area in which the slug coalescence complete and a much more stable slug spacing is established. They propose to calculate the maximum bed height underneath which the bed will be freely bubbling can be calculated from Equation 16:

$$H_{fb} = \left(\frac{D - 2,51D^{0,2}}{0,13D^{0,47}}\right) \qquad\qquad 16$$

Where:

H_{fb} : height of fluidized bed (cm)

D   : diameter of fluidized bed (cm)

Hovmand and Davidson (1971) suggest the operating superficial gas velocity Equation for the transition of bubbling to slug flow, which agrees with most experiments, as shown by Equation 17:

$$\frac{U - U_{mf}}{0,35\ (gD)^{\frac{1}{2}}} = 0,2 \qquad\qquad 17$$

When $U - U_{mf}$ is larger than the value found in Equation 17, the bed will change into the slugging region immediately.

2.10.4 Effect of fine coal accumulation and density

Mohanta *et al.* (2013) indicate that the distribution of bed beneficiation of coal by ADMFB mainly depends on the density differences of heavier and lighter coal particles in respect

of the density of the fluidized bed. Accordingly, the authors cited that the nature of density distribution inside the bed is an essential factor, which manipulates the sharpness of separation. In continuous operation, the fine coal particles (<1 mm) continuously accumulate in the fluidized bed because of the poor screening efficiency and affect the separation performance of the equipment (Mohanta *et al.*, 2013). Luo and Chen (2001b) studied the influence of fine coal accumulation and found that on precise control of fluidization velocity, 50 x 6 mm size coal can be successfully separated by using a mixture of magnetite powder (0,15 x 0,3 mm), and coal fines (0,45 x 0,9 mm) as the fluidizing medium. The authors also perceived that the fluidizing gas velocity could be adjusted over a wide range to sustain a stable bed.

With regard to the size difference, it is evident that the most prominent particles will commonly separate to some point below the smaller ones, except in the case where the size difference is insignificant or complicating aspects such as hydrodynamic instability, or bulk circulation can significantly blend the two particles thoroughly (Yang, 2003). In the event of a difference in shape, the materials with the greater size particle sphericity (ϕdp) will commonly segregate below. In the case of density difference, the stratification will be accentuated, if the difference in density of the particle is perceived to be in the same direction with the product ϕdp. When the density difference is in the opposite direction, depending on the degree of this difference, the stratification may be decreased during the whole voidage range as the liquid velocity is increased. This may be overturned over the complete voidage range, or it may be reversed at the lower voidage and decreased at the higher voidage (Yang, 2003).

He *et al.* (2003) investigated the density distribution in fluidizing bed for fine coal particles (0,15 x 0,3 mm) mixed with magnetite powder (0,15 x 0,3 mm) and perceived that density stratification does not appear beneath the fine coal concentration of 12%. Stratification of the fine coal increases rapidly when its concentration is above 18%.

2.10.5   Bed voidage

The system stability increases as the voidage drops. The systems tend towards the orthorhombic state, mainly in the case where a mechanical disturbance like vibration is associated with the systems. Also according to Yang (2003), the voidage of a bed of

same-size particles (monosized particles) is commonly about 0,395 after prolonged shaking, therefore approaching the features of an eight-point packing of orthorhombic.

Haughey and Beveridge (1969) categorise the packing into four distinct modes, namely very loose random packing, poured random packing, loose random packing and close packing. The poured and loose random packing are both equivalents to Scott's (1960) dense and loose random packing, whereas the very loose random packing relates to the situation where the bed is primarily fluidized, after which the gas is gradually decreased until it reaches below the minimum fluidization. Typically, the voidage of bed so formed is about 0,44. The close random packing is achieved by vigorously vibrating or shaking the bed; usually, the voidage approaches 0,359 to 0,375.

The bed porosity (ε) can be calculated by Equation 18:

$$\varepsilon = 1 - \frac{\rho_b}{\rho_p} \qquad\qquad 18$$

Where:

ε	: bed porosity
ρ_b	: density of the bed
ρ_p	: density of the particle

2.11 Conclusion

At the end of this chapter, there should be a clear understanding of ilmenite properties, its production, impurities and application of the mineral. This chapter also encompasses a thorough explanation of the different types of magnetic separation. The significant producers of ilmenite in South Africa are highlighted, actual available reserves and economic viability are discussed.

Emphasis has been placed on the essential coalfields in South Africa and their actual reserves and availability.

There should be an appreciation of the fundamental mechanism of separation in an air dense medium fluidized bed separator, medium parameters, the principle of fluidization, terminology and essential parameters.

3 METHODOLOGY

3.1   Introduction

The methodology was established to evaluate the performance and recovery of ilmenite from an air dense medium fluidized bed. It is essential to determine parameters, such as the minimum fluidizing velocity, bed composition of binary medium (ilmenite with fine coal and ilmenite with fine sand), bed density, Ecart Probable Moyen and the yield with two different coal samples.

The alternative materials contain ilmenite with sand and ilmenite with fine coal. It is perceived as an accessible material, which is mostly available in a wide variety of shapes and sizes, which makes the selection of sand critical for fluidized bed experiments.

The two coal samples used for this experimental test were from Greenside Colliery in Witbank, from No 1, 4, and 5 Seams. The coal samples were labelled as a run of mine coal sample (ROM) and feed to the plant coal sample (AFE). Each coal samples collected were weighted 80 kg and were visibly wet. The ilmenite sample used for this testwork was provided by Tronox Limited from Hillendale South Africa (120 kg). The sand sample was sourced from Rolfes Silica in Brits (50 kg), and the sample was already upgraded and sized. The fine coal came from sizing the coal samples (50 kg).

ASTM and ISO standard were used to determine the surface moisture, proximate analysis, calorific value and particle size distribution. In some cases, no standards were available, and so the methods used were discussed and approved by the supervisors and sponsors. The air dense medium fluidization bed and magnetic separation were done based on principles discussed in the literature.

3.2   Sampling characterisation of coal

3.2.1   Air drying of coal sample

The two samples AFE and ROM were visibly wet. It was thus essential to air dry the coal samples to be able to screen and split the sample in a ten-way rotary splitter.

The objective of air-drying coal is to bring its moisture content to equilibrium with the atmosphere at ambient temperatures. The samples were air dried on a drying floor, and then dispersed in a thick layer not surpassing a thickness of twice the nominal top size of the coal (ASTM D3302/D3302M-12). Air drying on a drying floor consumed all the time, as ASTM D3302/D3302M-12 suggests that the drying must stop when the loss in weight of the sample is less than 0,1% per hour.

Some precautions are needed to minimise the variance at this stage of sample preparation. Air drying the sample on a drying floor was carried out in a room free of dust and excessive wind. The residual moisture remained in the sample after air drying; only surface moisture was removed.

3.2.2 Screening coal samples

The coal samples ROM and AFE were screened using a vibrating horizontal screen. The sample was first screened at 13,2 mm. This was done to be able to create the sized feed (–50+13,2 mm) as is currently used by the Bohou process in China.

3.2.3 Materials handling

Coal samples are collected and prepared with the aim of conducting a test, which after analysis will offer results that are representative of the gross sample. The materials handling of prepared samples are an essential stage of the experiment, as inappropriate handling these samples could lead to unrepeatable outcomes.

The ASTM D2234/D2234M-16 standard for sample splitting was used to successfully prepare the samples and avoid biases. The loss of dust and particle degradation were minimised.

Precision, as specified by the reproducibility of the impartial results, is indicated by the nearness of the data to the concrete value in certain conditions. Sampling precision relies on coal variability, the number of increments containing each sample, the number of samples from a lot and the sample's mass relative to nominal top size.

Gross sample division

The first step in creating an unbiased sample is to homogenise the samples. Secondly, samples are split into ten increments, which is achieved by using a ten-way rotary splitter. Lastly, increments are added, and the process is repeated more than three times to ensure a correct sample representative (ASTM D2234/D2234M-16).

Figure 18 shows the ten-way rotary splitter.

Figure 18 Rotary splitter

When a given quantity of coal that is characterised as a single lot is split into multiple sub-lots, the inaccuracy of the representative sample is reduced, as shown by Equation 19 (ASTM D2234/D2234M-16).

$$Imprecision = 1 \div \sqrt{m} \qquad\qquad 19$$

Where:

m : number of sub-lots

In this study, a maximum error of 3% was permissible during splitting to ensure correct sample splitting. For example, the gross coal sample of 80 kg was divided into ten lots; then each lot had to weigh 8 ± 0,3 kg.

A graph illustrating the splitting procedure to achieve 160 samples of 0,5 kg each, from the gross sample, is shown in Figure 19. A cross selection of samples was applied to combine sub-samples through the whole splitting procedure.
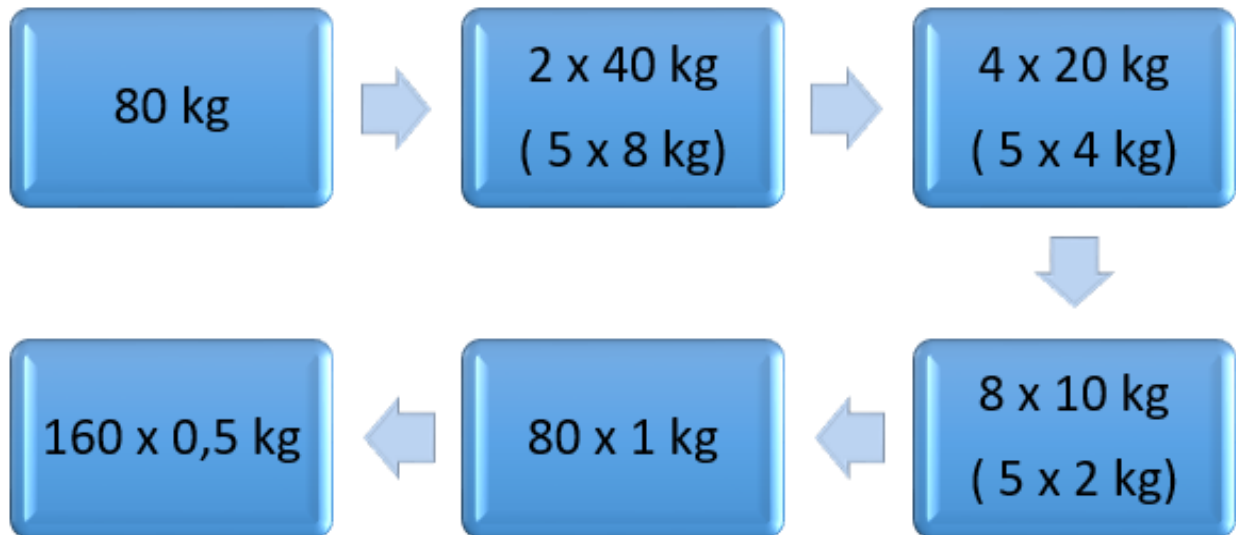
Figure 19 Graphical illustration of the rotary splitting

3.2.4 Material characterisation

The sample characterisation forms the foundation of the project, as it is essential to determine the chemical composition, the phase's identification, and the physical properties of samples. These parameters are the most significant factors in the evaluation of ilmenite as a possible medium in air dense medium fluidized bed process.

The sample was divided into 0,500 kg sub-samples, and three samples were picked by applying cross selection. Two of these 0,050 kg samples were combined to produce a single sample of 0,100 kg, which was pulverised and split into 0,010 kg samples, as shown in Figure 20. Three random samples of 0,010 kg were sent for chemical analysis. A small ten-way rotary splitter was used to split it into 0,010 kg sub-samples, and the sub-samples were dispatched to X-ray diffraction (XRD), X-ray fluorescence (XRF), micro XRF and scanning electron microscope (SEM) analysis, respectively. The sub-samples of 0,010 kg were split into increments of 0,001 kg using a small ten-way rotary splitter for proximate analysis and calorific value. The rest of the samples were used for particle size distribution (PSD) analysis.
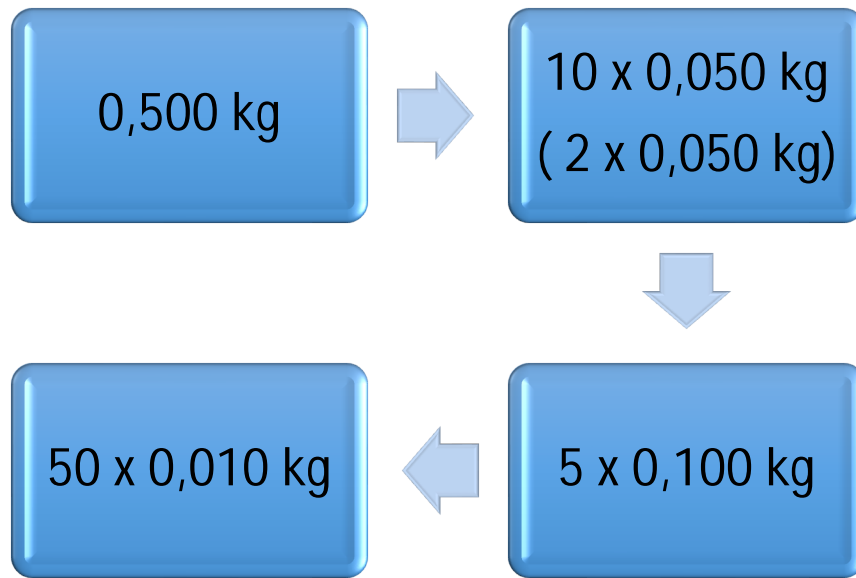
Figure 20 Graphical illustration of a material characterisation

The wet coal samples were prepared by adding water to the air-dried coal subsamples, according to Equation 20. The wet coal samples were conditioned for 24 hours, and the samples were weighed again to check if there were any variations in the surface moisture content.

$$Moisture\% = \frac{A-B}{B} \times 100 \qquad\qquad 20$$

Where:

      A   : weight of wet sample (grams), and

      B   : weight of dry sample (grams)

3.2.5 Proximate analysis

According to ASTM D5142, the proximate analysis was used to determine the volatile matter (VM), moisture content, ash content and, by difference, the fixed carbon within the coal sample. It is the most common and uncomplicated method used for coal samples. The total and residual moisture content of coal are determined through proximate analysis of moisture. Thus, the total moisture content of coal entails the surface and inherent moisture.

Ash content is ascertained by assessing the weight of residue remaining after burning 0,001 kg of coal under strictly controlled conditions to control the temperature, sample weight, time, atmosphere and equipment specifications.

The volatile matter is determined by the same principle which required 0,001 kg of coal sample with a top size of 250 microns. A total of 7 minutes is allowed to heat up the sample at a fixed temperature in a covered crucible.

The fixed carbon present in coal is the remaining carbon in the coal sample after driving off the volatile matter. The proximate and ultimate analysis of carbon content differs because of some carbon lost in hydrocarbons with volatiles. The measurement of burnout and combustion reactivity is determined by the ratio between fixed carbon and proximate volatile matter. The proximate analysis of coal samples was analysed at Mintek.

3.2.6 Calorific value

Calorific value (CV) is a direct indication of the heat content (energy value) of the coal. Coal's CV is one of the most vital factors in the mining of coal, as coal is used for combustion applications. CV is the most commonly used benchmark of coal quality and determines its economic value. The CV is usually expressed as the gross calorific value (the higher heating value) or the net calorific value (lower heating value). The difference between the gross calorific value (GCV) and the net calorific value (NCV) is the present heat of condensation of the water vapour produced during the combustion process (Zhu, 2014).

The bomb calorimeter provides the most suitable and accurate apparatus for determining the CV of liquid and solid fuels and is adopted in ASTM D5865-12. The calorific value was determined with a 0,00096 kg coal sample. The coal samples were then analysed with the bomb calorimeter at Mintek.

3.2.7 X-ray diffraction analysis for coal and ilmenite sample

The X-ray diffraction analysis (XRD) is one of the most advanced and most commonly employed method of identifying various mineral phases and crystal structures in the sample. The samples were prepared according to the standardised Panalytical backloading system, which provides nearly random distribution of the particles.

The samples were analysed using a Panalytical X'Pert Pro powder diffractometer in θ–θ configuration with an X'Celerator detector and variable divergence and fixed receiving slits with Fe filtered Co-Kα radiation (λ=1,789 Å). The phases were identified using *X'Pert High score plus® software.* The relative phase amounts (weight%) were estimated using the Rietveld method (Autoguan Program). Errors were on the 3-sigma level.

The XRD analysis was done for identifying mineral phases and minerals in coal and ilmenite samples in Stoneman at the University of Pretoria.

3.2.8 X-ray fluorescence analysis for ilmenite sample

X-ray fluorescence (XRF) analysis, also referred to as X-ray emission spectrography was used to determine the chemical composition of samples. The ARL Perform'X Sequential XRF instrument was used for the analyses. When the X-ray beam is directed at the sample produced in a high-intensity X-ray tube, the sample which is pulverised to a fine powder and compressed into a pellet using a binder absorbs the X-ray beam in a certain way according to Beer's Law. Analyses were executed using the *Quantas® software*. The software analyses all elements in the periodic table between Na and U, but only elements found above the detection limits were reported.

XRF analysis was done in Stoneman at the University of Pretoria.

3.2.9 Particle size distribution

By applying cross selection, two sub-samples of 0,500 kg each were added together to produce a sample of 1 kg. A particle size distribution was completed on the sample, using a laboratory sieve shaker. A Taylor sieve series was selected. The particle size distribution (PSD) study was executed with a 1 kg sample of ilmenite, sand, fine coal and coal which was screened for 10 minutes at an amplitude of 40% (ASTM D4749-87). Malvern equipment was used to measure the particle size distribution of the medium solids such as ilmenite according to ISO 13320:2009. A cross selection was employed to pick three sub-samples of 0,010 kg each and dispatched for Malvern test at the University of Pretoria.

The *Malvern 2000® software* was used to report accurately the level of signal the sample produces. The ilmenite sample was measured by monitoring the obscuration (10–20%)

of the laser beam produced by the sample. The software measured the size distribution calculated and the data was automatically saved.

3.3 Sample preparation of ilmenite

3.3.1 Scanning electron microscopy (SEM)

Scanning electron microscopy (SEM) analysis was done to create a backscatter image to investigative the specimen with an intense electron beam that is scanned across a rectangular area of the specimen (Zhu, 2014).

SEM JSM-IT300HR (Joel Oxford instrument) produces a considerable amount of information by creating numerous categories of emission signals, as well as secondary electrons cathodoluminescence emission, backscatter electrons and X-rays. SEM equipment was incorporated with *smile view lab® software* which linked stage navigation, stage positions, scanning electron microscopy images and energy dispersion spectroscopy (EDS) results. The ilmenite samples were mounted on a sticky material and analysed in each spectrum by using the backscatter electron technology which can determine various minerals according to the mean atomic number.

SEM analysis was done in the Industrial Metals and Minerals Research Institute (IMMRI) at the University of Pretoria.

3.3.2 Pycnometer

Gas pycnometry is known as one of the most reliable techniques for obtaining true and apparent volume. The AccuPyc II 1340 Series Pycnometer was rapid, fully automatic pycnometers that afford high-precision volume measurements, high-speed and calculations of correct density on a wide variety of powders. The test accuracy mode allows it to achieve high repeatability (Micromerities website). The ilmenite samples were analysed using a gas pycnometer in the mineral processing laboratory at the University of Pretoria. The gas pycnometer is displayed in Figure 21.

Instructions from gas pycnometer:

- Inert gas flows into the sample chamber
- Equilibrium is reached
- Gas flows into the second chamber for volume measurement

- Equilibrium is reached yet again

- Volume divided by sample weight determines the density

- Pressure vented off to the atmosphere

Figure 21 Gas pycnometry

3.3.3 Micro X-ray fluorescence

Micro X-ray fluorescence (µXRF) is a fundamental analysis method which depends on the same principles as X-ray fluorescence (XRF). The dissimilarity is that micro X-ray fluorescence has a spatial resolution with a diameter many orders of magnitude smaller than conventional XRF. While a smaller excitation spot can be achieved by restricting X-ray beam using a pinhole aperture, this method blocks much of the X-ray flux, which has a different effect on the sensitivity of trace elemental analysis ("Micro X-ray Fluorescence, "2018).

Ilmenite grains loosely packed in Al cups were mapped elementally using a Bruker M4 Tornado, an energy-dispersive micro-X-ray fluorescence spectrometer (µ-EDXRF). This instrument has a large analytical area, up to 200 x 160 mm, and can take a mass of up to 5 kg, so samples are cut and ground flat, with no further sample preparation required. The sample mapped measured 38,08 x 16,64 mm and had a mass of

approximately 0,050 kg. The great advantage of the instrument is that optical imaging is replaced by elemental imaging, and the image required can be assembled from addition of different element spectra to give the most effective visualisation. This, with the addition of a complete spectrum of each pixel, enables quantitative and qualitative elemental analysis of points and areas.

The instrument was configured with a Rhodium tube, which was operated at 50 kV, 500 µA and 30 W. The polychromatic beam (0–50 keV) is focused by means of a polycapillary lens to a spot size of <25 µm at this wavelength, with the incident beam and take-off angles at 51°. The instrument is equipped with two silicon drift detectors with an energy resolution of 145 eV for Mn Kα, which face each other at a 180° angle and 90° to the tube with respect to the sample surface. The sample chamber was evacuated to <20 mbar to enable light elements such as sodium to be measured. Step size and integration time per pixel were set to 50 µm and 50 ms.

The micro X-ray fluorescence was conducted identifying all elements on the surface of ilmenite sample in Stoneman at the University of Pretoria.

3.4 Air dense medium fluidized bed

The most common method of measurement is to measure the pressure drop across the bed against the superficial velocity. This superficial velocity must be increased stepwise through U_{mf} and beyond. U_{mf} is taken as the intersection of the straight lines corresponding to a fixed bed, and fluidized bed portions of the graph gained when ΔP_{bed} is plotted against U (superficial velocity) log-log coordinates.

The experiments were conducted in a laboratory air dense medium fluidized bed unit situated at the Council for Scientific Industrial Research in Pretoria (CSIR). A schematic air dense medium fluidized bed is shown in Figure 22.

Instructions from air dense medium fluidized bed:
- Blend medium in different ratio
- Load the medium into Perspex fluidized bed
- Switch on the compressor air
- Control volume of air with air bleed valve

- Open the air bleed valve stepwise and measure the superficial velocity using the manometer and convert it using superficial gas velocity versus orifice pressure drop (Appendix 11)
- Read the pressure drop over the bed through a manometer
- Plot the graph pressure drop versus superficial velocity

1. Compressed air; 2. Air bleed valve; 3. Orifice; 4. U-type manometer; 5. Pipe connector; 6. Perspex fluidised bed; 7. Distributor;
8. Bed pressure drop
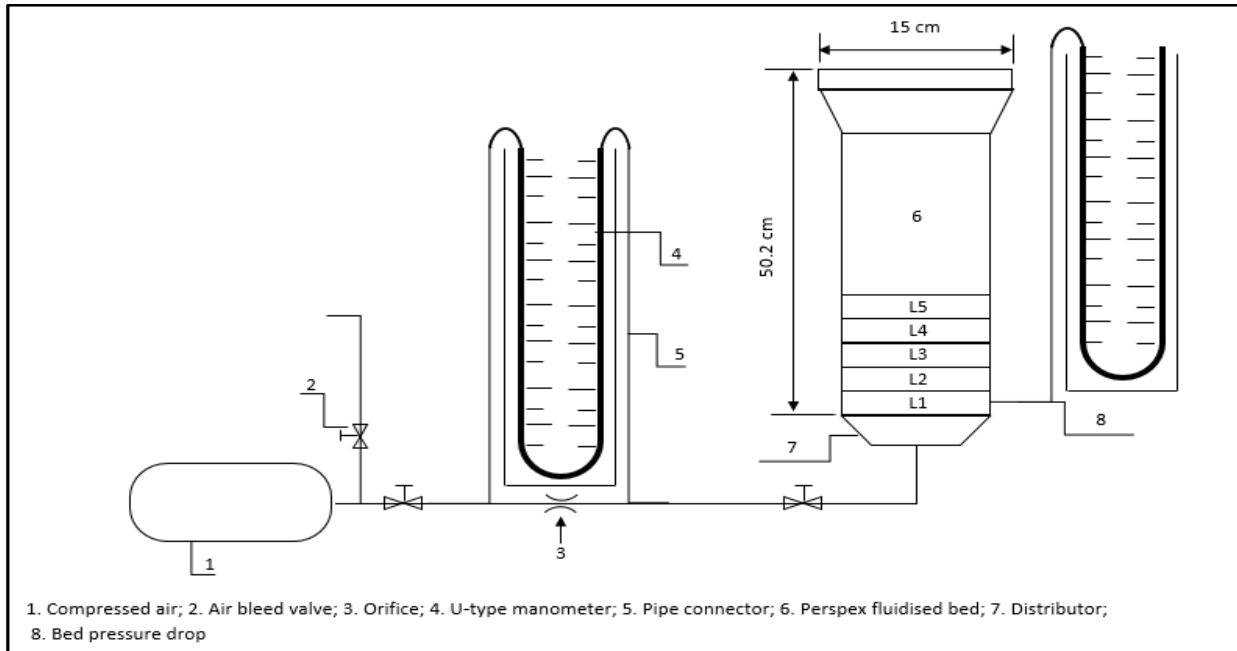
Figure 22 Schematic air dense medium fluidized bed (CSIR, Pretoria)

Parameters were determined by using the laboratory ADMFB, for instance:

- Compressed air: a pressure inlet of 88 kPa was used to fluidize the bed.
- Minimum fluidization: was experimentally determined for each bed composition medium solids: ilmenite with sand and ilmenite with fine coal.
- The U_{mf} of ilmenite, sand and fine coal were also calculated using the Ergun Equation 15:

$$\frac{1,75}{\phi_s \varepsilon_{mf}^3}\left(\frac{d_p u_{mf}\,g}{\mu}\right)^2 + \frac{150(1-\varepsilon_{mf})}{\phi_s^2 \varepsilon_{mf}^3}\left(\frac{d_p u_{mf}\rho_g}{\mu}\right) = \frac{d_p^3 \rho_g(\rho_s-\rho_g)g}{\mu^2} \qquad 15$$

- Maximum bed height: was calculated as the maximum bed height where the bed will be freely bubbling from Equation 16:

$$H_{fb} = \left(\frac{D-2,51D^{0,2}}{0,13D^{0,47}}\right) \qquad 16$$

- A static bed: was fixed at 120 mm due to the Equation 16, which was divided into 5 layers such as L5: 20 mm, L4: 20 mm, L3: 20 mm, L2: 20 mm and L1: 40 mm.

- Operating superficial gas velocity: for the transition from bubbling to slug flow using the Equation 17:

$$\frac{U - Umf}{0{,}35\,(gD)^{\frac{1}{2}}} = 0{,}2 \qquad\qquad 17$$

- The bed porosity (ε) can be calculated by Equation 18:

$$\varepsilon = 1 - \frac{\rho_b}{\rho_p} \qquad\qquad 18$$

- Ecart Probable Moyen was calculated to determine the efficiency of the process by using Equation 21 (Tromp, 1937):

$$EPM = \frac{\rho_{25} - \rho_{75}}{2} \qquad\qquad 21$$

Where:

ρ_{50} (SG50) : Cut point density at 50%

ρ_{25} : Cut point density at 25%

ρ_{75} : Cut point density at 75%

- Napier-Munn (1991) gives a good overview of the statistical calculations Equation 22, knowing the cut point at 50%, particle density and the EPM which correct the actual partition curve.

$$Y = 1/(1 + \exp[1{,}099 * (\rho_{50} - \rho)/Ep\,]) \qquad\qquad 22$$

Where:

Y : partition number

ρ_{50} : cut density, kg/m^3

ρ : particle density, kg/m^3

EP : separation efficiency (Ecart Probable Moyen)

1,099 : empirical constant

- Segregation of bed: was determined by grouping the bed layers into three groups (top (L5 & L4), middle (L3 & L2) and bottom (L1) layers).
- Ascertain the stereomicroscopy of bed medium.
- The Yield of coal samples AFE and ROM were calculated using Equation 23 (Gupta & Yan, 2006).

$$Yield = \frac{\text{Feed ash\%} - \text{Float ash\%}}{\text{Sink ash\%} - \text{Float ash\%}} \times 100 \qquad\qquad 23$$

3.5   Tracers particles

The specific gravity range of the tracers particles used for the tests was between 1300 to 3000 kg/m^3 and for each density value, there were ten tracers available. The tracer's particles are made of a magnetically susceptible material. They are cubic and with side dimensions of 12 mm. The tracer's particles are shown in Figure 23.

Figure 23 Tracers particles

3.6   Fluidization

Ten minutes was allowed for the fluidized bed to stabilise, and the tracers were then gradually introduced onto the surface of the fluidized bed. After stratification for 30 seconds, the air bleed valve stream was sharply closed off and all the stratified tracers were retained in their positions in the mixture. The static bed was divided into five layers which were three floats (L5, L4 & L3) and two sinks (L2 & L1); the tracers were discharged layer by layer using a scoop from top to bottom.

3.7   Recovery of ilmenite

The mixture 40% ilmenite with 60% fine coal medium was mixed with coal. Ilmenite was reused one time, four times and ten times. The mixtures (coal + medium) were sieved for 10 minutes on a sieve size of 3,350 mm at amplitude 40%. A dry high gradient magnetic separator (HGMS) of 4200 Gauss was used at a rotation speed of 60 rpm to recover the ilmenite from undersize. Each time ilmenite recovered was reused according to the number of reusing, fresh coal was introduced into the process as shown in Figure 24. Lastly, the Magna chute of 3150 Gauss was used to clean the magnetic ilmenite recovered to achieve a real account of the medium recovered. The loss of ilmenite was expressed in gram per kilogram using Equation 24:

$$Loss\ of\ ilmenite = \left(\frac{Initial\ ilmenite - Recovered\ ilmenite}{feed\ coal}\right) \qquad 24$$

Figure 24 Reused ilmenite medium circuit

3.8   Magnetic separator

The magnetic elements are constructed of blocks of high-temperature neodymium-iron-boron magnets (Eriez magnetics, 2008). The dry HGMS parameters are:

- Drum speed   : 40–80 rpm.
- Gauss Interpole magnetic element (average on drum surface): 4200 Gauss.

Figure 25 displays the dry high gradient magnetic separator from the mineral processing laboratory at the University of Pretoria parameters.

Instructions for high gradient magnetic separator:

- Discharge the undersize medium in the hopper.
- Switch on the motor of the drum at a speed of 60 rpm.
- Switch on the feeder.
- Collect the magnetic and non-magnetic.

Figure 25 High gradient magnetic separator

3.9   Magna chute

The Eriez Magna Chute Rare Earth was used to determine the ilmenite losses, as shown in Figure 26. The approximate magnetic strengths are 3150 Gauss (website Eriez). Instructions from Eriez lab equipment:

- The tray position is flat and in contact with the magnet discharge 1 litre of ilmenite.
- Carefully wash off coal/non-mags that become entrapped in magnetic particles.
- Lift the tray to a higher position away from the magnet.
- Rinse off magnetic.
- Collect, dry and weigh magnetic.

Figure 26 Eriez Magna Chute Rare Earth

3.10 Summary of experimental plan

Figure 27 summarises the preliminary plan of the project, starting from the coal sampling and ending with the recovery of ilmenite.
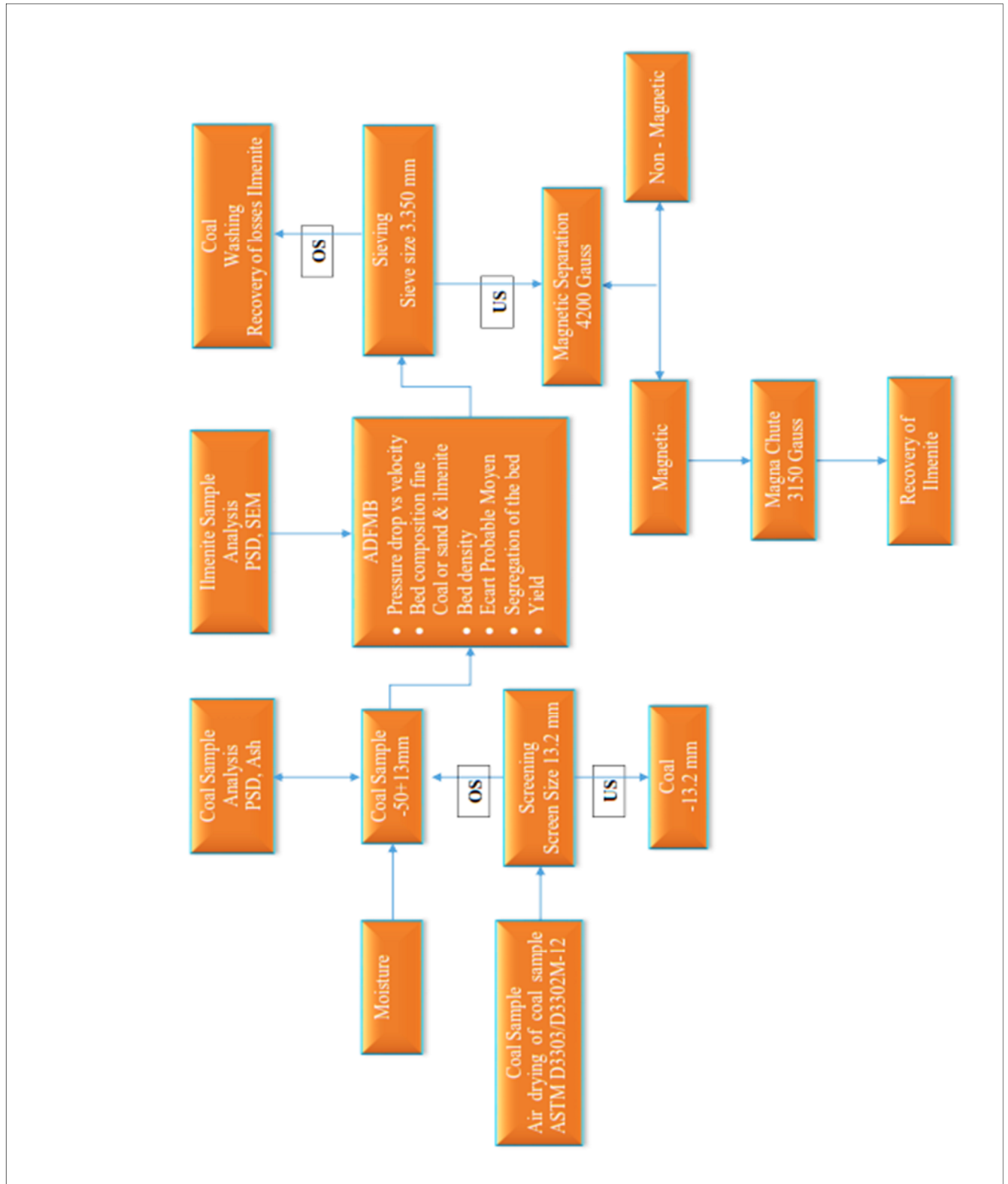
Figure 27 Summary of experimental plan

4 RESULTS AND DISCUSSIONS

4.1 Initial results: Coal samples

4.1.1 X-ray diffraction

The coal samples AFE and ROM were from Greenside Colliery in Witbank. As discussed in section 3.2.1, the samples were dried according to ASTM D3302/D3302M-12 and were screened to get the size range between –50+13,2 mm.

As discussed in section 3.2.7, three samples of each coal ROM and AFE were selected for the XRD analysis to determine the clays content in the bulk/gross sample and to confirm that the split samples are representative.

The XRD analysis of both coal samples shows the presence of quartz. Tables 5 and 6 show that minerals such as calcite, dolomite, kaolinite, and siderite were identified (data in Appendix 3). The ROM coal samples contain high kaolinite (73,58%) and low calcite (8,52%). The AFE coal samples contain high kaolinite (57,91%) and low siderite (6,82%) respectively.

As a final point, the results confirm that the samples handling and splitting were conducted successfully, as the standard deviation is close to zero.

Table 5 X-ray diffraction of ROM coal samples

Sample	Calcite%	Dolomite%	Kaolinite%	Quartz%
ROM 1-1	8,52	0	73,58	24,20
ROM 1-2	8,60	0	73,49	24,13
ROM 1-3	8,45	0	73,61	24,27
Average	8,52	0	73,58	24,20
Maximum	8,80	0	73,71	24,50
Minimum	8,40	0	73,35	24,12
Standard deviation	0,08	0	0,06	0,07

Table 6 X-Ray diffraction of AFE coal samples

Sample	Calcite%	Dolomite%	Kaolinite%	Quartz%	Siderite%
AFE 1-1	11,06	13,98	57,91	19,94	6,82
AFE 1-2	11,08	13,95	58,00	19,97	6,85
AFE 1-3	11,02	14,02	57,85	20,01	6,79
Average	11,06	13,98	57,91	19,97	6,82
Maximum	11,08	13,98	57,91	20,01	6,85
Minimum	11,02	13,95	57,85	19,94	6,79
Standard deviation	0,03	0,04	0,08	0,04	0,03

4.1.2 Calorific value

The bomb calorimeter method was used (as discussed in sections 3.2.6) to determine the calorific value of coal samples. The calorific value (Table 7) was determined with 0,00096 kg of three similar coal samples (section 3.24).

Table 7 Calorific value of coal samples

Name	Mass (kg)	CV (MJ/kg)	Method
COAL ROM	0,000966	18,170	ASTM D5865-12
COAL AFE	0,000966	14,298	ASTM D5865-12

4.1.3 Proximate analysis

The proximate analysis was conducted according to ASTM D5142 to determine the volatile matter (VM), inherent moisture content, ash and by difference, the fixed carbon within the coal samples as discussed in section 3.2.5. The proximate analysis was determined with three similar coal samples of 0,001 kg each (section 3.2.4). Table 8 contains the proximate analysis result of ROM and AFE coal samples. The ROM sample had higher moisture, volatiles and fixed carbon contents; the AFE sample had a higher ash content.

Table 8 Proximate analysis of Coal samples

Name	Method	Initial mass (g)	Moisture %	Volatile %	Ash %	Fixed Carbon
COAL AFE	ASTM D5142 Moisture Volatile Ash Coal	1,0022	1,61	20,14	49,22	29,03
COAL ROM	ASTM D5142 Moisture Volatile Ash Coal	1,0064	2,39	22,82	39,39	35,39

4.1.4 Particle size distribution

The bulk coal AFE and ROM samples were air-dried according to ASTM D3302/D3302M - 12 standards. A particle size distribution (PSD) was completed on the representative coal samples using a laboratory sieve shaker, as discussed in section 3.2.9. Figure 28 shows that coal sample ROM was coarser than AFE coal sample (data in Appendix 4). The PSD of ROM and AFE coal samples show 13% and 7% passing at 13,2 mm sieve size. The results of the three repetitions on the particle size distribution are similar samples, confirming that the handling and splitting were done representatively.
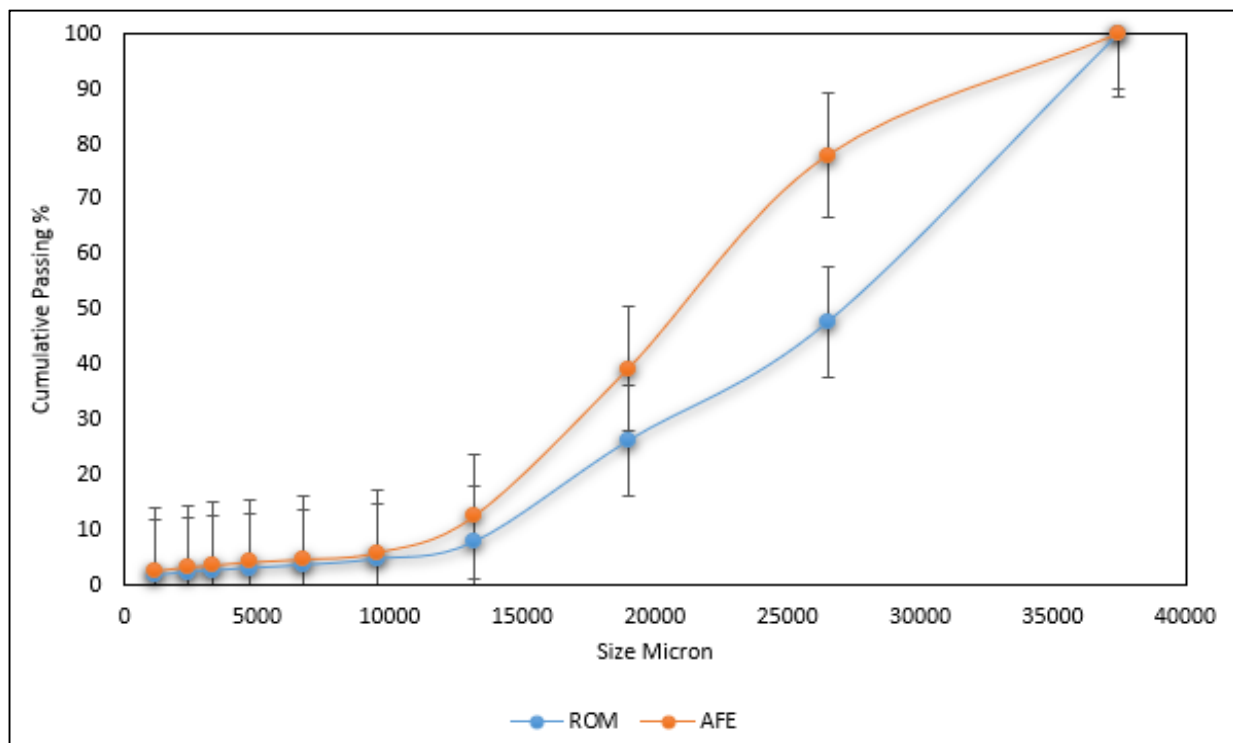
Figure 28 Particle size distribution of coal samples

4.2 Medium sample

4.2.1 Ilmenite sample chemical analysis

4.2.1.1 X-ray fluorescence analysis

The X-ray fluorescence (XRF) analysis was conducted to identify the chemical composition of the ilmenite sample, as discussed in section 3.2.8. Table 9 lists the results of the XRF analysis on ilmenite. As it can be seen from the XRF analysis on ilmenite in Table 9, titanium (Ti) and iron (Fe) elements were found to be the elements dominant at

an average of 37,50% and 48,37% respectively. The results once more indicated that samples handling and splitting were representative, as the standard error is close to zero.

Table 9 X-ray fluorescence analysis of ilmenite

Elements	Sample 1 %	Sample 2 %	Sample 3 %	Median%	Standard deviation
Si	6,66	6,59	6,7	6,66	0,06
Ti	**37,38**	**37,71**	**37,5**	**37,5**	**0,17**
Al	2,67	2,34	3,01	2,67	0,34
Fe	**48,37**	**48,54**	**48,13**	**48,37**	**0,21**
Mn	1,08	1,02	1,15	1,08	0,07
Mg	1,47	1,52	1,37	1,47	0,08
Ca	0,62	0,59	0,61	0,61	0,02
Na	0,03	0,02	0,03	0,03	0,01
K	0,11	0,15	0	0,11	0,08
P	0,05	0,05	0,04	0,05	0,01
Cr	0,47	0,4	0,42	0,42	0,04
Ni	0,02	0,02	0,02	0,02	0,00
V	0,52	0,48	0,56	0,52	0,04
Zr	0,37	0,41	0,33	0,37	0,04
S	0,01	0,01	0,01	0,01	0,00
Cl	0,02	0,02	0,02	0,02	0,00
Zn	0,04	0,03	0	0,03	0,02
La	0	0	0	0	0,00
Nb	0,11	0,1	0,1	0,1	0,01
Total	100	100	100	100	

4.2.1.2   X-ray diffraction analysis

As discussed in section 3.3.2, X-ray diffraction (XRD) analysis was completed to identify mineral phases in the ilmenite sample (ILM). Table 10 shows the results of mineral phases identified, such as actinolite, rutile, hematite, quartz and srebodolskite (data in Appendix 5). The average grade of the ilmenite was 63,70%.

Table 10 XRD analysis of ilmenite

Ilmenite sample	Actinolite %	Rutile %	Hematite %	Ilmenite %	Quartz %	Srebodolskite %
ILM 1-1	15,49	2,85	12,56	63,79	0,80	4,51
ILM 1-2	15,85	2,80	12,50	63,61	0,80	4,53
ILM 1-3	15,42	2,73	12,60	63,70	0,90	4,49
Median	15,49	2,80	12,56	63,70	0,80	4,51
Standard deviation	0,23	0,06	0,05	0,09	0,06	0,02

4.2.1.3   Scanning electron microscopy

As discussed in section 3.3.3, Figure 29 emphasised the smooth pebble-like nature and sphericity of ilmenite. This property will contribute to creating an excellent bed medium (data in Appendix 6). Ilmenite is considered due to its specific surface properties and sphericity. These properties give it an advantage as a medium in an air dense medium fluidized bed process.
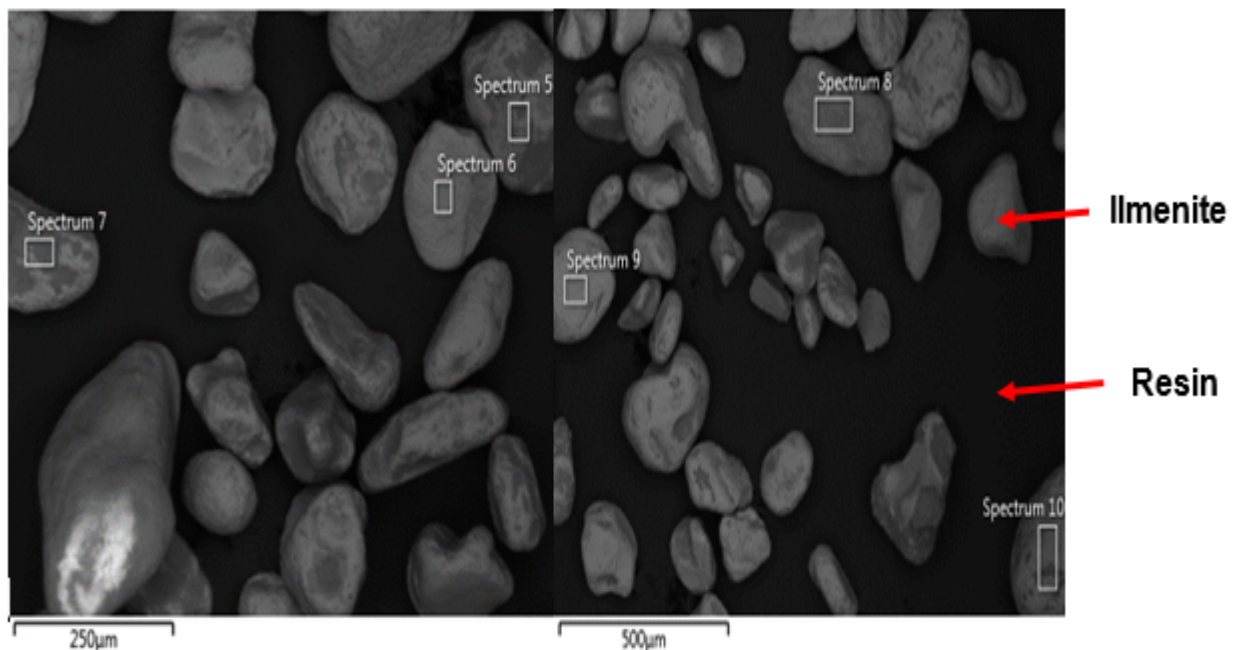
Figure 29 Scanning electron microscopy image ilmenite

4.2.2 Particle size distribution

A particle size distribution was completed on the representative ilmenite (ILM) samples using a laboratory sieve shaker, as discussed in section 3.2.9. The cut point at 50% (d_{50}) was read from Figure 30, which was 151 microns (data in Appendix 7). The Malvern test was conducted with 0,010 kg, and the cut point at 50% was found to be 154 microns (data in Appendix 8). Since the results of both sieve shaker and Malvern Mastersizer were much closer, it was preferred to use only the sieve shaker for representative samples. Also, the results of particle size distribution are similar for all the samples, indicating representative sampling of ilmenite.
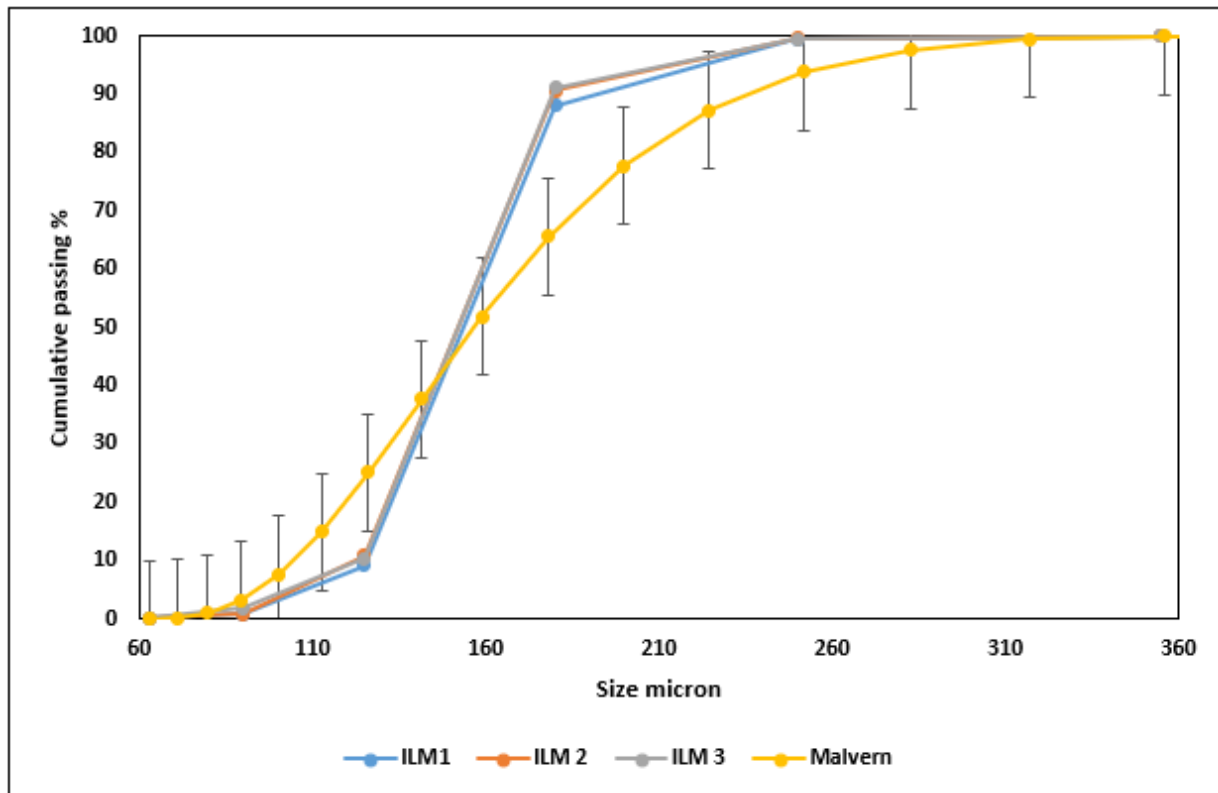
Figure 30 Particle size distribution of ilmenite

4.2.3 Fine coal sample

The minus 13,2 mm coal was sieved (discussed in section 3.2.9) to have the size range −300 microns and +53 microns. The fine coal was used to reduce the bed density. A binary medium of ilmenite with fine coal (group B) was used to achieve the bed split required in the coal beneficiation industry. A particle size distribution was completed on the representative fine coal sample using a laboratory sieve shaker. The cut point of fine coal at d_{50} was read from Figure 31, which was 155 microns (data in Appendix 9). The particle size distribution results once more indicated that samples handling and splitting were representative.
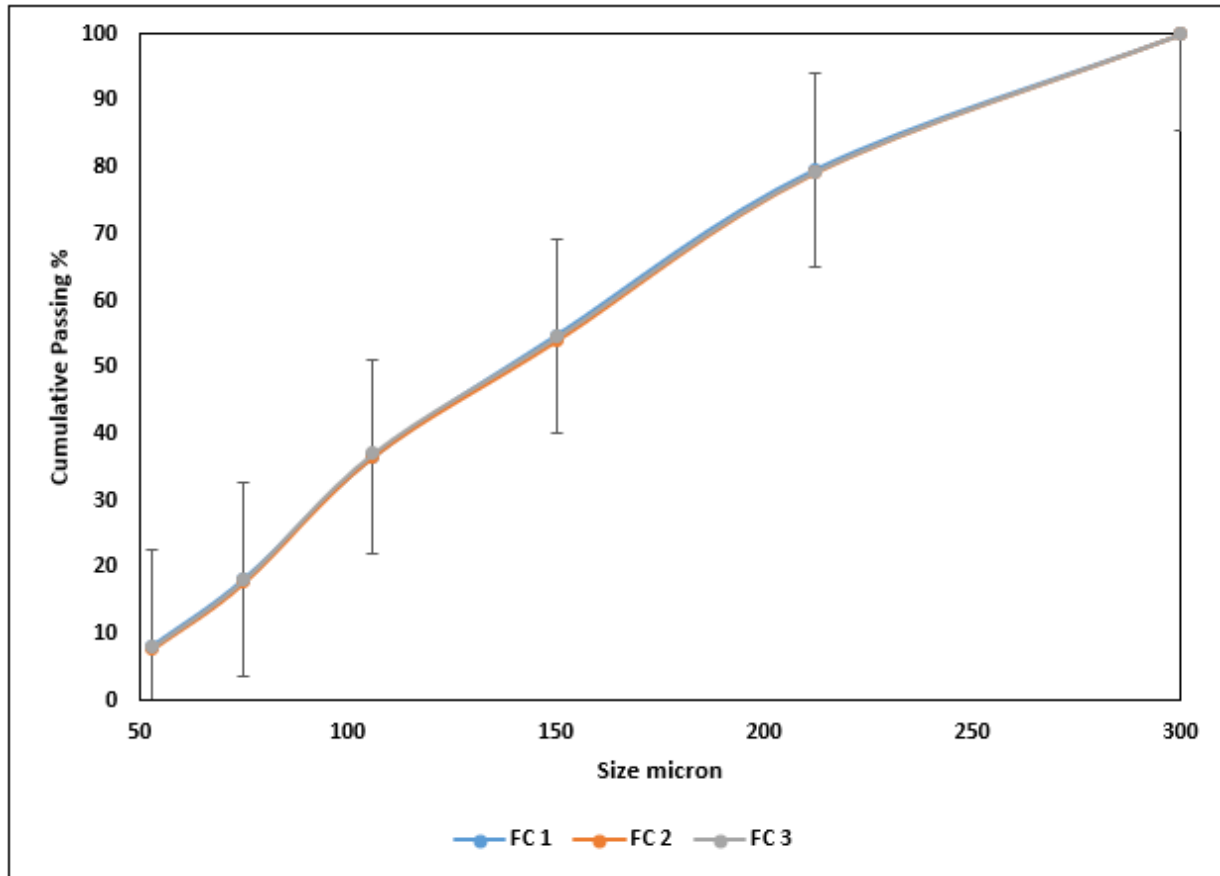
Figure 31 Particle size distribution of fine coal

4.2.4 Sand sample

Sand was used as a "proof of concept", to see if separation by density could be achieved in a fluidized bed. Sand is an oxide of silicon with the chemical formula SiO_2. It is available in abundant quantity and is a cheap material, with a wide range of PSD and sphericity. The size range was −300+53 microns and it was sourced from Rolfes Silica in Brits. A particle size distribution was completed on the representative sand sample using a laboratory sieve shaker (as discussed in section 3.2.9). The cut point of sand at 50% (d_{50}) was read from Figure 32, which was 191 microns (data in Appendix 10). The split of sand was representative.
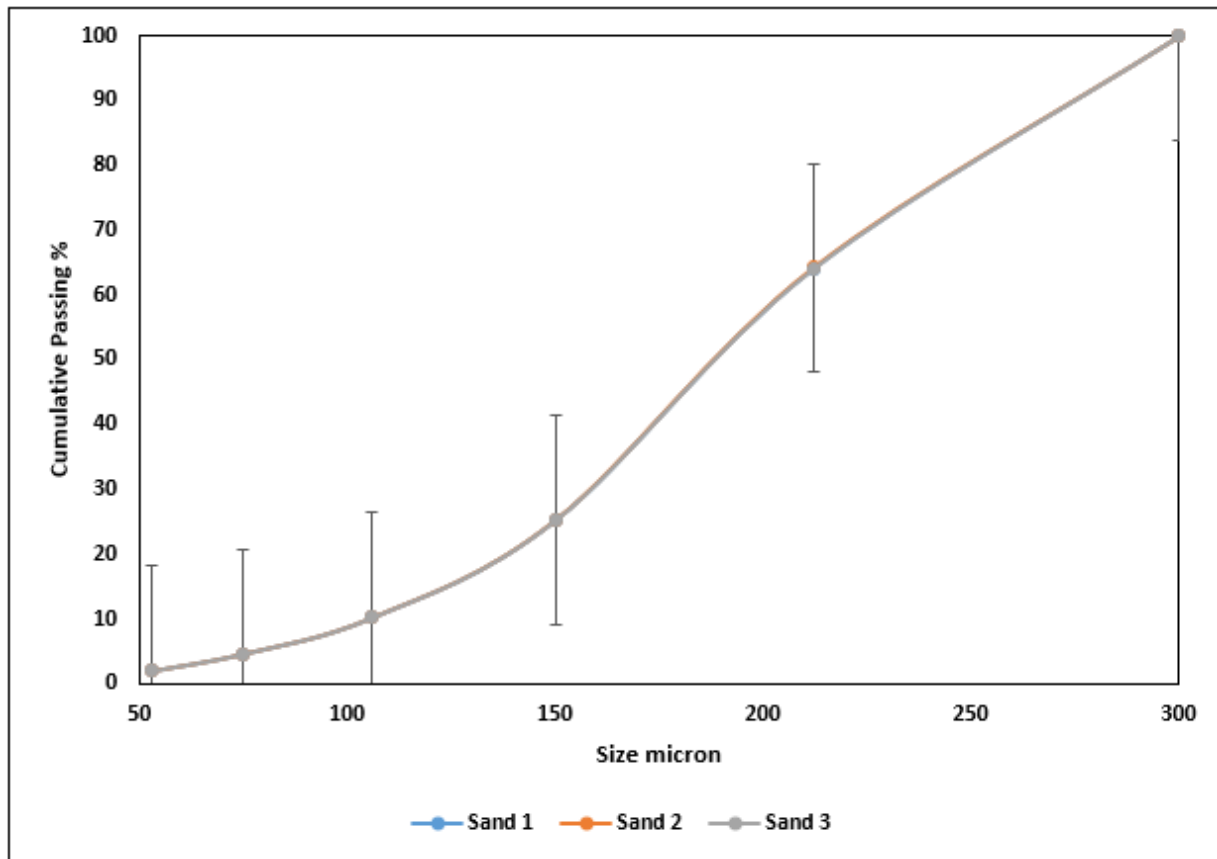
Figure 32 Particle size distribution of sand

4.3 Air dense medium fluidized bed

4.3.1 Determine the maximum bed height of the bed

The maximum bed height was calculated where the bed would be freely bubbling, and not slugging, by using Equation 16:

$$D = 15 \; cm$$

$$H_{fb} = \left(\frac{15 - 2,51 \times 15^{0,2}}{0,13 \times 15^{0,47}} \right) = 23,02 \; cm \; or \; 230,20 \; mm$$

The maximum bed height was found to be 230,20 mm underneath which the bed was freely bubbling, and the static bed height was fixed at 120 mm for all experiment.

4.3.2 Pressure drop vs superficial velocity of ilmenite

The ilmenite medium samples fall into group B of Geldart's classification powder, which means that the minimum fluidization velocity is equal to the minimum bubbling velocity

(U$_{mb}$) (Geldart, 1973). As discussed in section 3.4, a plot of bed pressure drop as a function of superficial gas velocity was experimentally determined (data in Appendix 11). The U$_{mf}$ is the superficial gas velocity at which the pressure drop is equal to the weight of the bed. Figure 33 shows that the U$_{mf}$ of the ilmenite sample was 0,030 m/s (data in Appendix 12). A similar result was found by (Luckos and Den Hoed, 2005).

The fluidized bed density of ilmenite 100% media was determined by using tracers; it was found that the observed bed split was at 3000 kg/m^3. The actual density of the ilmenite sample was calculated by using a gas pycnometer; it was found to be 4780 kg/m^3.

Equation 18 was used to determine the bed porosity (voidage) of ilmenite.

$$Bed\ porosity = 1 - \frac{3000}{4780} = 0,37$$
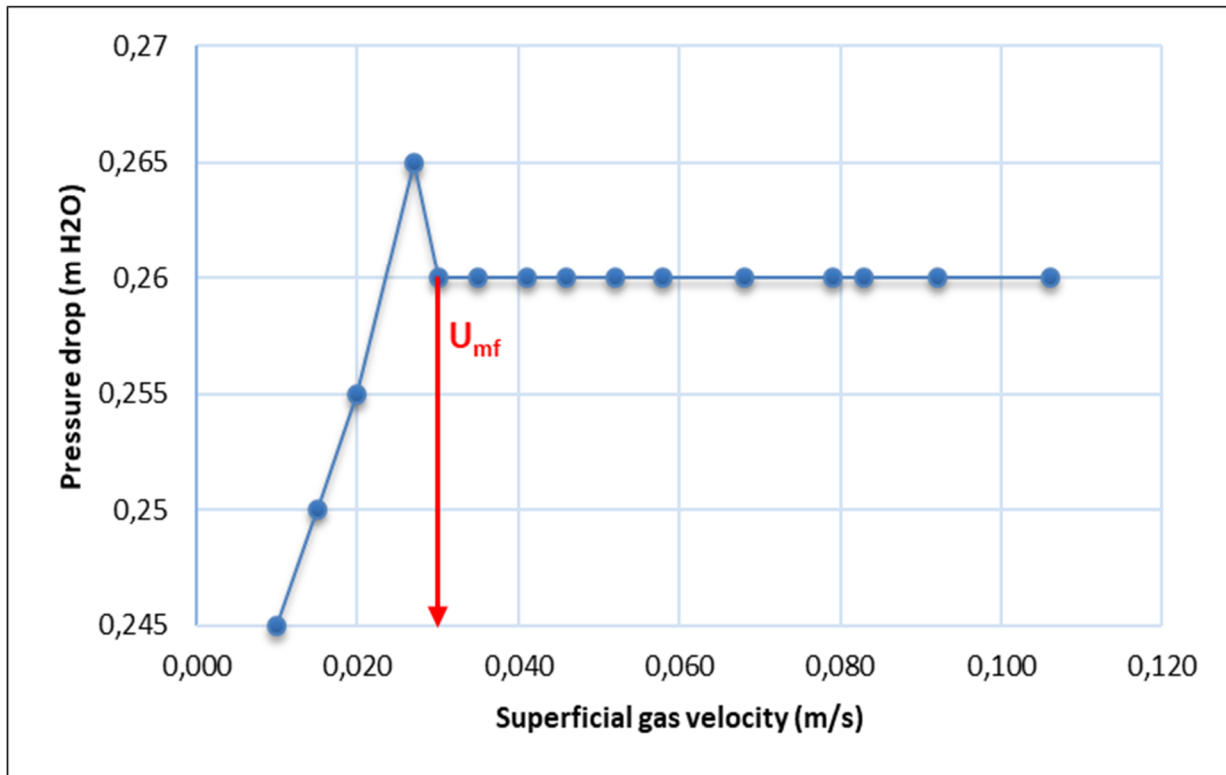
Figure 33 Pressure drop vs superficial gas velocity of ilmenite

The calculated U$_{mf}$ of ilmenite by using Equation 15 was found to be 0,031 m/s with bed voidage: 0,37 (0,44 recommended value by Haughey and Beveridge (1969)); particle diameter d50 (mm): 0,151; particle density (kg/m^3): 4780; gas pressure (kPa): 88; gas

temperature (°C): 25; molecular weight: 28,84; gas density (kg/m^3): 1,0244, and gas viscosity (Ns/m^2): 0,000018.

It was found that the lower bed voidage significantly affects the minimum fluidization velocity and would increase the drag component.

4.3.3 Ilmenite with sand medium

4.3.3.1 Sand medium

A plot of bed pressure drop as a function of superficial gas velocity was experimentally determined, as discussed in section 3.4. The minimum fluidization velocity is the superficial gas velocity at which the bed pressure drop becomes nearly constant, which is the same as the weight of the bed. Figure 34 shows the surface of the bubbling bed.

Figure 34 Surface of the bubbling bed

Figure 35 shows the U_{mf} of the sand sample was 0,052 m/s (data in Appendix 13). However, it was expected that, because sand has measured specific gravity (SG) of 2600 kg/m^3 and voidage of 0,48, the sand alone could not be used for coal beneficiation. The fluidized bed density of sand 100% medium was determined by using tracers, it was

found that the observed bed split was at 1350 kg/m^3. The density of the fluidized bed would be below the cut density.

Equation 18 was used to determine the bed porosity of sand.

$$Bed\ porosity = 1 - \frac{1350}{2600} = 0,48$$

The calculated U_{mf} of sand by using Ergun Equation 15 was found to be 0,056 m/s with bed voidage: 0,48 (0,44 recommended value by Haughey and Beveridge (1969)); particle diameter d50 (mm): 0,191; particle density (kg/m^3): 2600; gas pressure (kPa): 88; gas temperature (°C): 25; molecular weight: 28,84; gas density (kg/m^3): 1,0244; gas viscosity (Ns/m^2): 0,000018.
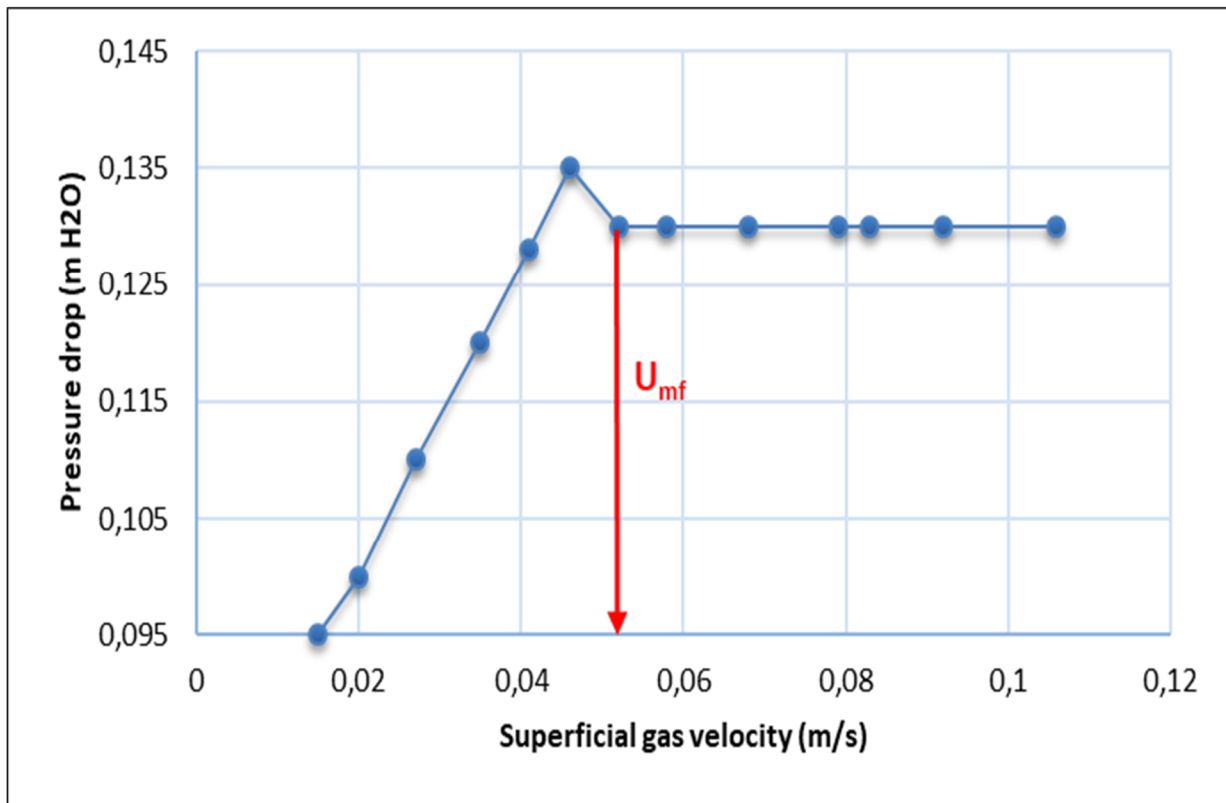
Figure 35 Pressure drop vs superficial gas velocity of sand

4.3.3.2 Pressure drop vs superficial gas velocity of different bed mixture ilmenite and sand medium

The experiment was first conducted using ilmenite alone as the medium; it was found that the bed split was at 3000 kg/m^3 (Figure 36). The observed split of ilmenite was too high for beneficiation of coal in the density ranging between 1300 kg/m^3 to 2300 kg/m^3.
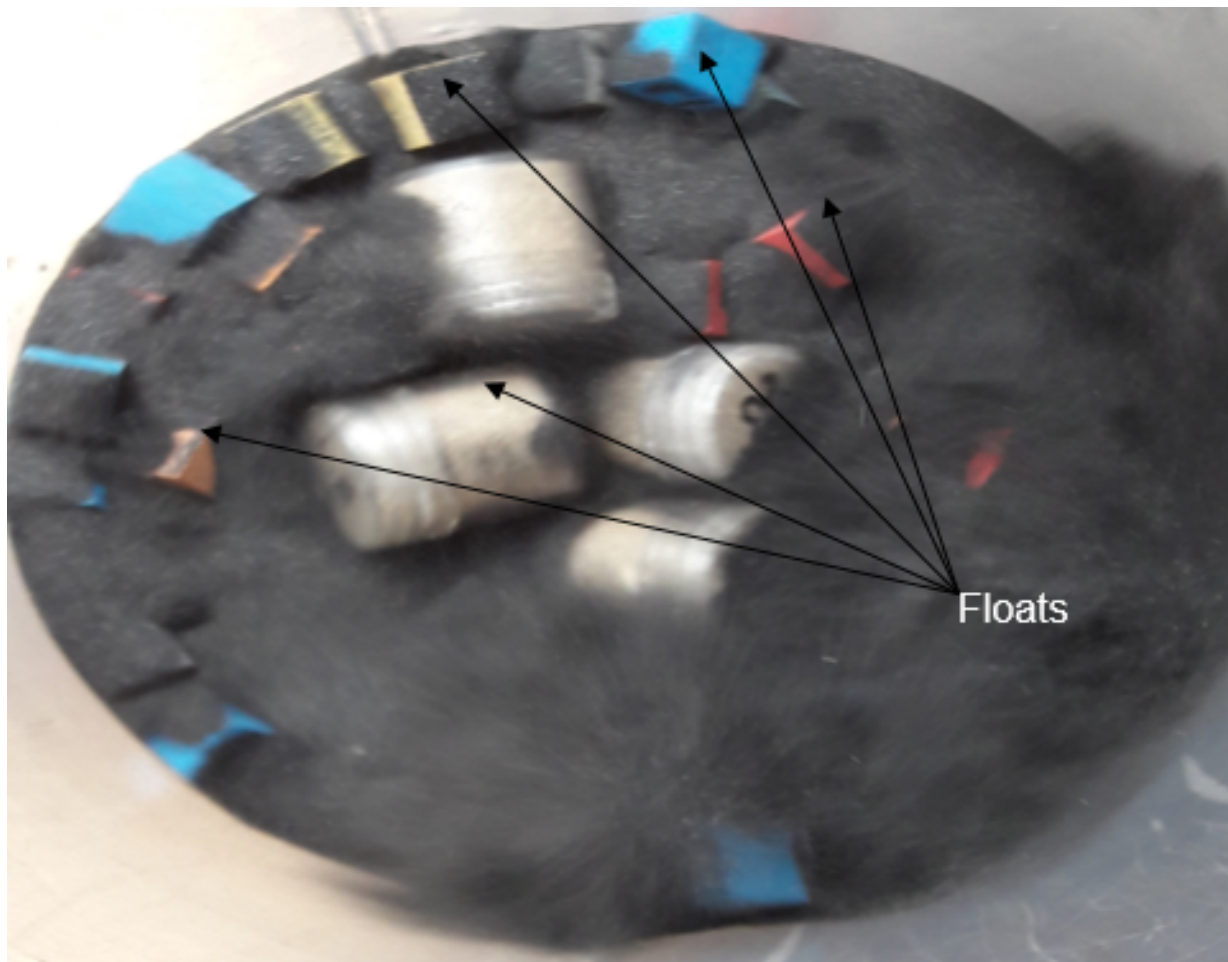
Figure 36 Surface of bubbling bed 100% ilmenite medium

As a result, the sand (–300 +53 µm) was used to reduce the bed density of the ilmenite. A binary medium of group B (ilmenite with sand) was used to achieve the bed split required in the coal beneficiation industry. The sand and ilmenite were mixed in different ratios and then used as a medium in the fluidized bed. The experiments were conducted at the bed height of 120 mm over the bed diameter of 150 mm to prevent the slugging regime, which takes place only in beds with a bed height (H) over bed diameter ratio (D) larger than 2. The results are shown in Table 11.

The average density of the bed was calculated using Equation 6. Figure 37 shows an illustration of 30% ilmenite with 70% sand medium, which was randomly picked sets of data coming from a larger pool (data in Appendix 14).
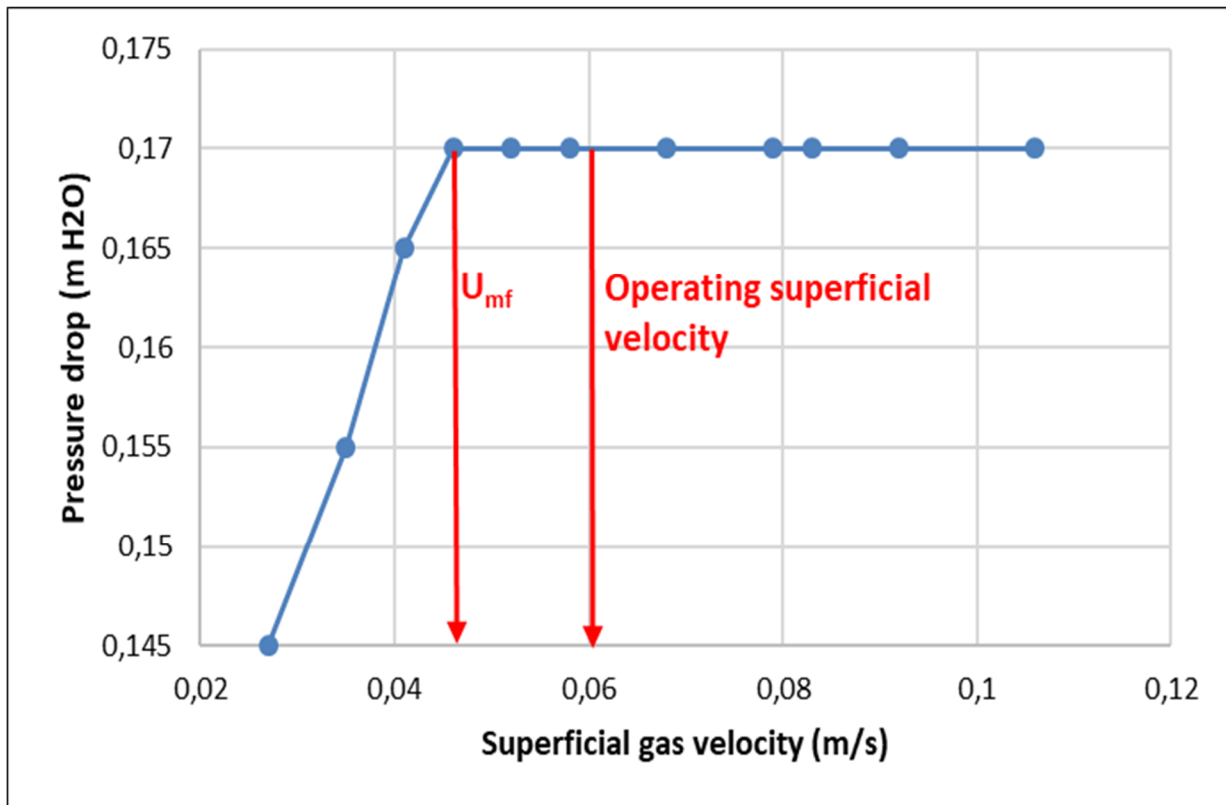
Figure 37 Pressure drop vs superficial gas velocity of mixture 30% ilmenite and 70% sand medium

The observed split given in Table 11 was obtained by using tracers and confirmed by the partition curve at cut point 50%.

Table 11 Split results at different mixture sand and ilmenite

Sand %	Observed U_{mf} (m/s)	Observed Pressure drop (m H2O)	Average SG (kg/m^3)	Observed split (kg/m^3)
0	0,030	0,260	2 940	3 000
10	0,032	0,240	2 780	2 750
20	0,034	0,235	2 620	2 600
30	0,034	0,235	2 470	2 450
40	0,035	0,215	2 310	2 300
50	0,036	0,210	2 150	2 100
60	0,042	0,185	1 990	2 000
70	0,046	0,170	1 830	1 800
80	0,048	0,160	1 670	1 650
100	0,052	0,130	1 360	1 350

The observed split was designed against the sand percentage added to the mixture. The resultant graph is displayed in Figure 38. The results offer an excellent trend between the observed split and the sand percentage, which can be seen in Figure 38. The trendline fitted linearly, which results in an R^2 value of 1.
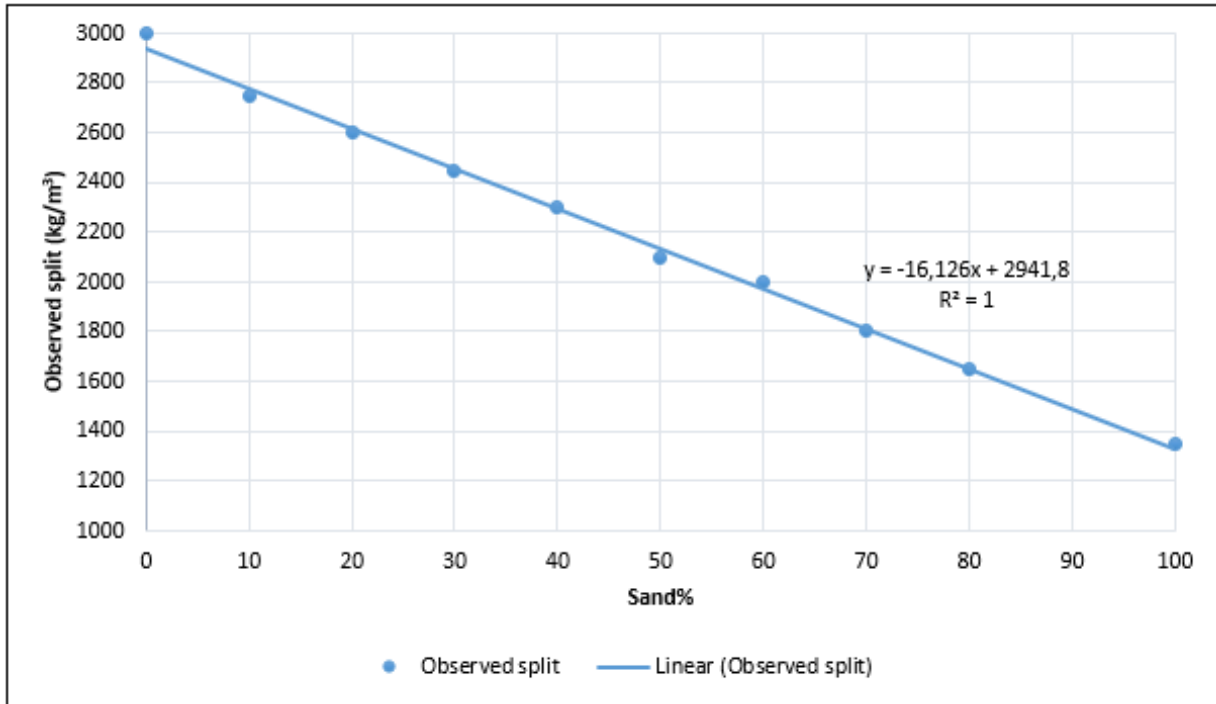
Figure 38 Density split at different mixture sand and ilmenite medium

4.3.3.3 Position of tracers in an air dense medium fluidized bed

According to Hovmand and Davidson (1971), the operating superficial gas velocity was found by using Equation 17 for the transition from bubbling to slug flow, as it gives a good correlation with most experiments. When $U - U_{mf}$ is larger than the value found from Equation 17, the bed will be in the slugging zone. The operating superficial gas velocity used was 0,060 m/s, which was in the bubbling zone. The results of bubbling zone are shown in Table 12.

Table 12 Transition region between bubbling and slugging

Sand %	Observed U_{mf} (m/s)	Transition region between bubbling and slugging ≤ 0,2
0	0,030	0,07
10	0,032	0,07
20	0,034	0,06
30	0,034	0,06
40	0,035	0,06
50	0,036	0,06
60	0,042	0,04
70	0,046	0,03
80	0,048	0,03
100	0,052	0,02

As discussed in section 3.6, some results of tracer's particles position in ADMFB are shown in figures 37 and 38 (data in Appendix 15). Figures 39 and 40 display the separation into the beds which were plotted in the three-dimensional graph, where the Y-axis is the number of tracers, the X-axis is the layers into the bed, and the Z-axis is the tracer's density.

Figure 39 shows that all the tracers were reported to the float layers 4 and 5.
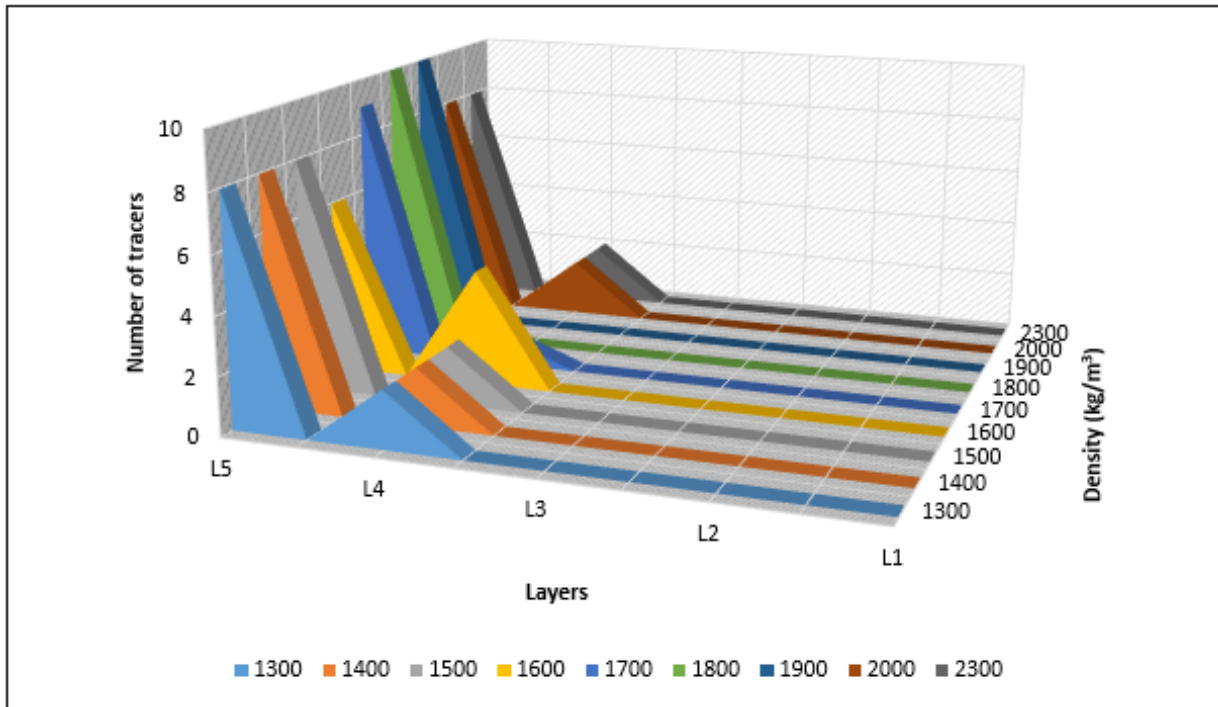
Figure 39 Position of tracers using 100% ilmenite medium in an air dense medium fluidized bed

Figure 40 shows that the tracers were reported to the float (L5, L4 &L3) and the sink (L2 & L1).
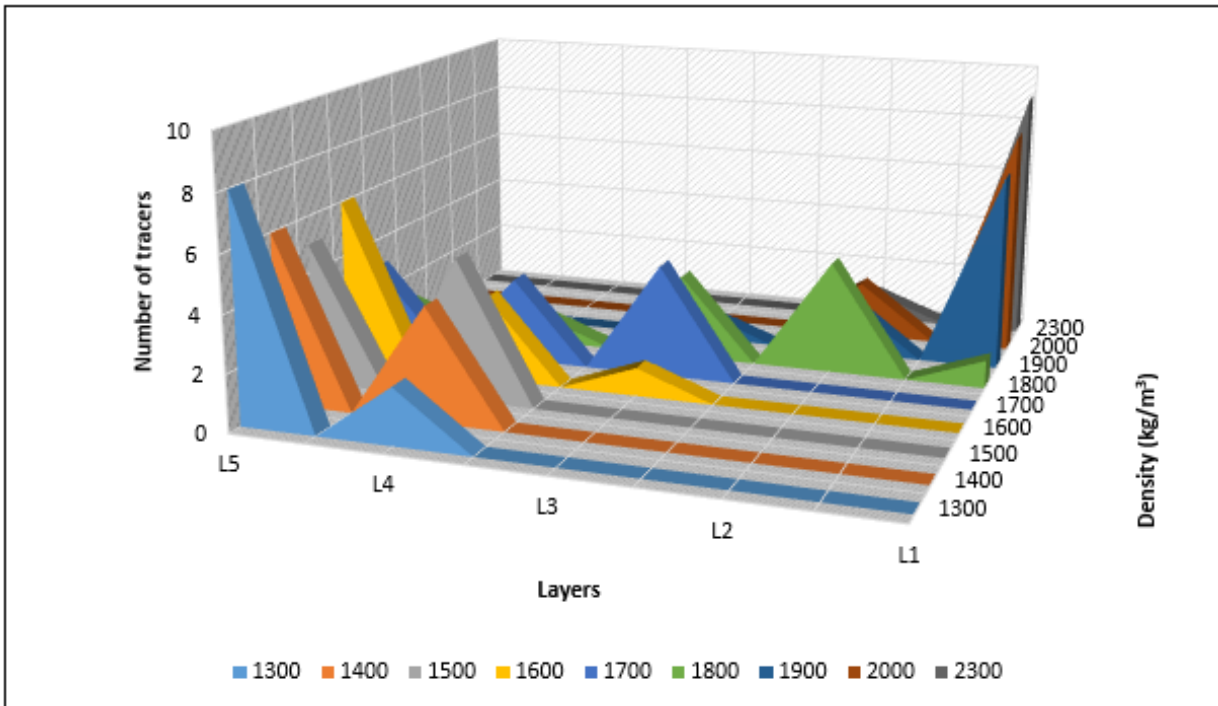
Figure 40 Position of tracers using 30% ilmenite and 70% sand medium in an air dense medium fluidized bed

4.3.3.4 Performance of air dense medium fluidized bed: Partition curve

The tracers were used to determine the EPM of the fluidized bed. It was found that the ADMFB was efficient when the EPM ranges from 0,04 to 0,12. The tracer particles were stratified into floats and sinks within the bed, in the same way in which coal would be separated. De Korte (2002) obtained similar results. The tracer particles recovered from the float and sink were sieved and counted, and the number of tracers recovered was then used to construct a partition curve. The EPM in Table 14 was calculated using Equation 21 and specific gravity of 50% (SG50). The cut point can be read from the partition curve, as illustrated in Table 13 or Figure 41, which is derived from picked sets of data coming from a larger pool (data in Appendix 16). The optimum condition was found to be a mixture of 30% ilmenite with 70% sand medium at the cut density (SG50) of 1800 kg/m^3.

Napier-Munn (1991) gives a good overview of the statistical calculations of Equation 22, knowing the cut point at 50% (required cut density), particle density and the EPM which correct the actual partition curve. As a result, the R^2 shows a much closer fit in Table 14.

Table 13 Partition curve of mixture 30% ilmenite with 70% sand medium

Relative density (kg/m^3)	Tracers	Float tracers	Sink tracers	Partition curve %	Model Partition curve %
1300	10	10	0	100	100
1400	10	10	0	100	100
1500	10	10	0	100	100
1600	10	10	0	100	99
1700	10	10	0	100	92
1800	10	5	5	50	50
1900	10	1	9	10	10
2000	10	0	10	0	0
2300	10	0	10	0	0
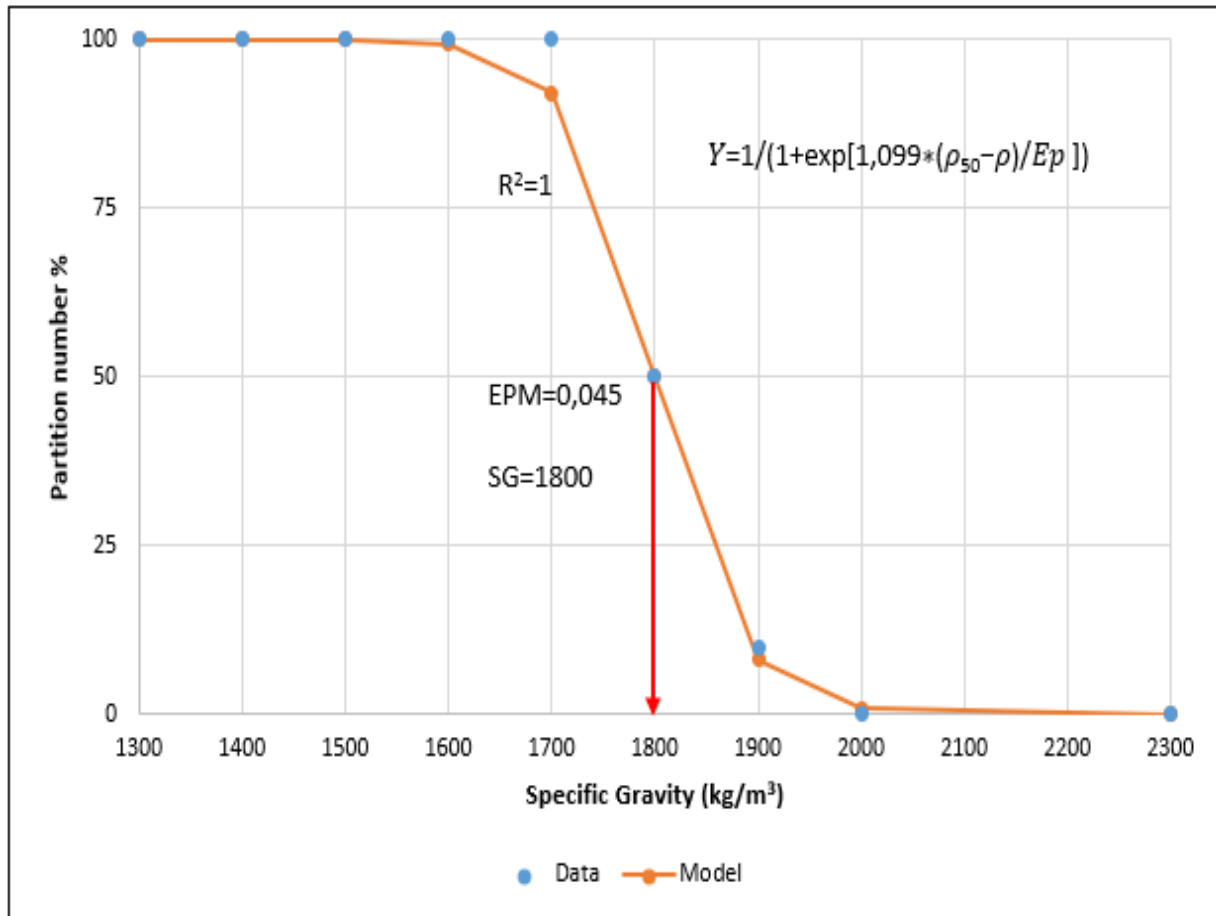
Figure 41 Partition curve of mixture 30% ilmenite and 70% sand medium

The EPM column in Table 14 of ilmenite with sand shows that all tracers floated from 0% to 40% sand. Consequently, the EPM could be calculated. The density distribution in a fluidized bed for sand size range from −300 microns to +53 microns mixed with ilmenite size range from −355 microns to +63 microns and observed that density stratification does not appear beneath the sand concentration of 40%. Stratification of the sand quickly increases when its concentration is above 50%, and the separation efficiency falls into the range of excellent separation in the air dense medium fluidized bed process. As a result, the correlation coefficient (R^2) showed a much better fit in Table 14.

Table 14 Ecart Probable Moyen at different mixture sand and ilmenite medium

Sand %	Ecart Probable Moyen	R^2
0	–	–
10	–	–
20	–	–
30	–	–
40	–	–
50	0,120	0,99
60	0,110	0,98
70	0,045	1,00
80	0,050	1,00
100	0,050	0,99

4.3.3.5 Segregation of bed

A binary medium of group B 30% ilmenite with 70% sand at a cut density of 1800 kg/m^3 was used as an optimum. As discussed in section 3.4, the bed was found to be uniform and stable with no segregation taking place, as illustrated in Figures 42 (data in Appendix 17).
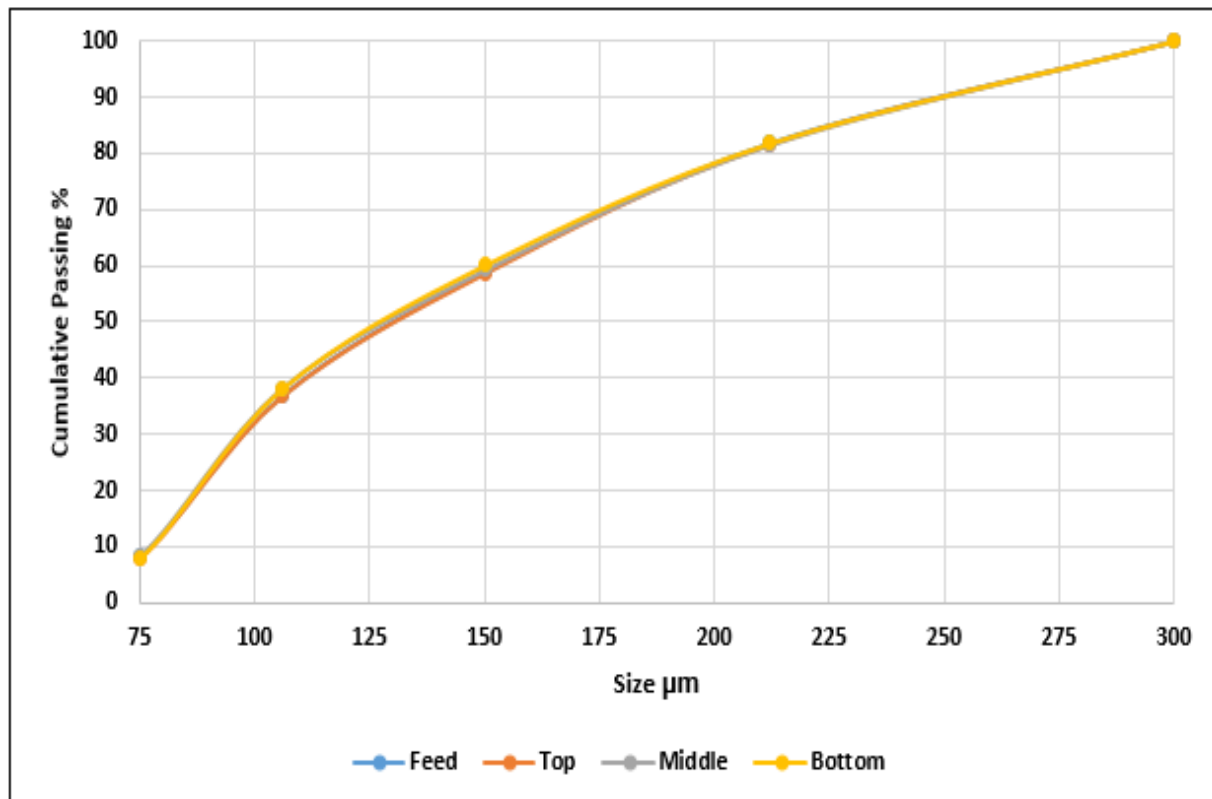
Figure 42 Segregation of bed by size of mixture 30% ilmenite and 70% sand medium

Figure 43 shows the stereomicroscopy distribution of mixture 30% ilmenite and 70% sand medium.
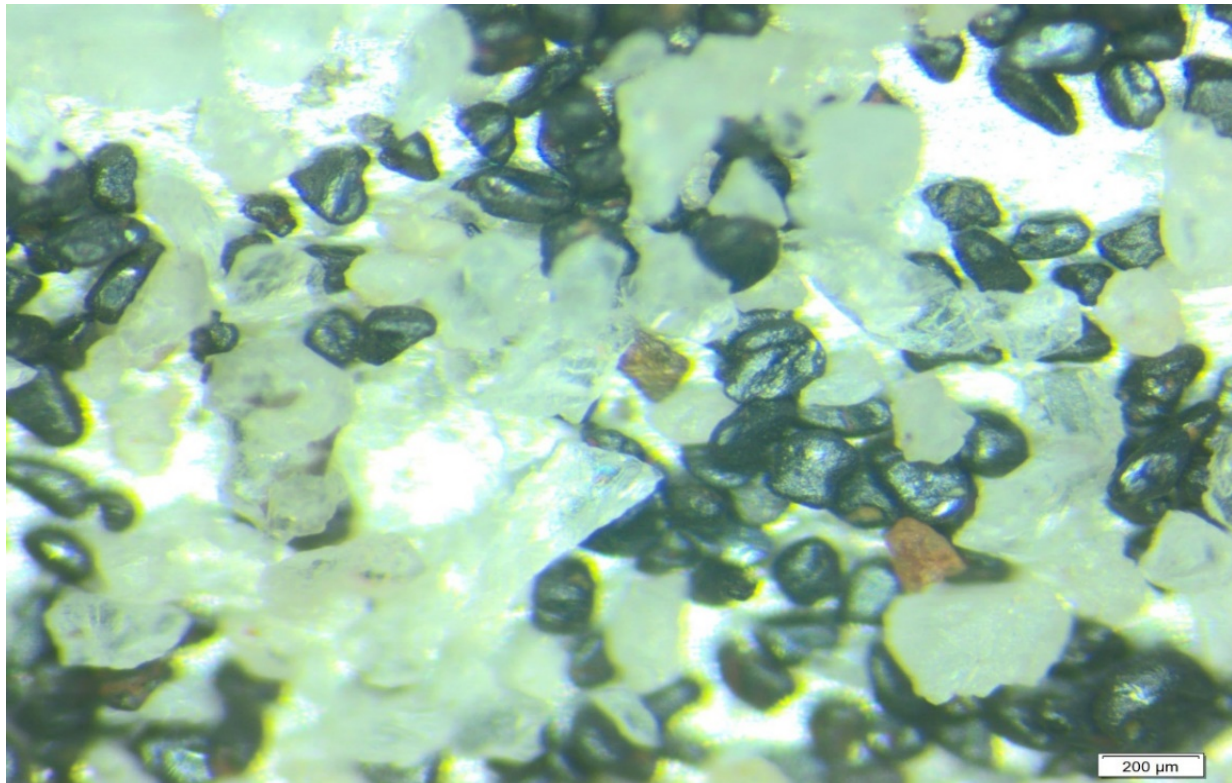
Figure 43 Stereomicroscopy distribution of mixture 30% ilmenite and 70% sand medium

4.3.4 Mixture of ilmenite with fine coal medium

4.3.4.1 Pressure drop vs minimum fluidization velocity of different bed mixture ilmenite and fine coal

Fine coal (−300+53 microns) is used in the process to decrease the bed density of ilmenite. This is what is used in China by Shenhua Xinjiang Energy Co. Ltd to decrease the bed density (Zhao et *al.*, 2017). A binary medium of group B ilmenite with fine coal was used to achieve the bed split required at 1500 kg/m^3 in the coal beneficiation industry. The fine coal and ilmenite were mixed in the different ratios and then used as a medium in the fluidized bed. The experiments were conducted at the bed height of 120 mm over the bed diameter of 150 mm to prevent the slugging regime, which takes place only in beds with a bed height (H) over bed diameter ratio (D) larger than about 2. The results are shown in Table 15.

The average density of the bed was calculated using Equation 6. The bed pressure drop as a function of superficial gas velocity was experimentally determined in the fluidized bed. Figure 44 shows the U_{mf} of the fine coal sample was 0,015 m/s (data in Appendix 18).
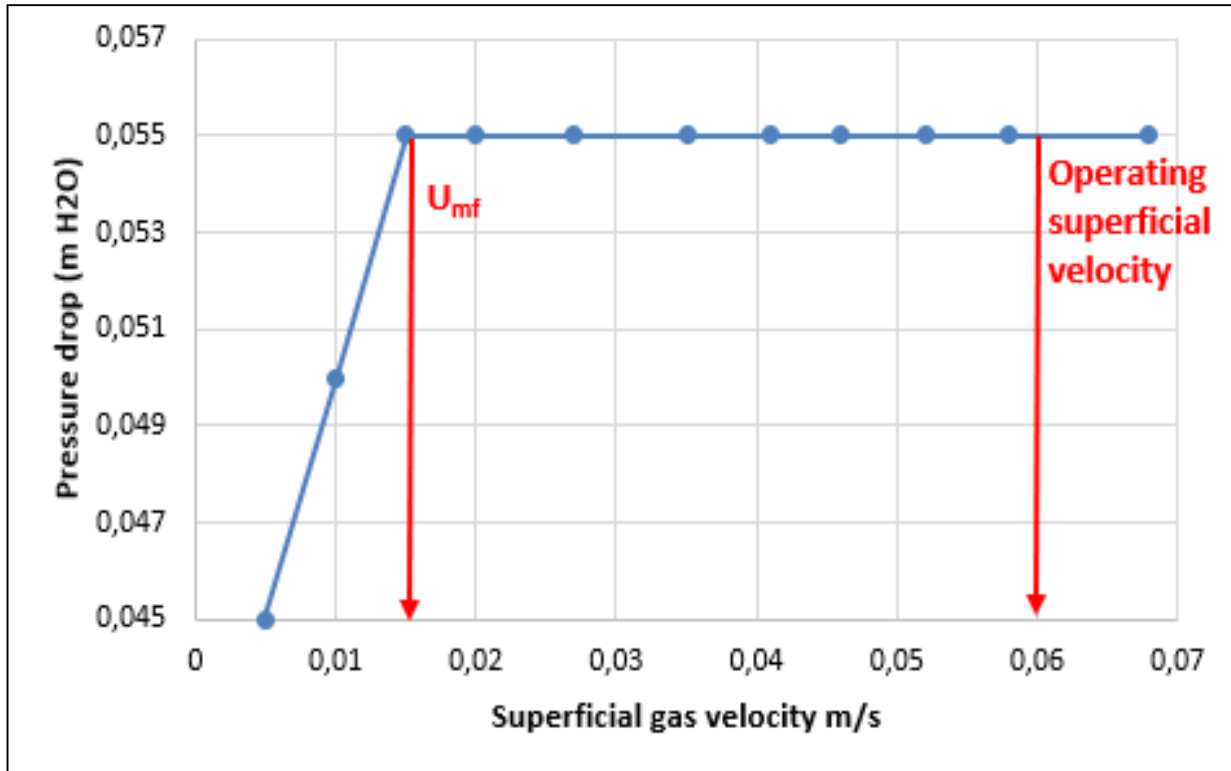
Figure 44 Pressure drop vs superficial gas velocity of 100% fine coal

It was expected that, due to the fine coal specific gravity (SG) of 1700 kg/m^3 and voidage of 0,59, fine coal alone could not be used for coal beneficiation. The density of the fluidized bed would be underneath the required cut density. The fluidized bed density of fine coal 100% medium was determined by using tracers, the observed bed split was at 700 kg/m^3. The density of the fluidized bed would be below the cut density.

The trial and calculated values were found to be at 0,015 and 0,024 m/s respectively.

$$Bed\ porosity = 1 - \frac{700}{1700} = 0,59$$

Where, bed voidage: 0,59 (0,44 recommended value); particle diameter d_{50} (mm): 0,155; particle density (kg/m^3): 1700; gas pressure (kPa): 88; gas temperature (°C): 25; molecular weight: 28,84; gas density (kg/m^3): 1,0244; gas viscosity (Ns/m^2): 0,000018.

Figure 45 displayed the U_{mf} of the mixture 40% ilmenite with 60% fine coal medium was 0,020 m/s (data in Appendix 19).
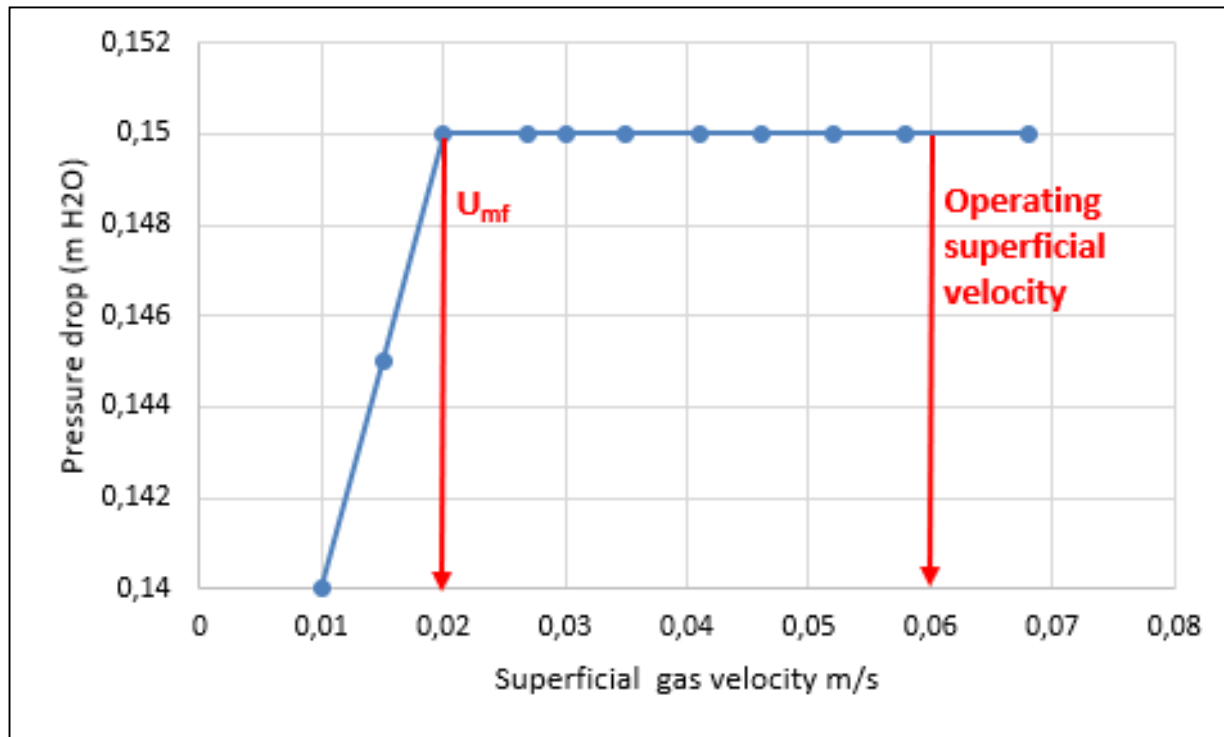
Figure 45 Pressure drop vs superficial gas velocity of mixture 40% ilmenite and 60% fine coal medium

The observed split given in Table 15 was obtained by using tracers and confirmed by the partition curve which SG50 was the bed split.

Table 15 Split results into different mixture fine coal and ilmenite medium

Fine coal (%)	Observed U_{mf} (m/s)	Observed Pressure drop (m H2O)	Average SG (kg/m^3)	Observed split (kg/m^3)
0	0,030	0,260	2 940	3 000
10	0,028	0,245	2 780	2 700
20	0,025	0,240	2 620	2 500
30	0,020	0,220	2 270	2 300
40	0,020	0,195	2 050	2 000
50	0,021	0,175	1 830	1 800
60	0,020	0,155	1 600	1 580
70	0,020	0,115	1 380	1 400
80	0,017	0,090	1 160	1 200
100	0,015	0,055	710	700

The observed split was plotted against the fine coal percentage added to the mixture. The resultant graph is displayed in Figure 46. The results offer an excellent trend between the split density and the fine coal percentage, which can be seen in Figure 46. The trendline fitted linearly, which results in an R^2 value of 1.
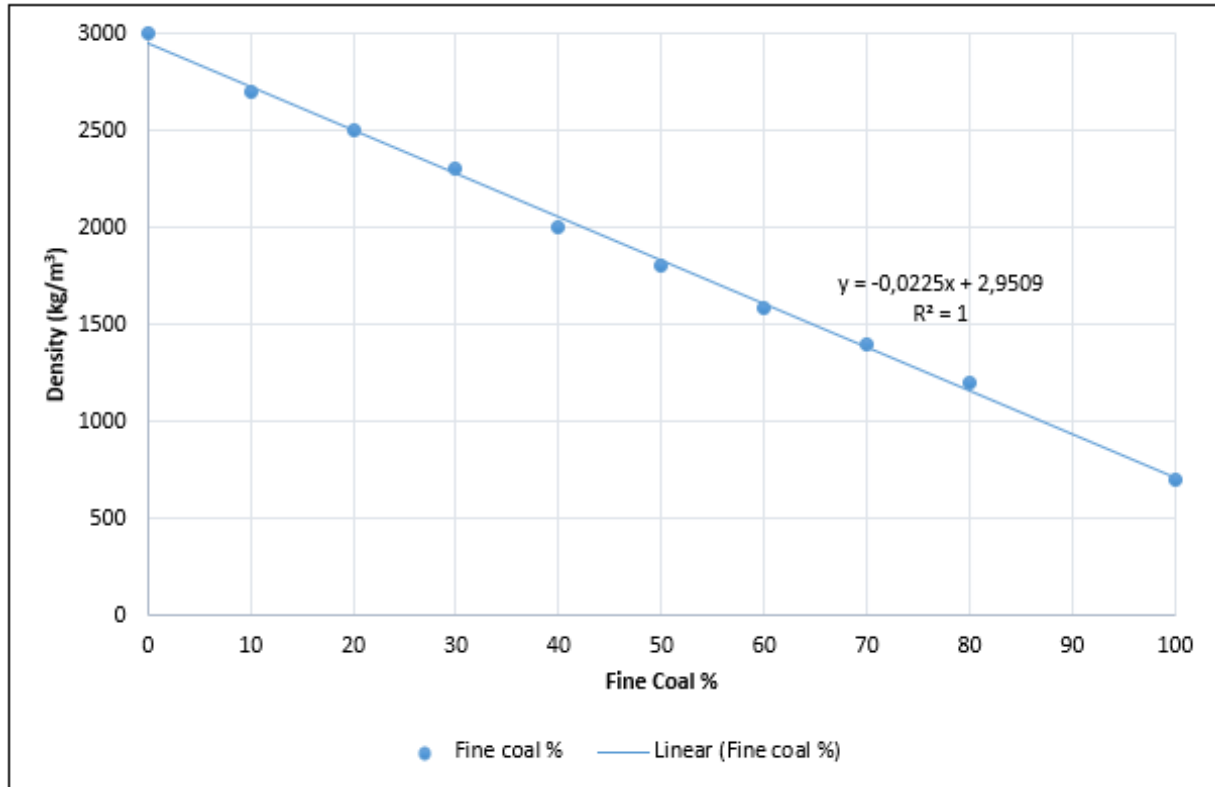
Figure 46 Density split into different mixture fine coal and ilmenite medium

4.3.4.2   Position of tracers in an air dense medium fluidized bed

As discussed in section 4.3.3.3, the bed was operating in the bubbling region with the transition region between bubbling and slugging which was lesser than 0,2. The results of transition region between bubbling and slugging are shown in Table 16.

Table 16 Transition region between bubbling and slugging

Fine coal %	Observed U_{mf} (m/s)	Transition region between bubbling and slugging ≤0,2
0	0,030	0,07
10	0,028	0,08
20	0,025	0,08
30	0,020	0,09
40	0,020	0,09
50	0,021	0,09
60	0,020	0,09
70	0,020	0,09
80	0,017	0,10
100	0,015	0,11

As discussed in section 3.6, one of the results is shown in Figure 47 (data in Appendix 20).
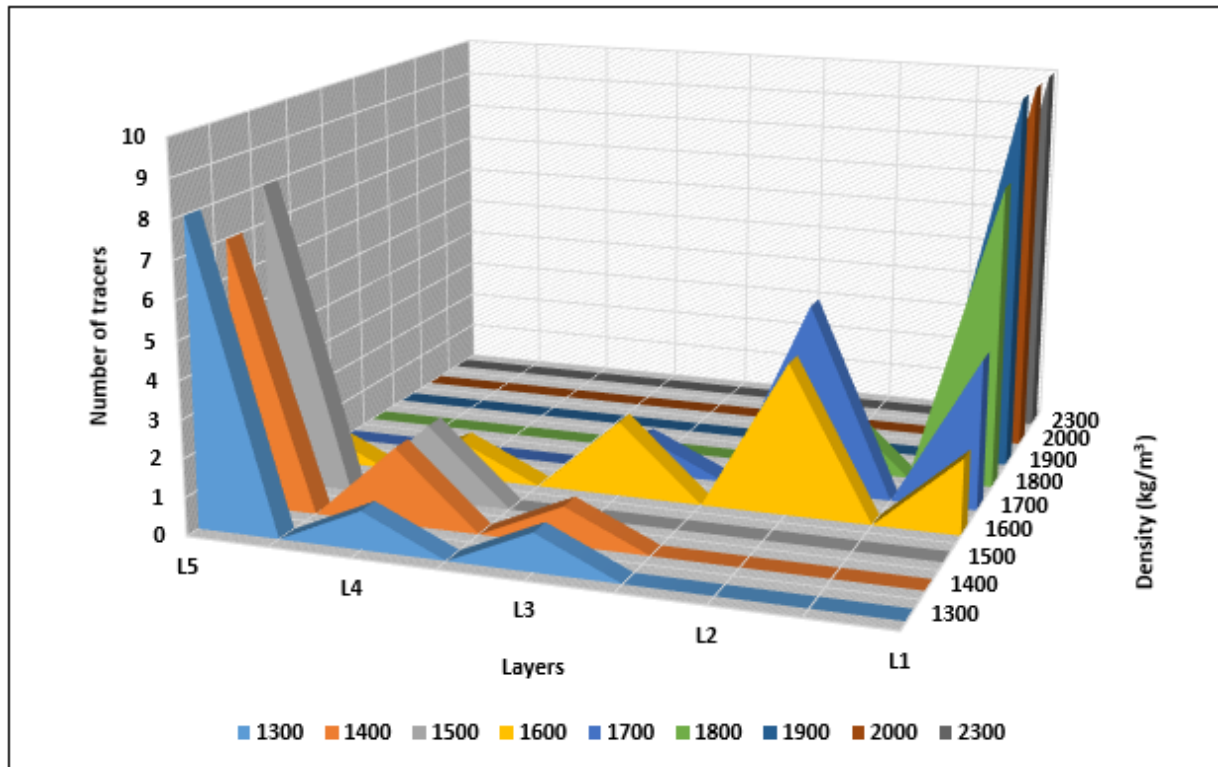
Figure 47 Position of tracers using mixture 60% fine coal and 40% ilmenite medium in an air dense medium fluidized bed

4.3.4.3 Performance of air dense medium fluidized bed: Partition curve

The cut point can be read (as discussed in section 4.3.3.4) from the partition curve. Table 17 shows the data, and Figure 48 shows the partition curve which is derived from the optimum condition mixture 60% fine coal and 40% ilmenite medium at a cut point of 1580 kg/m^3 (data in Appendix 21).

Table 17 Partition curve of mixture 60% fine coal and 40% ilmenite medium

Relative density (kg/m^3)	Tracers	Float tracers	Sink tracers	Partition Curve %	Model Partition curve float %
1300	10	10	0	100	100
1400	10	10	0	100	98
1500	10	10	0	100	85
1600	10	4	6	40	39
1700	10	1	9	10	7
1800	10	0	10	0	1
1900	10	0	10	0	0
2000	10	0	10	0	0
2300	10	0	10	0	0

$$Y=1/(1+\exp[1{,}099*(\rho_{50}-\rho)/Ep\;])$$

R²=0,99

EPM=0,05

SG=1580
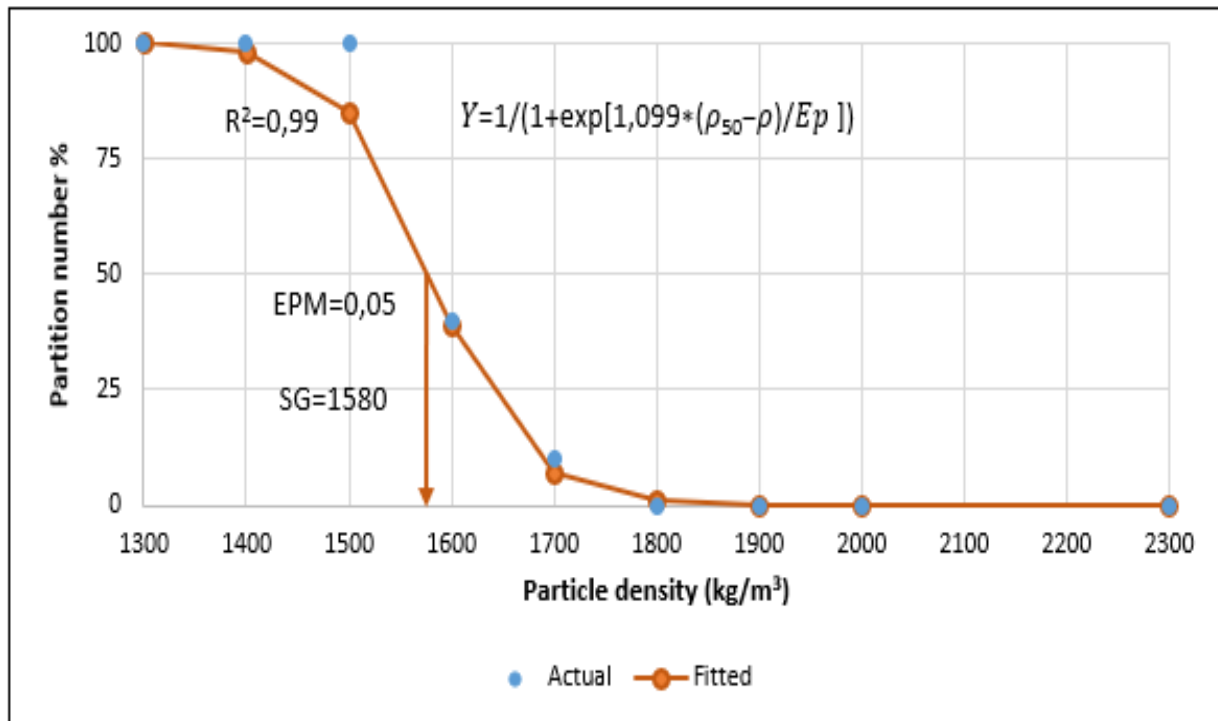
Figure 48 Partition curve of mixture 60% fine coal and 40% ilmenite in an air dense medium fluidized bed

The Ecart Probable Moyen column in Table 18 of ilmenite with fine coal shows that all tracers floated from 0% to 30% fine coal, and at 80% to 100% fine coal all tracers were found in the bottom region. The EPM could be calculated. The density distribution in the fluidized bed for fine coal (−300+53 μm) mixed with ilmenite (−355+63 μm) and perceived that density stratification does not appear beneath the fine coal concentration of 30%. Stratification of the fine coal quickly increases when its concentration is above 40%, and the separation efficiency falls into the range of excellent separation in the air dense medium fluidized bed process. As a result, the correlation coefficient (R^2) showed a much better fit in Table 18.

Table 18 Ecart Probable Moyen at different mixture fine coal and ilmenite medium

Fine coal %	Ecart Probable Moyen	R^2
0	–	–
10	–	–
20	–	–
30	–	–
40	0,11	0,99
50	0,06	0,99
60	0,05	0,99
70	0,07	0,99
80	–	–
100	–	–

4.3.4.4   Segregation of bed

A binary medium of group B 40% ilmenite with 60% fine coal at cut point of 1580 kg/m^3 was used to achieve the bed split required in the coal beneficiation industry. The bed was found to be uniform and stable with no segregation taking place, as illustrated in Figure 49 (data in Appendix 22).
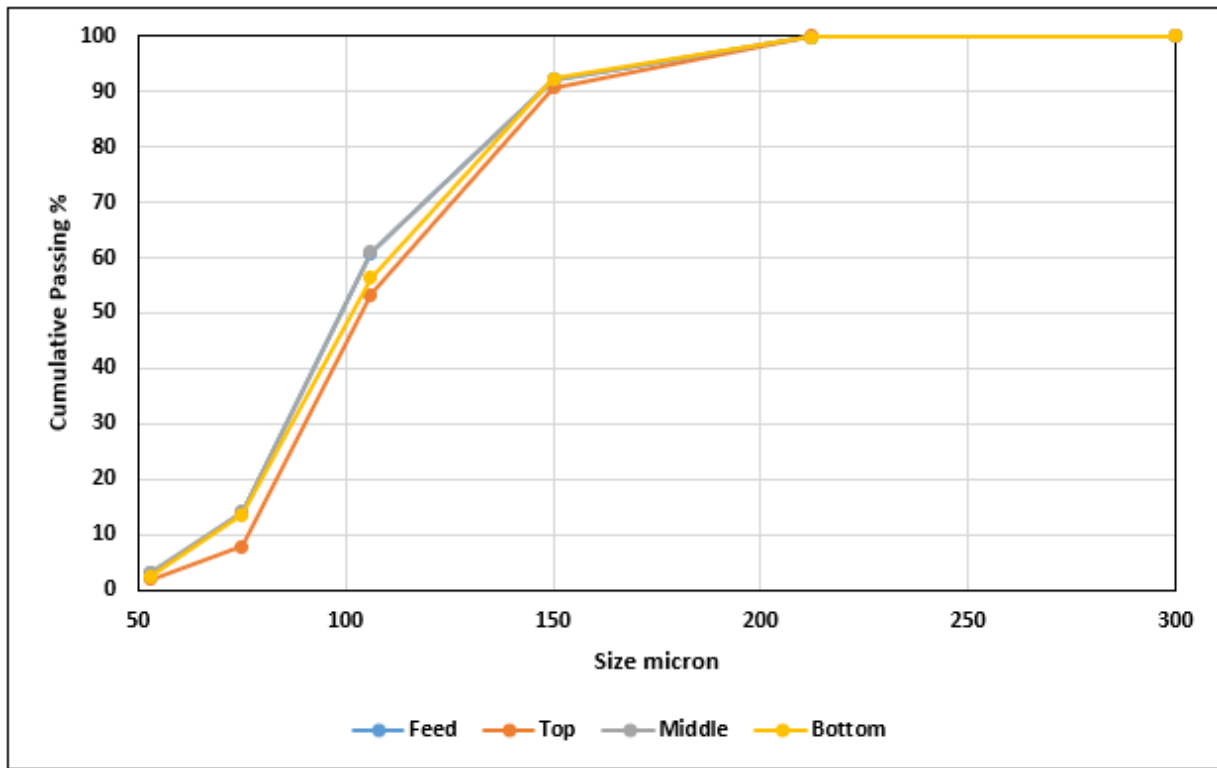
Figure 49 Segregation of bed by size of mixture 40% ilmenite with 60% fine coal medium

Figure 50 shows the stereomicroscopy distribution of bed mixture 40% ilmenite and 60% fine coal medium.
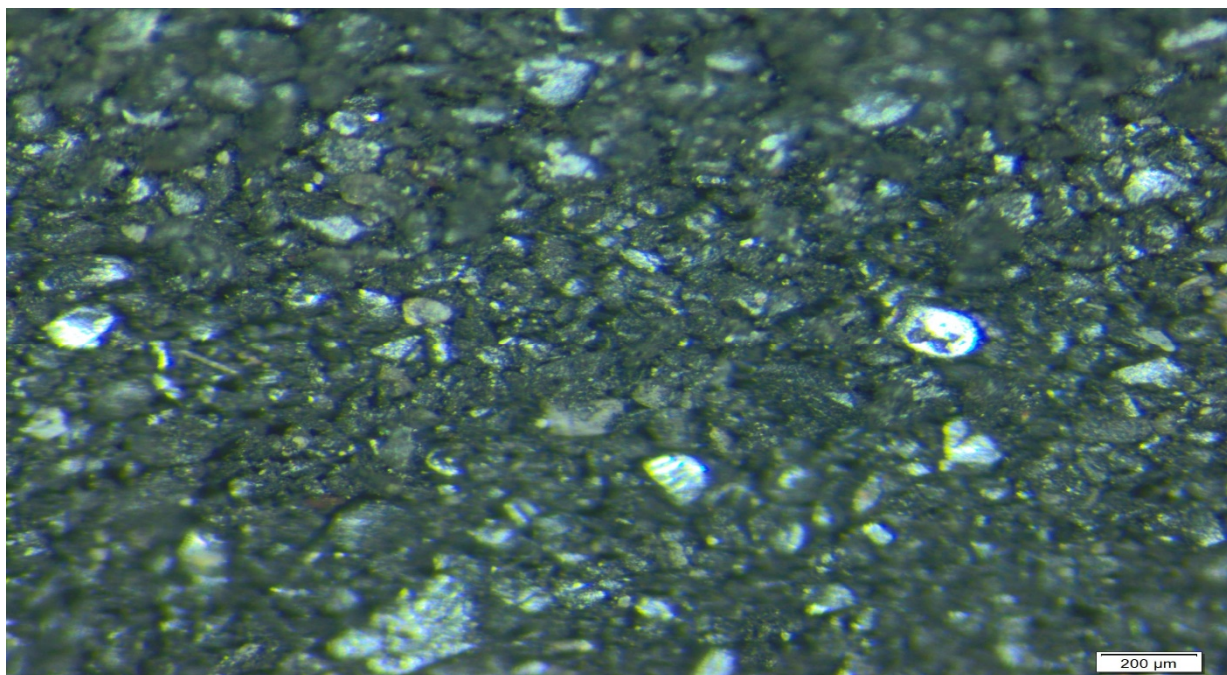
Figure 50 Stereomicroscopy distribution of bed mixture 40% ilmenite and 60% fine coal medium

4.3.4.5 Stratification in the bed of 40% ilmenite and 60% fine coal medium with AFE and ROM of coal

The cut density at 1580 kg/m^3 of medium 40% ilmenite with 60% fine coal seems to be acceptable by the coal beneficiation industry. The experiments were conducted at the cut point of 1580 kg/m^3, as discussed in section 3.6. The AFE and ROM coal particles (- 50+13,2 mm) were loaded into the bed after stratification and the air bleed valve was shut off. The static bed was divided into two layers, which were float (L5, L4 & L3) and sink (L2 & L1). The coal particles were discharged from the top to the bottom, and chemical analysis was conducted.

Table 19 shows the result of the chemical analysis on coal. The heavier coal particles reported to the bottom (sink), leaving behind the lighter coal particles (float) which remained in the float layer. The yield was calculated using Equation 23.

Table 19 Stratification in the bed of 40% ilmenite and 60% fine coal medium with coal samples

Coal	Bed location	Ash content (%)	Yield (%)
ROM	Float	11,0	61,44
	Sink	19,3	
AFE	Float	13,8	71,27
	Sink	55,6	

The yields of the ROM and AFE coals were 61,44% and 71,27%, respectively. These results proved that good splitting can be achieved using a binary medium of ilmenite mixed with fine coal.

4.3.4.6 Recovery of mixture 40% ilmenite with 60% fine coal medium using a dry high gradient magnetic separator

4.3.4.6.1 Dry coal

As discussed in section 3.7, three samples of dry coal were mixed with the binary medium of 40% ilmenite with 60% fine coal. It can be seen in Figure 51 that ilmenite one time used had the highest recovery of ilmenite 99,79% on dry coal. The recovery of 99,11% ilmenite was the lowest of ten times reused ilmenite on dry coal (data in Appendix 23).
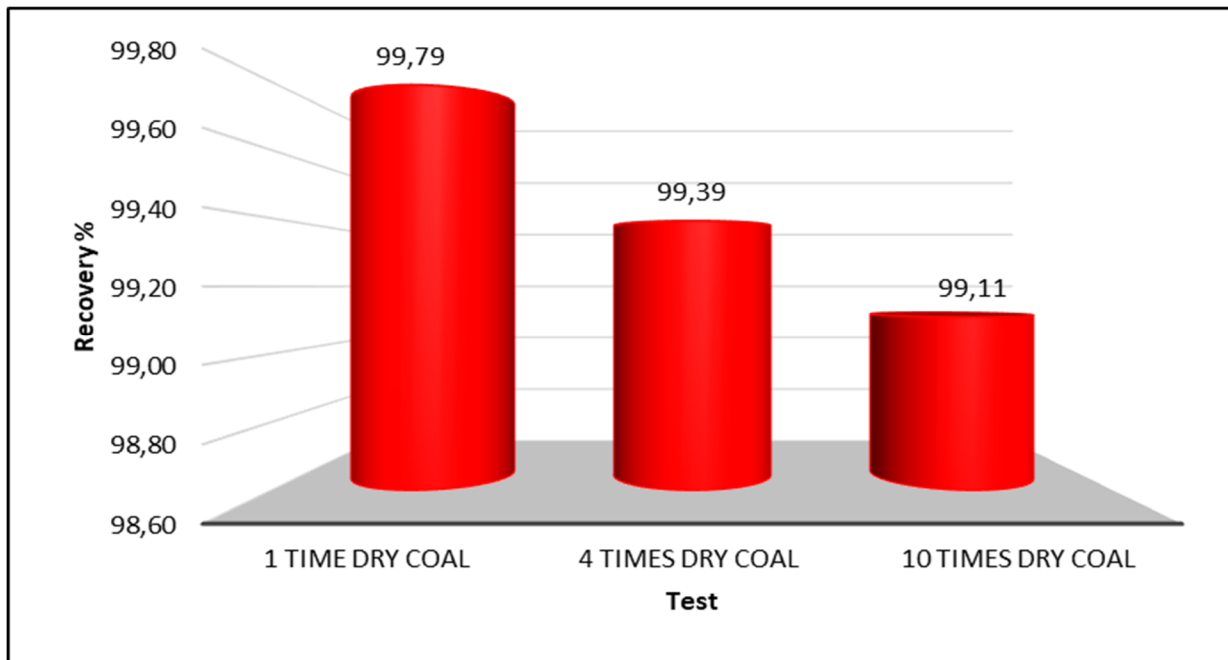
Figure 51 Recovery of ilmenite from dry coal using Magna chute

4.3.4.6.2 Wet coal

Four samples of wet coal (section 3.7) were mixed with the binary medium of 40% ilmenite with 60% fine coal. It can be seen in Figure 52 that 1% wet coal had the highest recovery of 99,74% ilmenite, and by increasing the moisture of coal, the recovery of ilmenite slightly decreased to reach 98,97% with 4% wet coal (data in Appendix 24).
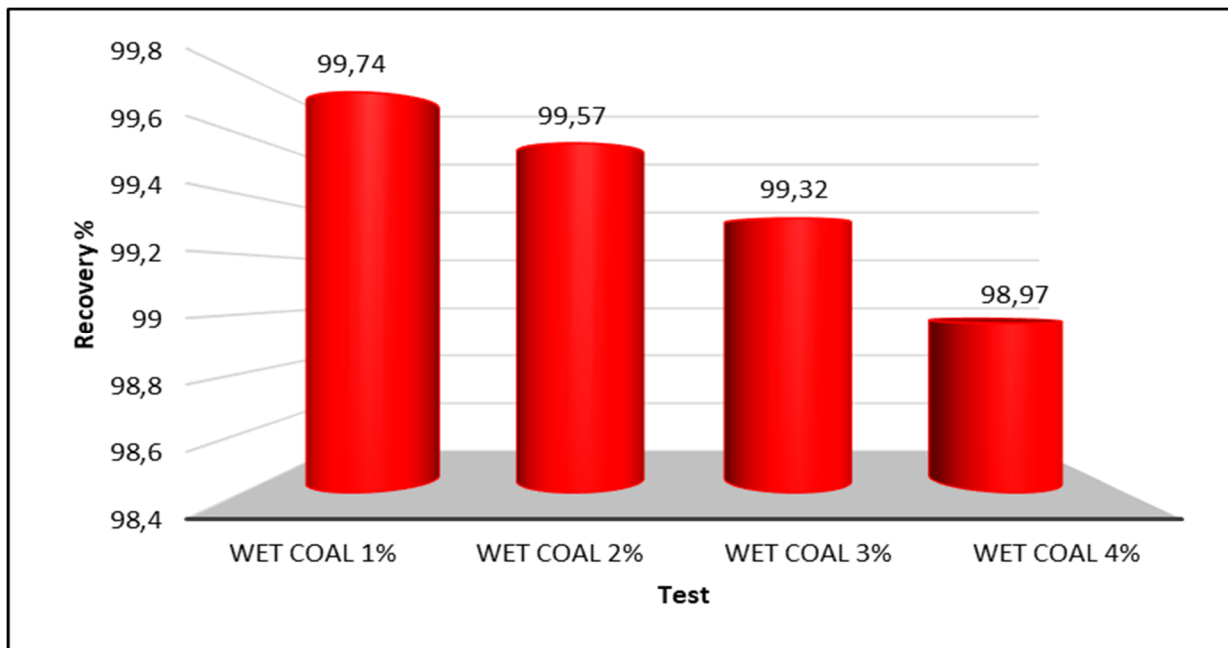
Figure 52 Recovery of ilmenite from wet coal using Magna chute

4.3.4.7 Losses of ilmenite

4.3.4.7.1 Dry coal

Figure 53 shows the run of mine coal sample before mixing with the medium.

Figure 53 Run of mine coal sample

It was found that ilmenite did not attach to the surface of dry coal (Figure 54).

Figure 54 Surface of dry coal sample

The losses of ilmenite occurred on the magnetic separator, as shown in Figure 55. The loss of ilmenite was expressed in gram/kilogram or kilogram/ton using Equation 24.

The lowest losses of 5,12 g/kg or 5,12 kg/t were seen in the one-time reused ilmenite, and ten times reused of ilmenite had the highest losses of 21,65 g/kg or 21,65 kg/t on the dry coal (data in Appendix 23).

$$Loss\ of\ ilmenite\ (1\ time\ used\ dry\ coal) = \left(\frac{1223 - 1220,43}{0,50142} \right)$$

$$= 5,12\ g/kg\ or\ 5,12\ kg/t$$
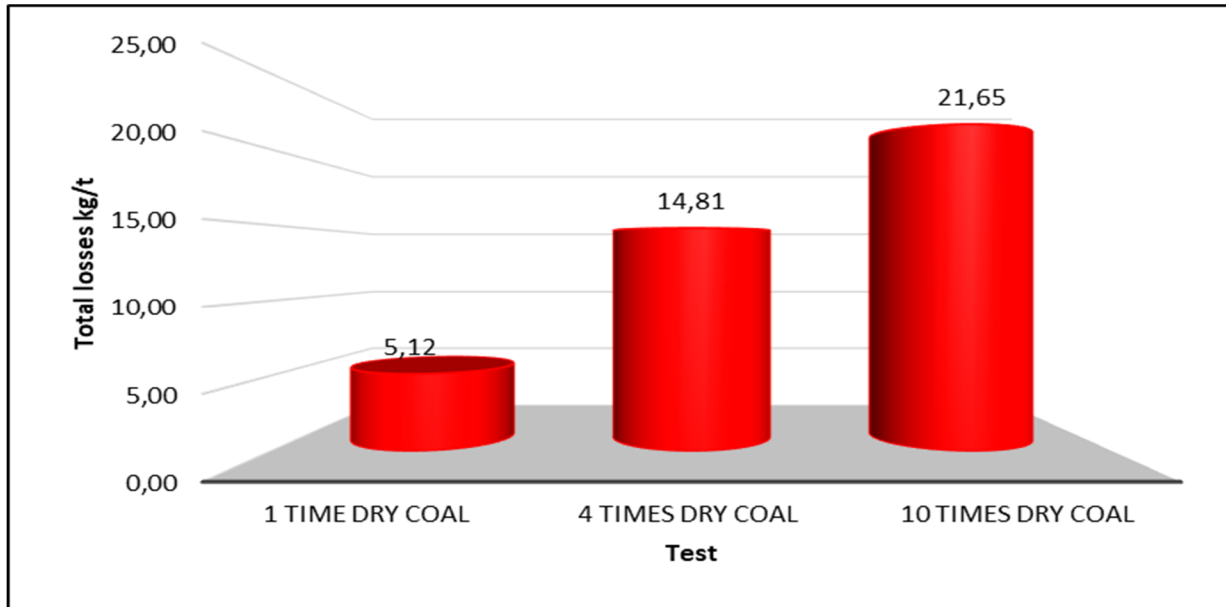
Figure 55 Total losses of ilmenite on dry coal

4.3.4.7.2 Wet coal

It was found that ilmenite did attach to the surface of wet coal (Figure 56 to 59).

Figure 56 Surface of 1% wet coal sample

Figure 57 Surface of 2% wet coal sample

Figure 58 Surface of 3% wet coal sample

Figure 59 Surface of 4% wet coal sample

The losses of ilmenite occurred both in the magnetic separator and on the wet coal surface, as shown in Figure 60 (data in Appendix 24). By using Equation 24, loss of ilmenite was expressed in gram/kilogram or kilogram/ton. The lowest losses of 6,13 g/kg or 6,13 kg/t were seen in the 1% wet coal, and 4% wet coal had the highest losses of 24,25 g/kg ilmenite.
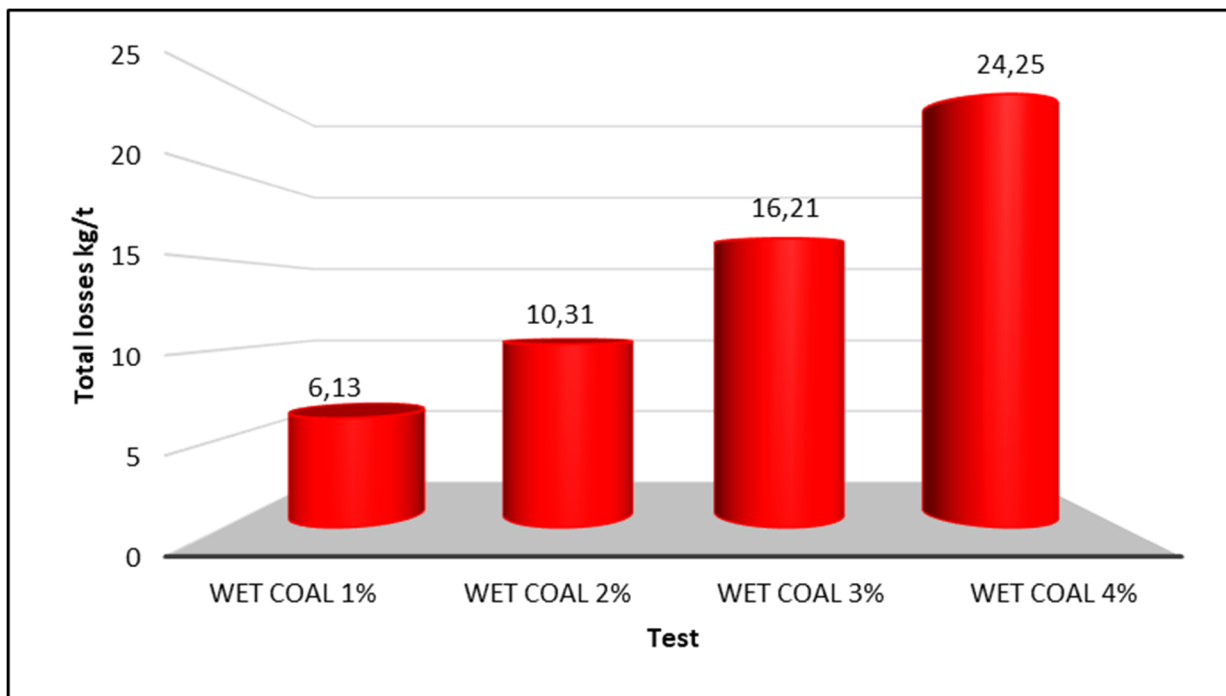
Figure 60 Total losses of ilmenite with wet coal

4.3.4.8   Assessment of the cost of losses

4.3.4.8.1 Dry coal

Figure 61 describes the cost of ilmenite losses in dry coal. The result shows that with dry coal, ilmenite losses in gram per kilogram resulted in $0,82 for ilmenite used once, $2,37 for ilmenite reused four times, and lastly $3,46 for ilmenite reused ten times. It is important to know that all the calculations were made based on an ilmenite price of $160 per ton (FOB), as shown in Figure 4.

Example:

- For dry coal used once
- Losses are 5,12 g/kg coal (or 5,12 kg/t coal)
- Ilmenite cost $160/t, or $0,160/kg ilmenite

Therefore, the losses can be calculated as follow:

$$Cost\ of\ ilmenite\ losses\ (dry\ coal\ used\ once) = \frac{5,12\ \cancel{kg\ ilmenite}}{tonne\ coal} \times \frac{\$0,16}{\cancel{kg\ ilmenite}}$$

$$= \$0,82/tonne\ coal$$
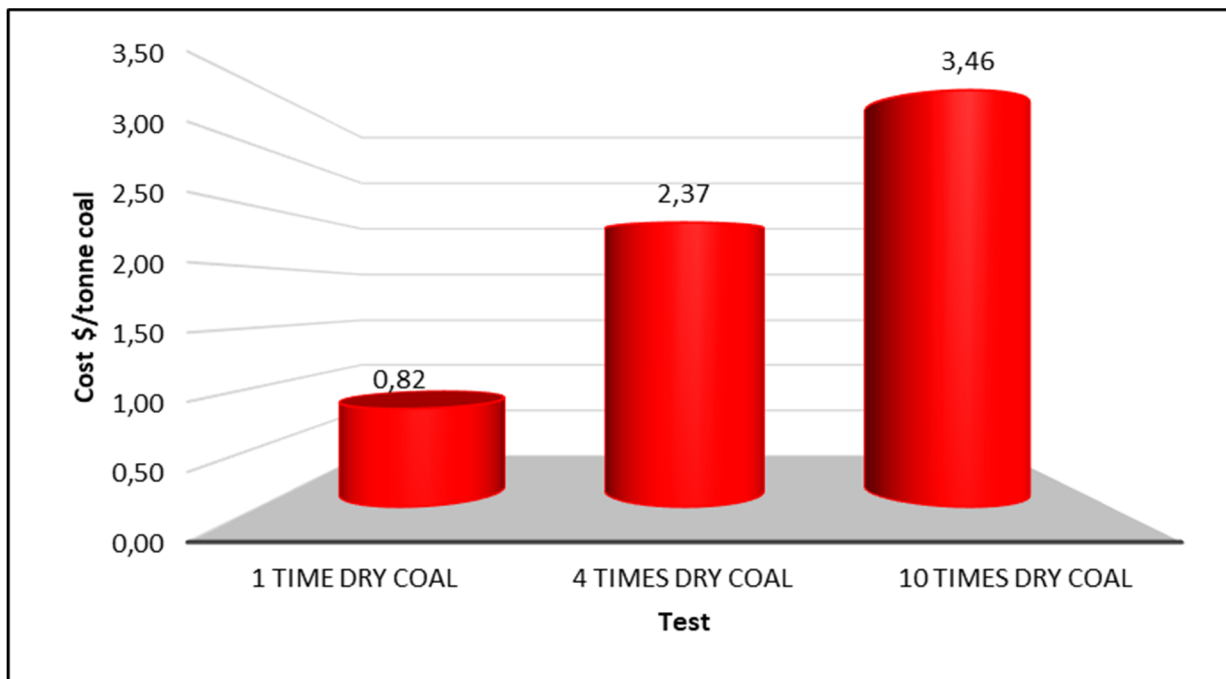
Figure 61 Losses of ilmenite cost with dry coal

4.3.4.8.2 Wet coal

Figure 62 describes the cost of ilmenite losses in wet coal. The result shows that with wet coal, ilmenite losses in gram per kilogram resulted in $0,98 for 1% wet coal, $1,65 for 2% wet coal, $2,59 for 3% wet coal, and lastly $3,88 for 4% wet coal. Similar to dry coal calculations, these calculations were made based on an ilmenite price of $160 per ton (FOB).

Example:

- For 1% wet coal
- Losses are 613 g/kg coal (or 6,13 kg/t coal)
- Ilmenite cost $160/t, or $0,160/kg ilmenite

Therefore, the losses can be calculated as follow:

$$Cost\ of\ ilmenite\ losses\ (1\%\ wet\ coal) = \frac{6,13\ \cancel{kg\ ilmenite}}{tonne\ coal} \times \frac{\$0,16}{\cancel{kg\ ilmenite}}$$

$$= \$0,98/tonne\ coal$$
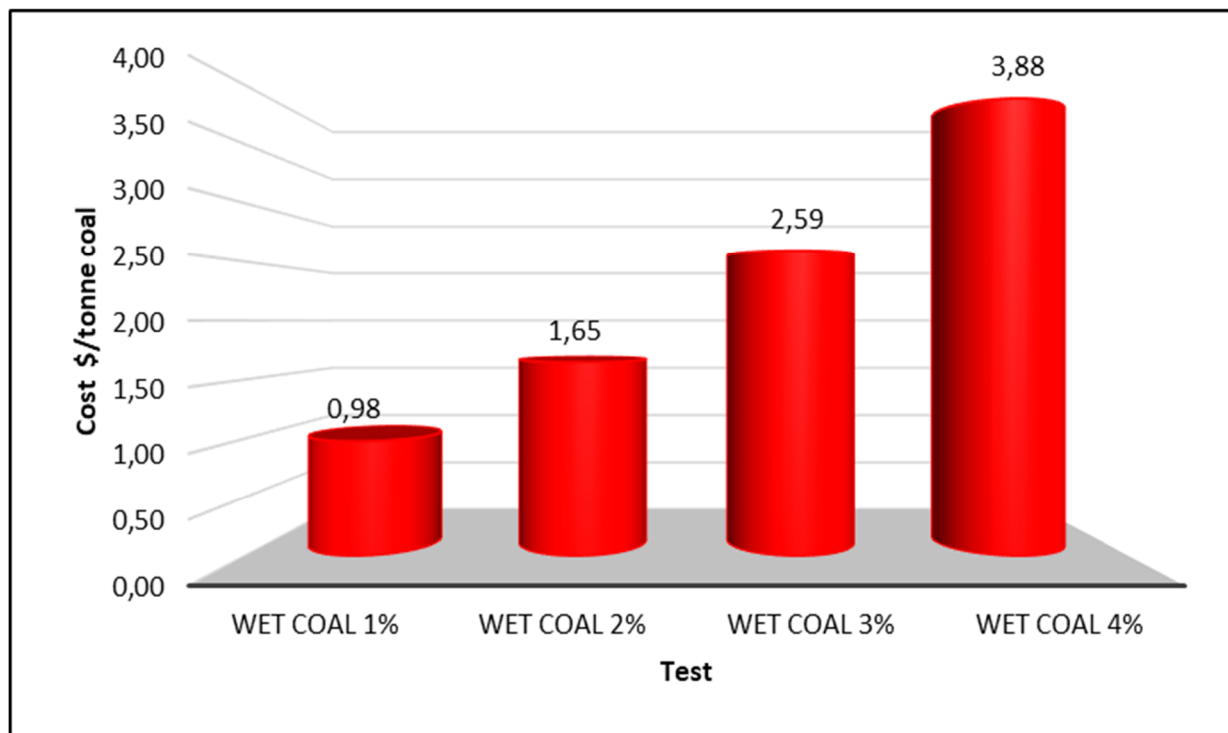
Figure 62 Losses of ilmenite cost with wet coal

4.3.4.9 Stereomicroscopy images of ilmenite

Figure 63 (section 3.3.3) indicates the stereomicroscopy results of ilmenite medium surface after the high gradient magnetic separator. This analysis showed that the surface of ilmenite used once was found to be similar to ilmenite reused ten times. Moreover, no clay materials attached to the surface.
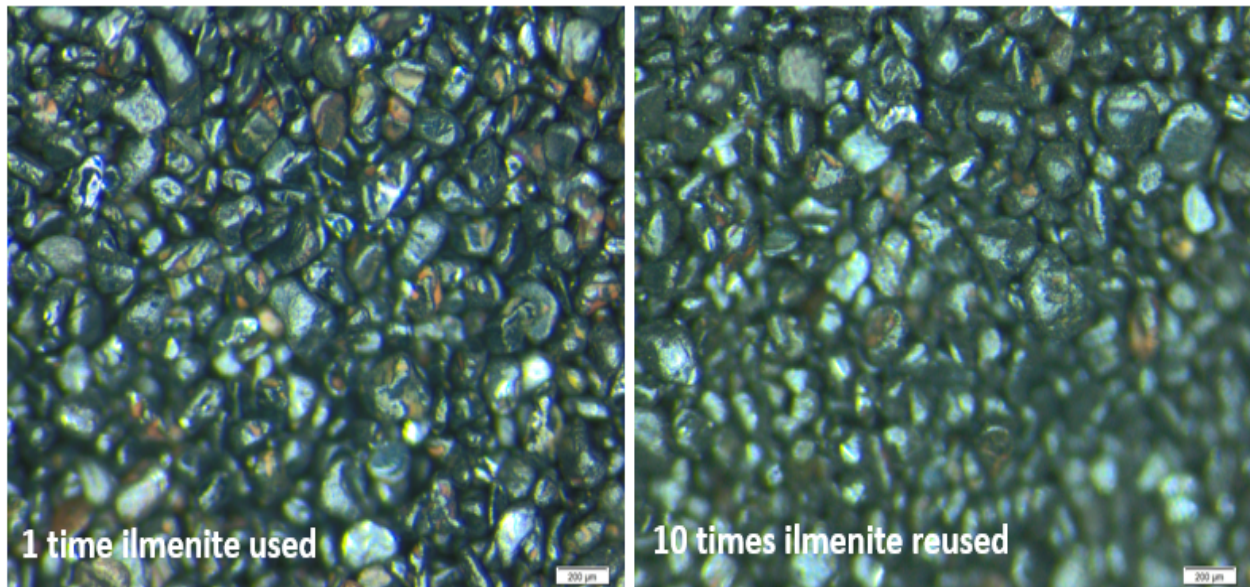
Figure 63 Stereomicroscopy of ilmenite medium surface after dry high gradient magnetic separator

4.3.4.10 Contamination of ilmenite after processed in the magnetic separator

Figure 64 contains the micro XRF analysis results of ilmenite medium surface after the high gradient magnetic separator. It can be seen that all of the analysis conducted, notably calcium (Ca), titanium (Ti), iron (Fe), silicon (Si), and sodium (Na), showed a similar ilmenite surface sample after using it once, or reusing it ten times (data in Appendix 24).
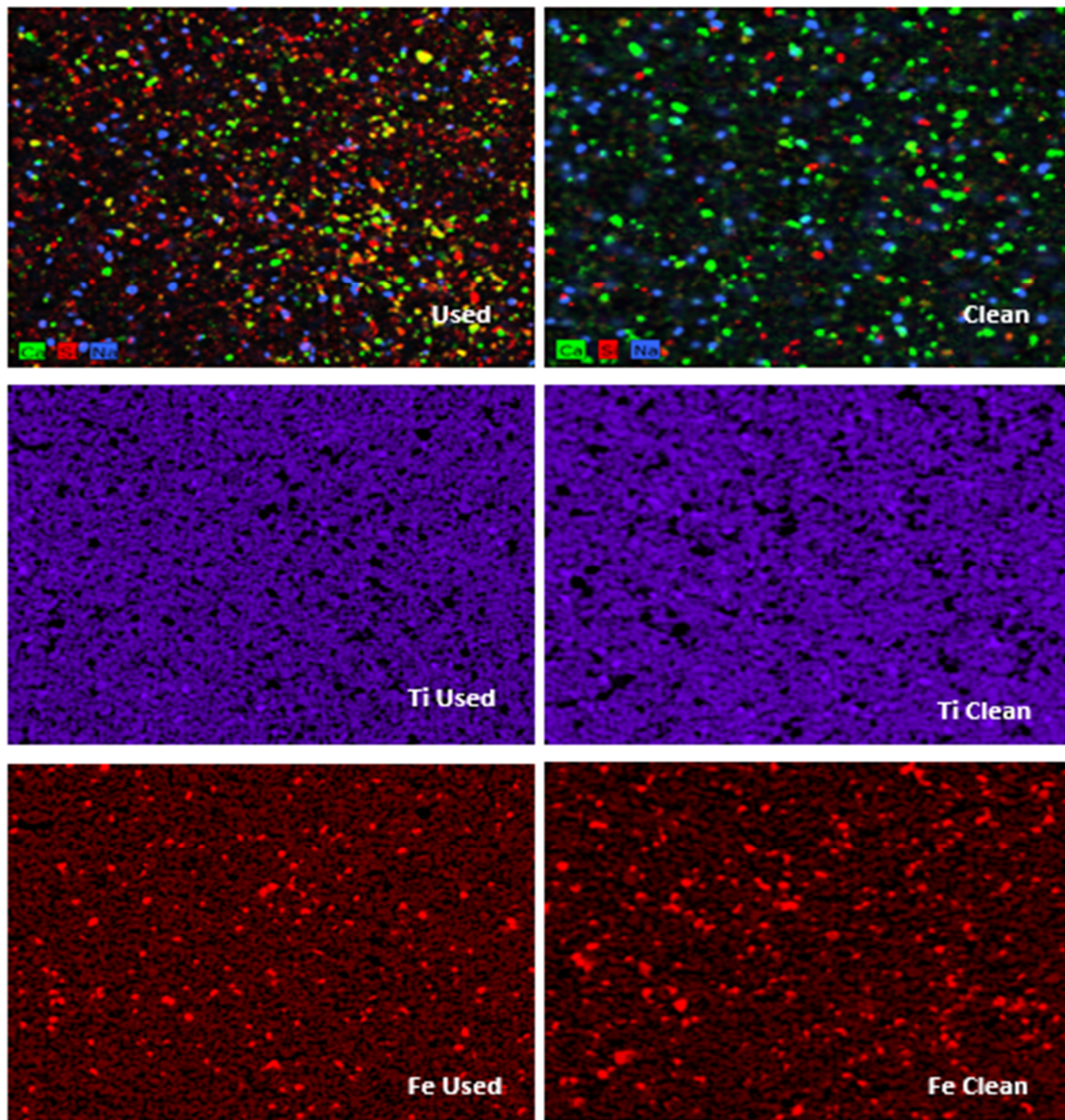
Figure 64 Micro XRF analysis after High gradient magnetic separator

4.4 Conclusion

In conclusion of this research chapter, ilmenite as a medium in an air dense medium fluidized bed was found to be an excellent alternative medium for dry coal beneficiation inside a laboratory batch ADMFB.

Through the fluidization of ilmenite as medium, some critical parameters were taken into consideration, such as particle size distribution, bed height, pressure drop versus

minimum fluidization velocity, and bed voidage, as well as the density of the bed, avoiding the slugging region and operating superficial velocity. In this study, different ratios of ilmenite/sand or ilmenite/fine coal as medium were tested to determine the density and minimum fluidization velocity. The tracers were fluidized and stratified into floats and sinks within the bed, in the same way that coal would be separated. The tracers recovered from the float and sink were sieved and counted, and the number of tracers recovered then used to construct a partition curve.

Sand or fine coal was used as a diluent to reduce the bed density of ilmenite in the experiments, which formed binary medium ilmenite with sand or ilmenite with fine coal. Moreover, tracers were used to determine the bed split, position of tracers in ADMFB, and Ecart Probable Moyen. The trend lines were fitted in an observed split with sand/ilmenite and fine coal/ilmenite ratio. The stratification was satisfactory with the bed split observed at 1580 kg/m^3 of the medium 40% ilmenite with 60% fine coal.

The binary medium of 40% ilmenite with 60% fine coal was mixed with both dry and wet coal and the ilmenite was recovered using a dry high gradient magnetic separator. It was found that ilmenite does not attach to the surface of dry coal with the highest recovery of 99,79%. The recovery of ilmenite slightly decreased by adding the surface moisture content of coal. The losses were found to be less than 25 g/kg at the external moisture content of 4% coal.

Furthermore, the micro XRF and stereomicroscopic analyses were done to analyse the contamination of ilmenite as medium; it was concluded that ilmenite once used and ilmenite ten times reused were similar.

5 CONCLUSIONS

The outcomes of this study on the evaluation of ilmenite as a possible medium in a dry dense medium fluidized bed provided some essential information which is projected in the near future development of a more efficient continuous air dense medium fluidized bed process. The critical parameters were taken into consideration, such as particle size distribution, bed height, pressure drop versus superficial gas velocity, bed voidage, the density of the bed, avoiding the slugging region and operating superficial velocity, which provides a good understanding and positive optimisations of an air dense medium fluidized bed process using ilmenite as a medium.

The ilmenite properties were studied to determine its possible use as a medium in dry coal beneficiation. It is considered due to its specific surface properties and sphericity. It was found that ilmenite as medium (−355+63 μm) presents some advantages, such as a hydrophobic surface with a contact angle of 14° degree and a clean surface. These properties give it an advantage compared to magnetite, as it does not attach to the coal particles as much as magnetite does.

This research has proven that there are available resources of ilmenite in South Africa, especially in the deposits located along the eastern, southern and northeastern coasts. Ilmenite as mineral is found in heavy mineral sands which typically contains 90% ilmenite, 5% Ti-hematite, 3% spinel (including chromite and magnetite) and 2% silicates by weight. Also, ilmenite minerals are recovered in three significant mines, namely Namakwa Sands (Tronox), Richard's Bay Minerals (Rio Tonto) and KwaZulu-Natal Sands (Tronox). Kenmare Resources (Moma) is also a potential producer of ilmenite in Mozambique. Based on USGS reported data of the world production of ilmenite in 2017, South Africa produced an average of 1,3 million metric tons of ilmenite.

In order to evaluate ilmenite as a possible medium in dry coal beneficiation, tracers particles of cubic shape and with side dimensions of 12 mm were used to determine the performance of fluidization process. The results of ilmenite as an alternative medium to the feasibility of dry coal in air dense medium fluidized bed beneficiation were positive, using a medium of fine coal with ilmenite, and sand with ilmenite.

Sand or fine coal (–300+53 µm) was used as a diluent to reduce the bed density of ilmenite in the experiments, which formed binary medium sand with ilmenite or fine coal with ilmenite. The results of ilmenite as an alternative medium to the feasibility of dry coal beneficiation were encouraging. The trend lines were fitted in density split with sand/ilmenite and fine coal/ilmenite ratio with R^2 of 0,997 and 0,998 respectively.

The density distribution in the fluidizing bed of sand with ilmenite medium perceived that density stratification does not appear beneath the sand concentration of 40%. However, stratification of the sand quickly increases when its concentration is above 50%, and the Ecart Probable Moyen ranged between 0,120 and 0,045. Thus, sand could not be used to separate coal at densities required by the coal industry. It was just proof of concept, at low densities. The fine coal with ilmenite medium observed that density stratification does not appear below the fine coal concentration of 30%. However, stratification of the fine coal quickly increases when its concentration is above 40%, and the Ecart Probable Moyen ranged between 0,11 and 0,05.

The coal can be efficiently separated in an air dense medium fluidized bed process (ADMFB). The yield of feed to the plant coal sample (AFE) and run of mine coal sample (ROM) of size range –50+13,2 mm were found to be 61,44% and 71,27% respectively, while using a binary medium of 60% fine coal with 40% ilmenite at bed split observed of 1580 kg/m^3 and at the Ecart Probable Moyen of 0,05.

The binary medium of 40% ilmenite with 60% fine coal was mixed with both dry and wet coal and the ilmenite was recovered using a dry high gradient magnetic separator. The results revealed that ilmenite does not attach to the surface of dry coal with the highest recovery of 99,79%. The recovery of ilmenite slightly decreased by adding the surface moisture content of coal. The losses were found to be less than 25 g/kg at the external moisture content of 4% coal, which was $4/t of coal.

The stereomicroscopy analysis results of ilmenite medium surface after the high gradient magnetic separator revealed that both the surface of ilmenite once used and ilmenite reused ten times were similar, and no clays attached to the surface.

The micro XRF analysis results of ilmenite medium surface after the high gradient magnetic separator indicated that all of the analysis constructs, notably Calcium (Ca),

Titanium (Ti), iron (Fe), silicon (Si), and sodium (Na) showed a similar surface of ilmenite sample and ilmenite reused ten times.

In conclusion, ilmenite is considered as a viable medium in a dry dense medium fluidized bed process, due to its material properties.

6 RECOMMENDATIONS

It is advised that the tests should also be conducted on a bigger experimental fluidized bed to avoid the effects of bed height to diameter ratio below 1 and possible wall effects on tracers.

It is suggested that the test should be examined in a continuous process to eliminate handling error and improve the recovery of ilmenite with the air flow in the bed.

The ilmenite recovery test was done using a laboratory sieve shaker; it is suggested that the high-frequency screen should be investigated to improve the recovery of ilmenite.

The recovery of ilmenite was conducted by using a dry high gradient magnetic separator; it is suggested that the test should be conducted with a high-intensity magnetic separator such as the SLon magnetic separator.

7 REFERENCES

Adán, C., Bahamonde, A., Oller, I., Malato, S., Martínez-Arias, A. 2014. Influence of iron leaching and oxidizing agent employed on solar photodegradation of phenol over nanostructured iron-doped titania catalysts, *Applied Catalysis B: Environment,* vol. 144, pp.269–276.

ASTM D2234 / D2234M-16, Standard practice for collection of a gross sample of coal, ASTM International, West Conshohocken, PA, 2016, www.astm.org

ASTM D3302 / D3302M-12, Standard test method for total moisture in coal , ASTM International, West Conshohocken, PA, 2012, www.astm.org

ASTM D4749-87(2012), Standard test method for performing the sieve analysis of coal and designating coal size, ASTM International, West Conshohocken, PA, 2012, www.astm.org

ASTM D5142-09, Standard test methods for proximate analysis of the analysis sample of coal and coke by instrumental procedures (Withdrawn 2010), ASTM International, West Conshohocken, PA, 2009, www.astm.org

ASTM D5865-12, Standard test method for gross calorific value of coal and coke, ASTM International, West Conshohocken, PA, 2012, www.astm.org

Babu, S. P., Shah, B., & Talwalker, A. 1978. Fluidization correlations for coal gasification materials – minimum fluidization velocity and fluidized bed expansion ratio. *Chemical Engineering Progress Symposium Series no. 176,* vol.74, pp.176–186.

Baeyens, J. & Geldart, D., 1974. An investigation into slugging fluidized beds. *Chemical Engineering Science*, vol. 29, pp. 255–265.

Balderson, G.F. 1999. Flowsheet development options for a greenfield titanium minerals project, in proceedings of heavy minerals. In *Symposium series S23*. Edited by R.G. Stimson. Johannesburg: The South African Institute of Mining and Metallurgy, pp.125–136.

Barker, O.B. 1999. A techno-economic and historical overview of the South African coal industry in the 19th and 20th centuries, *in Bulletin 113*. eds. Pinheiro, H.J. (South

African Bureau of Standards), pp. 1–63.

Bell, K. and Spurr, M.R. 1986a. The vryheid coalfield of Northern Natal. Anhaeusser, C.R. and Maske, S. (eds.). *Mineral Deposits of Southern Africa*, vol. II, pp. 2023–2032. Johannesburg: Geological Society of South Africa.

Bell, K. and Spurr, M.R. 1986b. The klip river coalfield of Northern Natal. Anhaeusser, C.R. and Maske, S. (eds.). *Mineral Deposits of Southern Africa*, vol. II, pp. 2033–2045. Johannesburg: Geological Society of South Africa.

Bennett, L.H., *et al.* 1978. Comments on units in magnetism. *Journal of research of the National Bureau of Standards*, vol. 83, no. 1, pp.9–12.

Bin´, A. K. 1994. Prediction of the minimum fluidization velocity. *Powder Technology*, vol. 81, pp.197–199.

Bourgeis, P. & Grenier, P. 1968. Ratio of terminal velocity to minimum fluidization velocity for spherical particles. *Canadian Journal of Chemical Engineering*, vol. 46, pp. 325.

Carvill, M. 2017. *Kenmare buoyed by ilmenite market improvement, record production potential*. [Online]. Available: http://m.miningweekly.com/article/kenmare-buoyed-by-ilmenite-market-improvement-record-production-potential. [Cited:11/10/2017].

Chan, E. W. & Beeckman, J. M. 1982. Pneumatic beneficiation of coal fines using the counter-current fluidized cascade. *International Journal of Mineral Processing*, vol. 9, pp.157–165.

Chen, Q. & Wei, L., 2003. Coal dry beneficiation technology in China: the state-of-the-art. *China Particuology*, vol. 1, no. 2, pp.52–56.

Chiba S, Chiba T, Nienow A.W., Kobayashi H. 1979. The minimum fluidization velocity, bed expansion and pressure-drop profile of binary particle mixtures. *Powder Technology,* vol. 22, pp. 255–269.

Chikerema, P. & Moys, M. 2012. Effects of particle size, shape, and density on the performance of an air fluidized bed in dry coal beneficiation. *International Journal of Coal Preparation and Utilization,* vol. 32, no. 2, pp. 80–94.

Choung, J., Mak, C. & Xu, Z. 2006. Fine coal beneficiation using an air dense medium

fluidized bed. *Coal Preparation*, vol. 26, pp.1–15.

Christie, A.D.M.1989. Demonstrated coal resources of the Springbok Flats Coalfield, Geological Survey of South Africa *Internal Report No. 1989–0069*.

Coltters, R. & Rivas, A.L. 2004. Minimum fluidization velocity correlations in particulate systems. *Powder Technology,* vol. 147, pp.34–48.

Coulter, T. 1957. The history and development of coal washing in South Africa. Fuel Research Institute Symposium, Pretoria.

Council for Geoscience. 2002. Simplified geology and titanium deposits South Africa, Lesotho and Swaziland.http://www.geoscience.org.za/index.php/publication /downloadable-material.[Cited 14/02/2018].

Crişan, M., Răileanu, M., Drăgan, N., *et al*. 2015. Sol-gel iron-doped TiO2 nanopowders with photocatalytic activity, Applied Catalysis A: General, vol. 504, pp.130–142.

Crowe, C.T. 2006. *Multiphase flow handbook*. Boca Raton, FL: CRC Press.

Ctibor, P., Pala, Z., Stengl, V., Musalek, R. 2014. Photocatalytic activity of visible-light-active iron-doped coatings prepared by plasma spraying, Ceramics International, vol. 40, pp.2365–2372.

Dahlin, D.C. & Rule, A.R. 1993. Magnetic susceptibility of minerals in high magnetic fields. Report RI 9449, *US Bureau of Mines*.

Dardis, K. A., 1987. The design and operation of heavy medium recovery circuits for improved medium recovery. *Proceedings of the Dense Medium Operators Conference*. Brisbane: Australasian Institute of Mining and Metallurgy, pp. 157–184.

De Jager, F.S.J. 1986. Coal occurrences in the central, northwestern, northern and eastern Transvaal. Edited by Anhaeusser, C.R. and Maske, S.(eds.), *Mineral Deposits of Southern Africa*, I. Geological Society of South Africa, pp.1315.

De Korte, G.J. 2002. Plant efficiency measurement: Coaltech 2020, Division of Mining Technology, pp.1–30.

De Korte, G.J. 2010. Coal preparation research in South Africa. *The Southern African*

Institute of Mining and Metallurgy, vol. 110, pp. 361–364.

De Korte, G.J. 2013. Dry processing versus dense medium processing for preparing thermal coal. 17th International Coal Preparation Congress, pp.1–6: Istanbul, Turkey.

De Korte, G.J. 2015. Processing low-grade coal to produce high-grade products. *The Southern African Institute of Mining and Metallurgy*, vol. 115, pp. 569–572.

Dhanraj, K. 2016. Air quality management plan, dust management strategy for the Hillendale and Fairbreeze mines, pp.1–71.

Dong, X. & Beeckmans, J.M. 1990. Separation of particulate solids in a pneumatically driven counter-current fluidized Cascade. *Powder Technology*, vol. 62, pp.261–267.

Drzymala J., Lekki J. 1989b. Flotometry – another way of characterizing flotation. *Journal of Colloid and Interface Science*, vol. 130, no. 1, pp.205–210.

Drzymala, J. 2007. *Mineral processing: foundations of theory and practice of minerallurgy*. Wroclaw: Wroclaw University of Technology.

Dwari, R.K. & Hanumantha R.K. 2007. Dry beneficiation of coal—A review. *Mineral Processing and Extractive Metallurgy Review*, vol. 28, pp.177–234.

Dworzanowski, M. 2014. Maximising hematite recovery within a fine and wide particle-size distribution using wet high-intensity magnetic separation. *The Journal of The South African Institute of Mining and Metallurgy*, vol. 114, no. 7, pp. 559–567.

Elias, S.J., 2016. *Mineralogy and provenance of the TiO2- Ilmenite Heavy mineral sand deposit of Nataka.* MSc. thesis. Cape Town: University of Cape Town.

Ergun S. 1952. Fluid flow through packed columns. *Chemical Engineering Progress*, vol. 48, pp. 89–94.

Eriez Magnetics, 2008. Eriez model 610 dia. x 170 magnet width RE Magnetic drum separator, Eriez magnetics SA (PTY) LTD.

Eriez, 2017. Laboratory equipment, magna chute. https://www.eriezlabequipment.com/products/magnetic-separators/separation/htm.

[Cited 14/02/2017].

Eriez, G., 2014. Reliable WHIMS with maximum recovery. Eriez Manufacturing Company, Erie, PA, USA, pp.1–12.

Falcon, R.M.S., & Snyman, C.P. 1986. *An introduction to coal petrography: Altas of petrographic constituents in the bituminous coals of South Africa*. Johannesburg,Geological Society of South Africa.

Fisher-White, M., Freeman, D., Grey, I., Lanyon, M., Pownceby, M. & Sparrow, G. 2007. Removal of chrome spinels from Murray Basin ilmenites by low-temperature roasting. *Mineral Processing and Extractive Metallurgy*, vol. 116 no. 2, pp.123–132.

Frantz, Y. F. 1966. Minimum fluidization velocities and pressure in fluidized beds. *Chemical Engineering Progress Symposium Series*, vol. 62, pp.21–31.

Fujii, T., Oohashi, H., Tochio, T., *et al.* 2011. Speculations on anomalous chemical states of Ti ions in $FeTiO_3$ observed by high-resolution X-ray Kβ emission spectra. *Journal of Electron Spectroscopy and* Related *Phenomena*, vol. 184, pp.10–15.

Geldart, D. 1973. Types of gas fluidization. *Powder Technology,* vol. 7, pp.285–292.

Giaquinta, D.M., zur Loye, H.C. 1994. Structural predictions in the ABO_3 phase diagram. *Chemistry of Materials*, vol. 6, pp. 365–372.

Gilligan, R.N.1986. OFS—Vierfontein coalfield. *Mineral Deposits of Southern Africa*, vol. II. Edited by C.R. Anhaeusser and S. Maske. Johannesburg: Geological Society of South Africa, pp.1929–1937.

Greenshields, H.D. 1986. Eastern transvaal coalfield. *Mineral Deposits of Southern Africa*, vol. II. Edited by C.R. Anhaeusser and S. Maske. Johannesburg: Geological Society of South Africa, pp. 1995–2010.

Gupta, A. & Yan, D.S. 2006. *Mineral processing design and operation an introduction*,published in Perth, Australia by Elsevier,pp. 549.

Gupta, C.K., & Sathiyamoorthy. D. 1999. *Fluid bed technology in materials processing*, Published in Boca Raton (Fla.) by CRC press, pp. 498.

Hand, P.E., England, T., Michael, D.C., Falcon, L.M. & Yell, A.D. (eds). 2002. *Coal preparation in South Africa.* Johannesburg: The South African Coal Processing Society, pp. 298.

Haughey, D.P., Beveridge, G.G. 1969. Structural properties of packed beds—a review. *Canadian Journal Chemical Engineering*, vol. 47, pp.130–140.

He, Y., Zhao, Y. & Chen, Q. 2003. Fine particle behavior in air-fluidized bed dense medium dry separator. *Coal Preparation*, vol. 23, pp.33–45.

He, Y., Zhao, Y., Chen, Q., Luo, Z., & Yang. Y. 2002. Development of the density distribution model in a gas-solid phase fluidized bed for dry coal separation. *Journal of the South African Institute of Mining and Metallurgy,*vol.102, pp.429–434.

Henderson, R.E. 1986. South rand coalfield.. In *Mineral Deposits of Southern Africa*, vol. II. Edited by C.R. Anhaeusser and S. Maske. Johannesburg: Geological Society of South Africa, pp.1953–1961.

Hovmand, S. & Davidson J.F. 1971. Pilot plant and laboratory scale fluidized reactors at high gas velocities: the relevance of slug flow. In: *Fluidization*. Edited by J.F.Davidson and D. Harrison. New York: Academic Press, pp.193–259.

Iluka Resources, 2014. The Mineral sands industry factbook. [Online]. Available at https://www.iluka.com/docs/default-source/industry-company-information/the-mineral-sands-industry-factbook-(Feb-2014). [Cited 11/03/2017].

ISO 13320:2009. The International standard for particle size analysis by laser diffraction, providing a methodology for proper quality control.

Izvorni, Z.R., Findorák, R., Fröhlichová, M., Legemza, J. 2014. Potential of ilmenite sand application in the iron ore materials agglomeration. *Metalurgija,* vol. 53, no. 1, pp. 9–12.

Jeffrey, L.S. 2005b. Challenges associated with further development of the Waterberg Coalfield. *The Journal of The South African Institute of Mining and Metallurgy*, vol.105, pp.453–458.

Jeffrey, L.S. 2005a. Characterization of the coal resources of South Africa. *The Journal*

of The South African Institute of Mining and Metallurgy, pp.7–9.

Jordaan, J. 1986. Highveld coalfield. *Mineral Deposits of Southern Africa.* vol. II. Edited by C.R. Anhaeusser and S. Maske. Johannesburg: Geological Society of South Africa, pp.1985–1994.

Kim, Y.J., Gao, B., Han, S.Y., *et al*. 2009. Heterojunction of FeTiO3 nanodisc and TiO2 nanoparticle for a novel visible light photocatalyst. *The Journal of Physical* Chemistry, vol. 113, pp.19179–19184.

Knowlton T.M. 1977. High-pressure fluidization characteristics of several particulate solids. *AIChE Symposium Series*, vol. 73, no. 61, pp.22–28.

Kozanoglu, B., Levy, E.K., Ulge, T., Sahan, R., & Schmitt, T. 1993. Prediction of rates of coal cleaning in a fluidized bed of magnetite. *AIChE Symposium Series*, vol. 89, pp.150–161.

Kunii, D., & Levenspiel, O. 2005. *Fluidization engineering,* 2nd ed*.* Newton, MA: Butterworth-Heinemann, pp.491.

Lee, R.B., Juan, J.C., Lai, C.W., Lee, K.M. 2017. Ilmenite: Properties and photodegradation kinetic on Reactive Black 5 dye.*Chinese Chemical Letters*, vol. 28, pp. 1613–1618

Liferovich, R.P., Mitchell, R.H. 2006. Mn, Mg & Zn ilmenite group titanates: a reconnaissance Rietveld study, Crystallography,vol. 51, pp.383–390.

Lippens, B.C. & Mulder. J. 1993. Prediction of the minimum fluidization velocity. *Powder Technology*, vol. 75, pp.67–78.

Luckos, A., & Den Hoed, P. 2005. A study into the hydrodynamic behaviour of heavy minerals in a circulating fluidized bed. *IFSA 2005, Industrial Fluidization South Africa*. Edited by A. Luckos and P. Smit. Johannesburg: South African Institute of Mining and Metallurgy, pp. 345–355.

Luo, Z. & Chen. Q. 2001a. Dry beneficiation technology of coal with an air dense-medium fluidized bed. *International Journal of Mineral Processing,* vol. 63, pp.167–175.

Luo, Z. & Chen. Q. 2001b. Effect of fine coal accumulation on dense phase fluidized bed

performance. *International Journal of Mineral Processing*, vol. 63, pp.217–224.

Luo, Z., Chen, Q. & Zhao. Y. 2002. Dry beneficiation of coarse coal using an air dense medium fluidized bed (ADMFB). *Coal Preparation,* vol. 22, pp.57–64.

Luo, Z., Zhao, Y., Chen, Q., Tao, X. & Fan, X. 2003. Separation lower limit in a magnetically gas-solid two-phase fluidized bed. *Fuel Processing Technology*, vol. 85, pp.173–178.

Luo, Z., Zhao, Y., Chen, Q., Tao, X. & Fan, X. 2004. Effect of gas distributor on performance of dense phase high-density fluidized bed for separation. *International Journal of Mineral Processing*, vol. 74, pp.337–341.

Luo, Z.F., Zhu, J.F., Tang, L.G., Zhao, Y.M., Guo, J., Zuo, W., Chen, S.L. 2010. Fluidization characteristics of magnetite powder after hydrophobic surface modification. *International Journal of Mineral Processing*, vol. 94, no. 3–4, pp.166–171.

Mak, C., Choung, J., Beauchamp, R., Kelly, D. J. A. & Xu, Z. 2008. Potential of air dense medium fluidized bed separation of mineral matter for mercury rejection from Alberta sub-bituminous coal. *Industrial and Engineering Chemistry Fundamentals*, pp.115–132.

Mehdilo, A., Irannajad, M. & Rezai, B. 2013. Colloids and Surfaces A: Physicochemical and Engineering Aspects Effect of chemical composition and crystal chemistry on the zeta potential of ilmenite. *Colloids and Surfaces A: Physicochemical and Engineering Aspects*, vol. 428, pp. 111–119.

Mehdilo, A., Irannajad, M. & Rezai, B. 2015. Chemical and mineralogical composition of ilmenite: Effects on physical and surface properties. *Minerals Engineering*, vol. 70, pp. 64–76.

Micrometrics, 2017. Accupyc II gas displacement pycnometry system. [Online]. Available: http://www.micromeritics.com/Product-Showcase/Density.aspx.htm.   [Cited 22/02/2018].

Micro X-ray Fluorescence,2018. Micro X-ray Fluorescence (µXRF). [Online]. Available:

https://www.xos.com/Micro-XRF. [Cited 12/07/2018].

Mlinar, M. & Petersen, T. 2017. Pilot-Scale demonstration of ilmenite processing Technology. *Natural Resources Research Institute Technical Report.* Minnesota: University of Minnesota Duluth.

Moctezuma, E., Zermeño, B., Zarazua, E., Torres-Martínez, L.M., García, R. 2011. Photocatalytic degradation of phenol with Fe-titania catalysts. *Topics in Catalysis*, vol. 54, pp. 496–503.

Mohanta, S. & Meikap, B.C. 2015. Influence of medium particle size on the separation performance of an air dense medium fluidized bed separator for coal cleaning. *South African Journal of Chemical Engineering*, vol. 115, pp. 761–766.

Mohanta, S., Daram, A. B., Chakraborty, S., Meikap, B.C. 2013. Applicability of the air dense medium fluidized bed separator for cleaning of high-ash Indian thermal coals: An experimental study. *South African Journal of Chemical Engineering*, vol. 16, no.1, pp. 50–62.

Mohanta, S., Rao, C.S., Daram, A.B., Chakraborty, S. & Meikap, B.C. 2013. Air dense medium fluidized bed for dry beneficiation of coal. Technological Challenges for Future. *Particulate Science and Technology*, pp.16–27.

Motsie, R. 2008. An overview of South Africa's titanium mineral concentrate industry. [Online]. Available at: http://www.dme.gov.za. [Cited 21/05/2017].

Nagata, T. 1961. *Rock magnetism.* Tokyo: Maruzen Company Limited.

Napier-Munn T.J. 1991. Modelling and simulating dense medium separation processes, *Minerals Engineering*, vol. 4, no. 3/4, pp.329–346.

Navrotsky, 1998. Energetics and crystal chemical systematics among ilmenite, lithium niobate, and perovskite structures, *Chemistry Materials*, vol. 10, pp.2787–2793.

Nell, J. & Den Hoed, P. 1997. Separation of chromium oxides from ilmenite by roasting and increasing the magnetic susceptibility of Fe,O,-FeTiO3, (ilmenite) solid solutions. In *Proceedings of Heavy Minerals*. Edited by R.E. Robinson, Symposium series S17. Johannesburg: South African Institute of Mining and Metallurgy, pp. 75–78.

Nguyen, T.H. & Grace, J. R. 1978. Forces on objects immersed in fluidized bed. *Powder Technology*, vol. 19, pp. 255–264.

Norrgran, D. 2010. Wet drum magnetic separators for heavy media application, operation, and performance. Society for Mining, Metallurgy & Exploration, Inc. (SME) Retrieved from www.knovel.com. Eriez, Erie, Pennsylvania, United States.

Ortlepp, G.J. 1986. Limpopo coalfield, 2057–2061. *Mineral Deposits of Southern Africa*. Edited by C.R. Anhaeusser and S. Maske. Johannesburg: Geological Society of South Africa, pp.1315.

Ortlepp, G.J.1986. Limpopo coalfield, 2057–2061. *Mineral Deposits of Southern Africa*. Edited by C.R. Anhaeusser and S. Maske. Johannesburg: Geological Society of South Africa, pp.1315.

Osborne, D.G. 1988. *Dense-medium separation. In Coal preparation technology*, vol.I. London: Graham and Trotman Limited, pp.199–276.

Outotec, 2013. SLon vertically pulsating high-gradient magnetic separator. 1-4. Outotec. [Online]. Available: www.outotec.com/ [Cited 22/09/2017].

Parapari, P.S., Irannajad, M., & Mehdilo, A. 2016. Modification of ilmenite surface properties by superficial dissolution method. *Minerals Engineering*, vol. 92, pp. 160–167. [Online]. Available at: http://dx.doi.org/10.1016/j.mineng.2016.03.016. [Cited 12/06/2016].

Philander, C. & Rozendaal, A. 2009. Geometallurgical intricacies of the Namakwa sands mineral resource: International Heavy Minerals Conference, 7th, South Africa, Proceedings, pp. 99–105.

Philander, C. & Rozendaal, A. 2015. Geology of the cenozoic Namakwa sands heavy mineral deposit, West Coast of South Africa: A World-Class Resource of Titanium and Zircon, Society of Economic Geologists, Inc. *Economic Geology*, vol. 110, pp. 1577–1623.

Pinetown, K.L., Ward, C.R., and van der Westhuizen, W.R. 2007. Quantitative evaluation of minerals in coal deposits in the Witbank and Highveld Coalfields, and the potential

impact on acid mine drainage. *International Journal of Coal Geology*, vol. 70, pp. 166–183.

Pownceby, M. 2005. Compositional and textural variation in detrital chrome-spinels from the Murray Basin, southeastern Australia. *Mineralogical Magazine*, vol. 69, no. 2, pp. 191–204.

Prashant, D., Xu, Z., Szymanski, J., Gupta, R., Boddez, J. 1997. *Dry cleaning of coal by a laboratory continuous air dense medium fluidized bed separator*, pp. 608–616.

Prevost, X.M. 2002. *Coal. South Africa's Mineral Industry 2001/2002*. Pretoria, Minerals Bureau.

Ramos, G., García Ruiz, M., Prieto Marqués, J.J., & Guardiola Soler, J. 2002.Minimum fluidization velocities for gas-solid 2d beds. *Chemical Engineering and Processing*, vol 41, no. 9, pp. 761–764.

Reina, J., Velo, E. & Puigjaner, L. 2000. Predicting the minimum fluidization velocity of polydisperse mixtures of scrap-wood particles. *Powder Technology*, vol. 111, pp. 245–251.

Rozendaal, A., Philander, C. & Carelse, C. 2010. Characteristics, recovery and provenance of rutile from the Namakwa Sands heavy mineral deposit, South Africa. *Journal of the South African Institute of Mining and Metallurgy*, vol. 10, pp. 67–74.

Sahan, R. A. & Kozanoglu, B. 1997. Use of an air-fluidized bed separator in a dry coal cleaning process. *Energy Conversion and Management*, vol. 38, pp. 269–286.

Sahu, A. K., Biswal, S. K. & Parida. A. 2009. Development of air dense medium fluidized bed technology for dry beneficiation of coal—A review. *International Journal of Coal Preparation and Utilization*, vol. 29, pp. 216–241.

Sample graph of ilmenite forecasts for the next six quarters (Energy & Metals Consensus Forecasts, June 2015). [Online]. Available at: http://www.consensuseconomics.com/Ilmenite_Price_Forecasts.htm access on 14/08/2016. [Cited 14/08/2016]

Scott, G.D. 1960. *Packing of spheres*, Nature (London), vol. 188, pp. 908–911.

Smith, D.A.M. & Whittaker, R.L.G. 1986. The Springs-Witbank coalfield. *Mineral Deposits of Southern Africa,* vol. II. Edited by C.R. Anhaeusser and S. Maske. Johannesburg: Geological Society of South Africa, pp.1969–1984.

Snyman, C.P. 1986. Coal. M.G.C Packing of spheres*. Nature,* vol. 188. *The Mineral Deposits of South Africa.* Edited by M.G.C. Wilson and C.R. Anhaeusser. Council for Geoscience, pp.136–205.

Song, Q., Tsai, S.C. 1989. Flotation of ilmenite using benzyl arsonic acid and acidified sodium silicate. *International Journal Mineral Processing*, vol. 26, pp. 111–121.

Spurr, M.R., Gillard, T.D., and Bell, K. 1986. The Utrecht coalfield of the Northern Natal. *Mineral Deposits of Southern Africa*. vol. II. Edited by C.R. Anhaeusser and S. Maske. Johannesburg: Geological Society of South Africa, pp. 2011–2022.

Svoboda, J. 1994. *The effect of magnetic field strength on the efficiency of magnetic separation, Minerals Engineering*, vol. 7, no. 5/6, pp. 747*.*

Svoboda, J. 2004. *Magnetic Techniques for the treatment of materials,* Johannesburg, South Africa, Kluwer Academic Publishers New York, Boston, Dordrecht, London, Moscow.

Taggart, A.F. 1927. *Gravity concentration*, In *Handbook of mineral dressing*. New York: John Wiley and Sons, pp. 1–140.

Tang, X., Hu, K.A. 2006. The formation of ilmenite $FeTiO_3$ powders by a novel liquid mix and H_2/H_2O reduction process. *Journal of Materials Science*, vol. 41, pp. 8025–8028.

Tao, T., Glushenkov, A.M., Liu, H.W., *et al.* 2011. Ilmenite $FeTiO_3$ nanoflowers and their pseudocapacitance, *Journal of Physics Chemistry* C, vol. 115, pp. 17297–17302.

Tarling, D.H. & Hrouda, F. 1993. *The magnetic anisotropy of rocks*. London: Chapman & Hall, pp.217.

Tromp, K.F. 1937. New methods of computing the washability of coals. *Gluckauf*, vol. 73, pp. 125–131.

Truong, Q.D., Liu, J.Y., Chung, C.C., Ling, Y.C. 2012. Photocatalytic reduction of CO2 on $FeTiO_3/TiO_2$ photocatalyst, *Catalysis Communications*, vol. 19, pp. 85–89.

U.S. Geological Survey (USGS) Titanium, 2017. *USGS Mineral Commodity Summaries*, pp.176–179.

Van Ommen, J.R. & Ellis, N. 2015. Particle mixing and separation in a binary solids floating fluidized bed. *Powder Technology*, vol. 147, no. 3–4, pp. 178–186. [Online]. Available at: http://dx.doi.org/10.1016/j.fuel.2016.01.006. [Cited 04/04/2016].

Wei, L., Chen, Q. & Liang, C. 1996. Study on the mechanisms of coarse material separation in the air-dense medium fluidized bed. *Journal of China University of Mining and Technology*, vol. 25 (1), pp.12–18.

Wei, L., Chen, Q. & Zhao, Y. 2003. Formation of double-density fluidized bed and application in dry coal beneficiation. *Coal Preparation*, vol. 23, pp. 21–32.

Wills, B. A. 2016. *An Introduction to the practical aspects of ore treatment and mineral recovery*, Amsterdam ; Boston, MA : Elsevier, pp. 496.

Wilson, M.G.C. & Anhaeusser, C.R. (eds.). 1998. *The mineral resources of South Africa*. Pretoria: Council for Geoscience, pp. 740.

Xiong, D.H. 1994. New development of the SLon vertical ring and pulsation HGMS separator. *Magnetic Electric*, pp. 211–222.

Xiong, D.H. 2004. SLon magnetic separators applied in the ilmenite processing industry. *Physical Separation Science Engineering*, vol. 13, no. 3–4, pp. 119–126.

Yang W.C. 2003. *Handbook of fluidization and fluid-particle systems.* Edited by W.C. Yang. UK: Siemens Westinghouse Power Corporation, pp. 851.

Yang, Z, Tung, Y., Kwauk, M. 1985. Characterizing fluidization by the bed collapsing method. *Chemical Engineering Communications*, vol. 39, pp. 217–232.

Zeng, W., & Dahe, X. 2003. The latest application of SLon vertical ring and pulsating high-gradient magnetic separator. *Minerals Engineering*, vol. 16, no. 6, pp. 563–565.

Zhao, Y., Li, G., Luo, Z., Zhang, B., Dong, L., Liang, C., & Duan, C. 2017. Industrial application of modularized dry coal beneficiation technique based on a novel air dense medium fluidized bed. *International Journal of Coal Preparation and Utilization*, DOI: 10.1080/19392699.2015.1125344.

Zhao, Y., Zhang, B., Luo, Z., He, J., Dong, L., Peng, L., Cai, L. 2015. Effect of lump coal shape on separation efficiency of gas-solid fluidized bed for dry coal beneficiation. *Procedia Engineering*, vol. 102, pp. 1123–1132.

Zhenfu, L., & Qingru, C. 2001. Dry beneficiation technology of coal with an air dense-medium fluidized bed. *International Journal of Mineral Processing*, vol. 63, no. 3, pp. 167–175.

Zheng, S. 2016. Large-scale high separation precision air dense medium dry coal beneficiation system. *XVIII International Coal Preparation Congress*, Saint-Petersburg, Russia.

Zhou, F., Kotru, S., Pandey, R.K. 2003. Nonlinear current-voltage characteristics of ilmenite-hematite ceramic. *Materials Lett*ers, vol. 57, pp. 2104–2109.

Zhu, Q., 2014. Coal sampling and analysis standards. *IEA Clean Coal Centre*, London United Kingdom, pp. 123.

8 APPENDICES

8.1 Appendix 1 Summary of coal quality in the South African coalfields (Jeffrey, 2005)

Coalfield	Coal quality
Limpopo (Tuli)	"The washed coal characteristics indicate yields of 53–47% with ash values of 12–10%, volatiles of 35,5–36,5%, sulphur of ~ 1,1%, and swelling indices of 8,0–8,5 (Ortlepp,1986)."
Waterberg (Ellisras)	"Little information is published regarding the overall coal qualities of the Waterberg (Ellisras) Coalfield, although it is known that the coal rank increases steadily from west to east. It must be assumed that qualities observed at GCM are potentially representative of the entire coalfield (de Jager,1986)."
Soutpansberg	"The Soutpansberg Coalfield is known to have some hard coking, but little other quality information is available."
Springbok Flats	"Analysis of coal qualities in the Springbok Flats Coalfield has resulted in the establishment of a well-defined CV to ash relationship. The linear relationship has been found at all fractional yields, and this is very useful regarding exploration (Christie,1989). Down-hole geophysical methods can be used not only to identify coal seams within the coal zone but also to determine ash and CV values for the identified seams in each borehole. Sulphur content in raw coal ranges from 2% to 4% and averages ± 1,5% in the beneficiated product."
Witbank	"In some areas of the Witbank Coalfield, the No. 1 Seam is a source of high-grade steam coal suitable for export after beneficiation (Smith, Whittaker & Snyman, 1986). According to Barker (1999), the No. 1 Seam often has very low phosphorus content, and in such cases, it is frequently mined separately as metallurgical feedstock. The No. 2 Seam contains some of the best quality coal. It displays

	well-defined zoning with up to seven (five in some areas) distinct coal zones of different coal quality with the three basal zones being mined mainly for the production of low-ash metallurgical coal and export steam coal. The upper part of the seam is shaly and unmineable; selective mining takes place within the better quality lower part of the seam (Smith & Whittaker, 1986). The No. 4 Seam is typical of poor quality and consists of predominantly dull to dull lustrous coal with the upper portion being of poor quality. Mining is thus restricted to the lower 3,5 m portion of the coal seam, which is mainly used as a power station feedstock and as domestic steam coal (Smith & Whittaker, 1986). The No. 5 Seam has been mined as a source of blend coking coal and for metallurgical uses, especially in the central Witbank area where it is of higher quality (Smith & Whittaker, 1986)."
Free State	"The Free State Coalfield's Bottom Seam is of low-grade steam coal with poor washing characteristics. The Top Seam comprises lustrous coal with bright stringers and is of better quality than the Bottom Seam (Gilligan, 1986)."
South Rand	"The South Rand's No. 2 Seam is composed mainly of dull coal, but with relatively constant coal quality throughout the seam (Henderson, 1986). The Ryder Seam is generally of low quality with a CV of about 18 MJ/kg and is prone to spontaneous combustion (Henderson & Snyman, 1986)."
Highveld	"The No. 2 Seam contains low-grade bituminous coal with an ash content of 22–35% and a CV of 20–23 MJ/kg. In areas where the No. 2 Seam is of better quality and has excellent washability characteristics, like in Leandra, a coal product of 27 MJ/kg at yields of greater than 70% can be produced. The No. 4 Seam contains mainly low-grade bituminous coal with an ash content of 20–35% and a CV of 18–25 MJ/kg. However, the ash content can increase to 40%, and CV can drop to 15 MJ/kg in the upper one to two meters. In areas

	where the seam is much thicker, the ash can be as low as 21% with the CV about 23 MJ/kg in the lower three to four meters of the seam (Jordaan, 1986). The No. 4 Upper Seam quality is extremely variable, but the seam contains low-grade bituminous coal with approximately 25% ash content and a CV of 22 MJ/kg (Jordaan, 1986)." "The No. 5 Seam has better quality coal than the other seams, with a raw in-situ CV of > 25 MJ/kg, ash and volatile matter contents of 19% and 32% respectively. It can be a source of metallurgical coal, such as is mined at the No. 2 Mine at Kriel Colliery (Barker, 1999)."
Ermelo	"The Ermelo Coalfield's E Seam is of reasonable quality, but the economic potential of the seam decreases southwards as it becomes torbanitic and shaly, whereas in other areas it might be too thin to be viable for mining (Greenshields, 1986). The D Seam is of high quality and has no clastic partings but has a significant proportion of vitrain with minor durain bands (Greenshields & Snyman, 1986). The C Lower Seam is an essential seam, as it is the primary source of export coal (Barker, 1999). The C Upper Seam is generally of poorer quality, has no in-seam partings and may be torbanitic in the upper part; however, the lower part of the seam is usually of high quality, making it the main target for mining. It is typically mined to supplement the C Lower (Snyman, 1986 & Barker, 1999). The B Seams are low quality, dull coal that contains fewer vitrain bands compared with the lower portion of the C Upper Seam (Greenshields, 1986)."
Klip River	"The Bottom Seam in the Klip River Coalfield (equivalent to the Gus Seam) is high in sulphur and phosphorus, with sulphur usually ranging from 1,3 to 1,8% (Bell & Spurr, 1986b and Snyman, 1986). The Top Seam (corresponding to the Alfred Seam) has a smaller bright coal proportion than the Bottom Seam, but like the Bottom Seam, the rank of the Top Seam ranges from bituminous to anthracitic with generally high sulphur and phosphorus content

	(Snyman, 1986). In general, the Klip River Coalfield contains bright coal with the rank ranging from bituminous to anthracite; in the central part of the coalfield, good coking coal has been produced in the past."
Utrecht	"In the Utrecht Coalfield, the seams have been a primary source of moderately good coking coal and require little beneficiation (Spurr, 1986). The Lower Dundas Seam rank varies from medium volatile bituminous to anthracitic, with the coal mined as a source of bituminous coal in the northeastern sector of the coalfield and as anthracite in the southern sector".
	"However, the sulphur content can be high—more than one percent (Spurr, 1986). The Gus Seam is subdivided into three coal quality zones with the upper part comprising mainly dull coal, the central part predominantly bright coal and the bottom section mainly poor-quality coal with shale partings. The seam has elevated methane gas concentration (Spurr & Snyman, 1986). The Alfred Seam is of better quality in the Utrecht Coalfield, particularly towards the bottom portion of the seam. The seam is high in ash and sulphur content, but beneficiation can produce relatively large quality, low ash coal with low sulphur and phosphorus (Snyman, 1986)."
Vryheid	"In the Vryheid Coalfield of KwaZulu-Natal, the Coking Seam is high-grade bright coal with excellent coking properties at the average rank and commonly contains very low ash of between seven and eight percent (Bell & Spurr, 1986a). The Lower Dundas Seam is mined as coking or steam coal in the Vryheid Coalfield (Bell & Spurr, 1986a). Good quality coke has been produced from the Gus Seam in the Vryheid Coalfield, where it is unaffected by dolerite intrusions, and high-quality anthracite, where the seam has been metamorphosed (Bell & Spur, 1986a). The Alfred Seam (Vryheid Coalfield) is of low grade with an average CV of 26–27 MJ/kg, the ash content of 16–35% and poor coking properties. The Fritz Seam is generally of

	relatively high grade, but high sulphur content and is usually mined together with other seams in opencast operations (Bell & Spur, 1986a)."
Nongoma	"The A coal zone in the Nongoma Coalfield has a thin A1 Seam and a thicker A2 Seam with raw ash values of between 33–42%. Anthracite occurs in the lower A Zone (Snyman, 1986). The B Zone consists of four seams with raw ash values of 25%; anthracite occurs in the upper part of the B Zone. Plant-scale wash tests on the Somkhele project indicate the anthracite is of high quality with a significant reactive component, low to medium ash, low phosphorus calcium oxide in the ash and low sulphur."
Molteno-Indwe	"Only the Indwe, Guba and the Molteno seams in the Molteno-Indwe Coalfield have economic potential in places; however, they are mainly of poor quality. Analyses show that the Indwe and Guba seams have high ash content of 31–51% unwashed and between 26–27% when washed, high moisture content of 7–11%, low volatile matter (VM) of 7–12% and a CV of 23,9–25,9 MJ/kg (Prevost, 2002)."

8.2 Appendix 2 Summary of ilmenite minerals reserve across South Africa (Wilson & Anhaeusser, 1998)

Provinces	Location	Characteristics	Reserves
KwaZulu-Natal Province	Cape Vidal	The dune sand consists of quartz grains, shell fragments and the heavy minerals ilmenite (3,20%), rutile (0,34%), zircon (0,74%) and leucoxene.	About 104 Mt of ore-grade sand.
	St Lucia and Tojan	The sand consists mainly of quartz grains, some shell fragments and the fragments and the heavy minerals ilmenite (3,2%), rutile (0,34) and leucoxene.	Deposit 351 Mt of ore- grade sand.
	Zululand Titanium (reserve No.4) North of Richards Bay	About 10% of the sand consists of heavy minerals composed of 6,08% ilmenite, 0,28% rutile and 0,83% zircon	Deposit 199 Mt of ore-grade sand.
	Richards Bay	The heavy mineral suite, about 70% of which is of economic value, consists of ilmenite (4,77%), rutile (0,28%), zircon (0,53%), leucoxene, magnetite, minor monazite, augite, hornblende and almandine garnet.	Deposit 770 Mt of ore to last until the end of the century.
	Port Durnford (ISCOR's Hillendale)	Heavy-mineral sand containing 4,77% ilmenite, 0,28% rutile and 0.53% zircon.	Deposit 450 Mt of heavy mineral sand.
	Zululand Titanium (Reserve No.10 or Mtunzini State Forest)	Sand contains 18,84 Mt of ilmenite, 2,37 Mt of zircon and 1,11 Mt of rutile.	Deposit 395 Mt of heavy- mineral sands.
	Umgababa	The sand, which consists mainly of quartz rains and subordinate feldspar, contains just over 11% heavy minerals, including (9%), rutile ((2%), zircon, garnet and tracers of monazite.	Not yet quantified.

| Provinces	Location	Characteristics	Reserves
Eastern Cape Province	Xolobeni	Ilmenite (3%)	Sand reserve is estimated to be as high as 500 Mt, of which 300 Mt may contain some 3% ilmenite.
	Mngazana	3,85% ilmenite, 0,16% rutile and 0,21% zircon	Reserve of 10 Mt.
	Bowker (Cede Deposit)	5,78% ilmenite, 0,26% rutile and 0,49% zircon	Reserve of 7.5 Mt.
	Sandy point	Ilmenite (5,2%), rutile (0,2%) and zircon	Sandy deposits 150 Mt, containing 17,5 Mt, ilmenite, 0.5 Mt rutile and 1,2 Mt zircon.
	Wavecrest	Ilmenite (6,1%), rutile (0,23%) and zircon	Reserve of 164,7 Mt.
	Kobonqaba	Ilmenite (5.0%) and rutile (0,2%)	Estimated a reserve 90 Mt of sand.
	Morgan Bay	Ilmenite (2,8%), rutile (0,14%) and zircon	Deposit of 64 Mt of unconsolidated Aeolian sand.
	Continental shelf	Ilmenite	Viable deposit.
	Nickolas	Ilmenite (3,26%), rutile (0,15%) and zircon	Resource of 64 Mt of sand.

Provinces	Location	Characteristics	Reserves
Northern Cape Province	Namaqua Sands (Graauw Duinen)	Grading at 9% total heavy minerals	Reserves of 530 Mt, lifetime of 35 years.
	Roode Heuwel	Ilmenite 11,9%, rutile 7,9% and zircon 0,7%	Not yet quantified.
	Soutfontein	Ilmenite 8,8%, rutile 0,1% and zircon 1,8%	Not yet quantified.
	Alexander Bay		Estimated resource of 324 000 t of ilmenite, 7 000 t of rutile, 13 000 t of zircon and 5 000 t of monazite.

| Provinces	Location	Characteristics	Reserves
Northern Province	Rooiwater	8% to 9% ilmenite	Eastern and Western deposits, containing 50 and 8 Mt of ore.
	Waterberg Group	Contain 50 to 60% of ilmenite and 2 to 10% zircon	Not yet quantify
Provinces	**Location**	**Characteristics**	**Reserves**
North West, Free State, Mpumalanga Provinces	Karoo Supergroup		Deposits of 96,55 Mt.

8.3   Appendix 3 XRD of coal samples
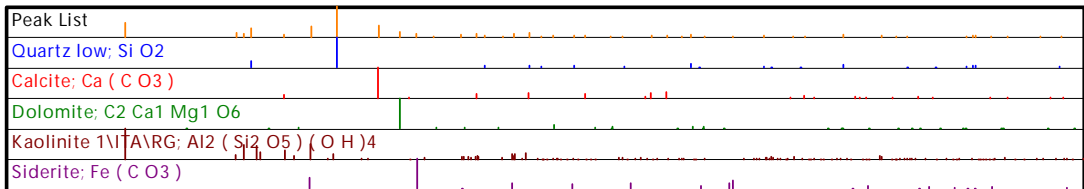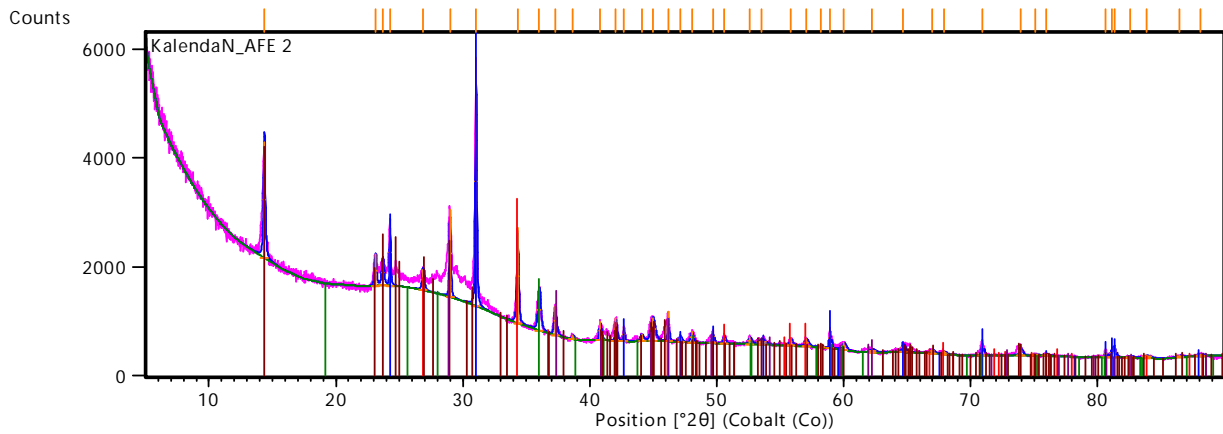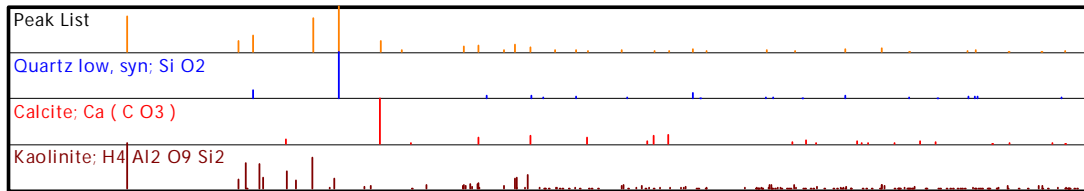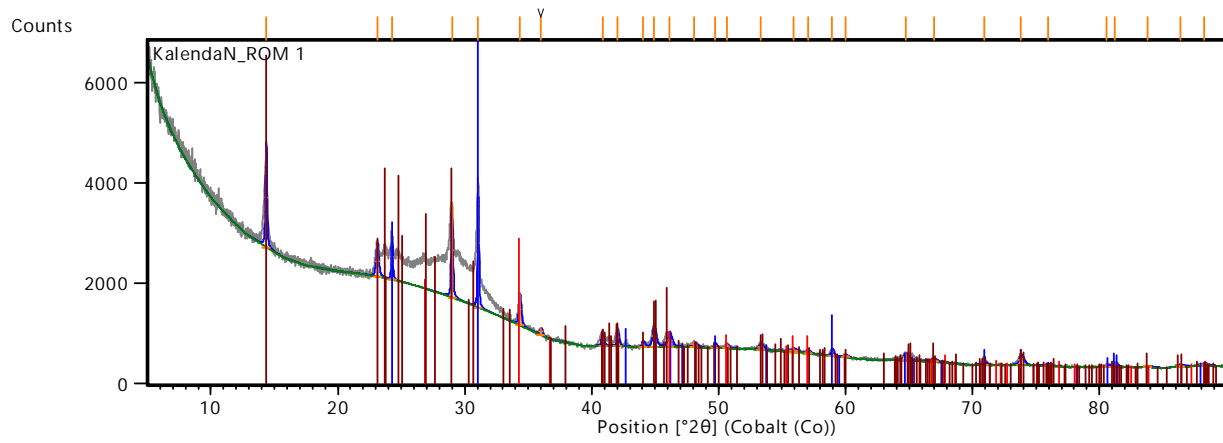
8.4   Appendix 4 Particle size distribution of coal samples

| Sample ID		Coal ROM			Coal AFE		
Total weight Sample (g)		1001,23			1002,9		
Sample loss		1,23			1,4		
Log Size	Sieve Size (um)	Weight (g)	Mass %	Cumulative Passing %	Weight (g)	Mass %	Cumulative Passing %
4,57	37500	-	-	100	-	-	100
4,42	26500	523,89	52,39	47,61	221,22	22,09	77,91
4,28	19000	214,10	21,41	26,20	386,73	38,61	39,30
4,12	13200	182,99	18,30	7,90	266,98	26,66	12,64
3,98	9500	30,95	3,10	4,81	66,45	6,63	6,00
3,83	6700	11,01	1,10	3,71	11,56	1,15	4,85
3,68	4750	5,42	0,54	3,16	5,36	0,54	4,31
3,53	3350	4,30	0,43	2,73	5,38	0,54	3,78
3,37	2360	3,16	0,32	2,42	3,87	0,39	3,39
3,07	1180	5,41	0,54	1,88	6,48	0,65	2,74
	Pan	18,77	1,88	-	27,47	2,74	-
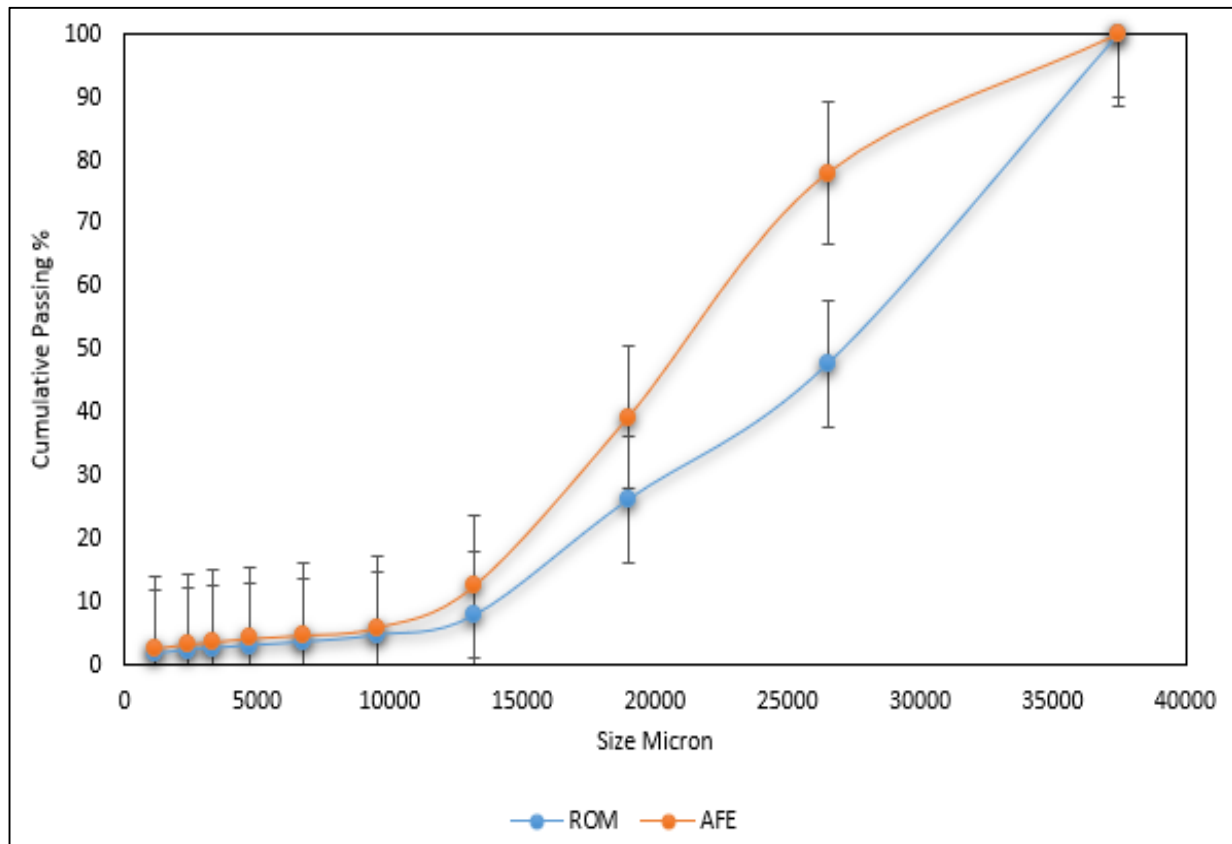
## 8.5   Appendix 5 XRD analysis of ilmenite samples
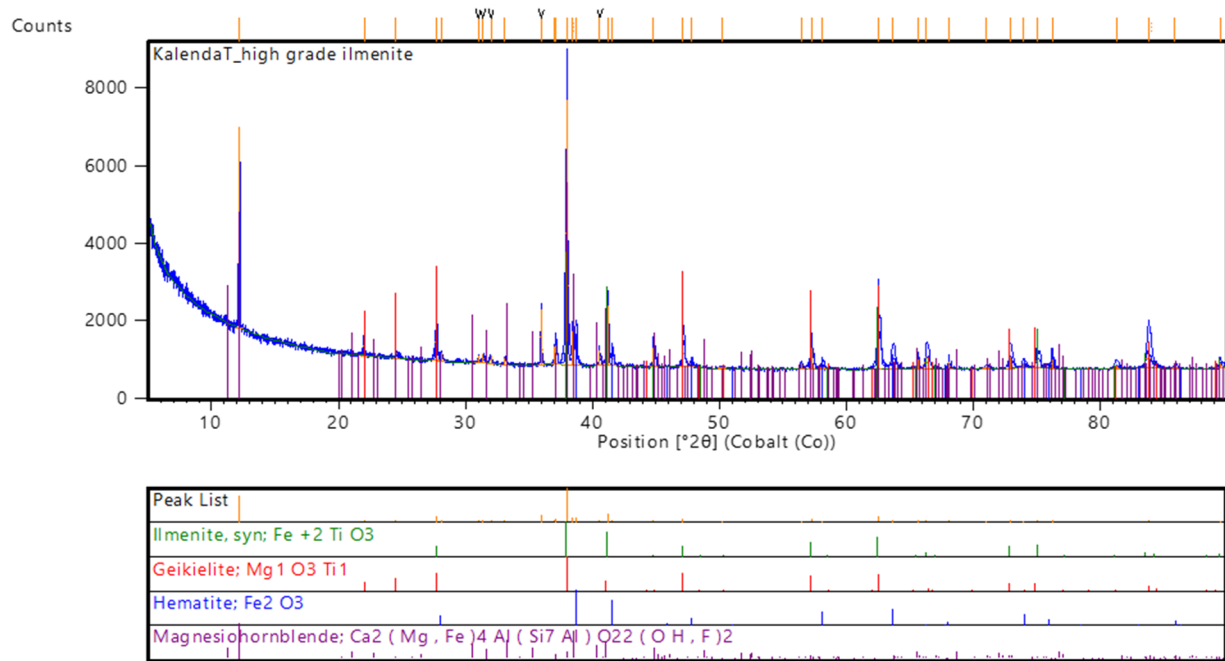
8.6 Appendix 6 Scanning electron microscopy of ilmenite
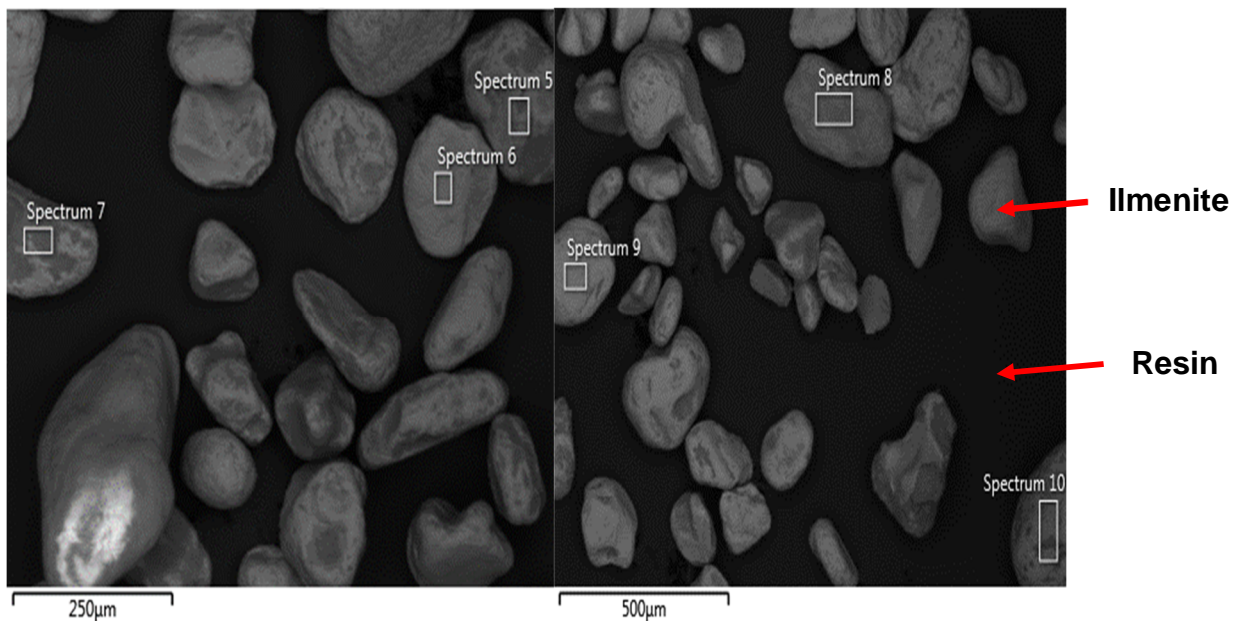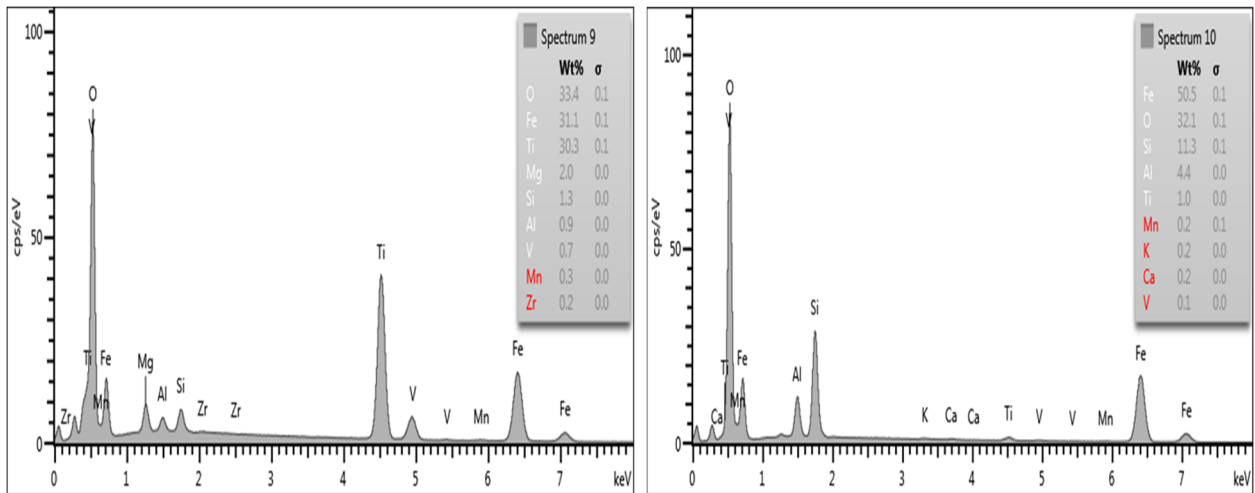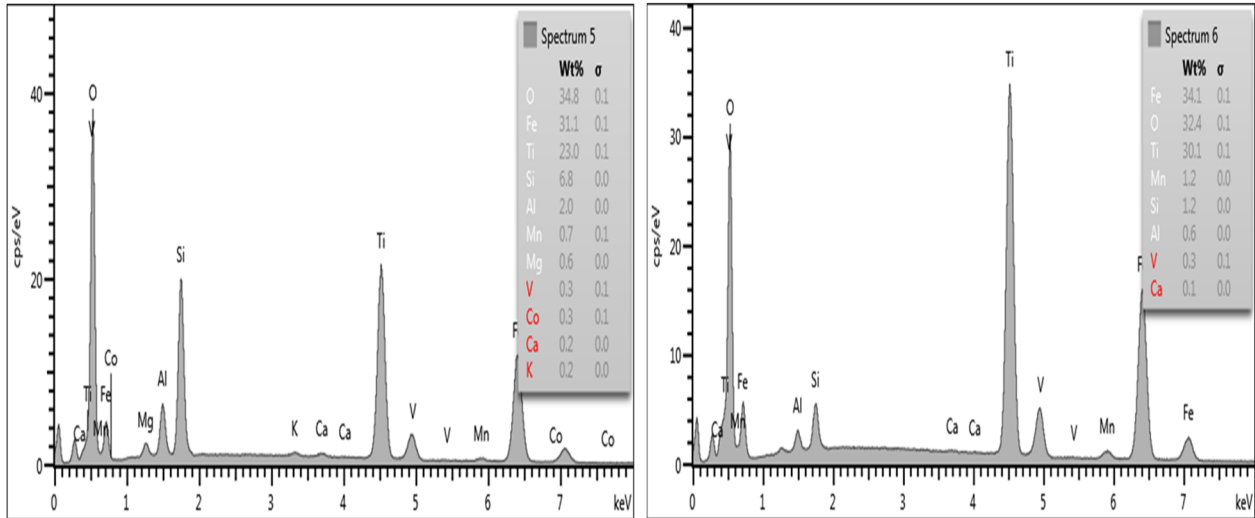
8.7 Appendix 7 Particle size distribution of ilmenite (sieve shaker)

Sieve size in Micron	Log size	Mass (g)			Mass %			Cumulative Passing		
		ILM1	ILM2	ILM3	ILM1	ILM2	ILM3	ILM1	ILM2	ILM3
355	2,55							100	100	100
250	2,40	5,36	4,55	5,90	0,54	0,45	0,59	99,46	99,55	99,41
180	2,26	113,24	88,82	83,04	11,32	8,86	8,29	88,14	90,69	91,12
125	2,10	790,85	800,77	808,89	79,09	79,89	80,77	9,05	10,80	10,35
90	1,95	83,34	99,60	85,48	8,33	9,94	8,54	0,72	0,86	1,82
63	1,80	6,86	8,35	17,62	0,69	0,83	1,76	0,04	0,03	0,06
Pan		0,35	0,31	0,56	0,04	0,03	0,06	0,00	0,00	0,00
	Total	1000,00	1002,40	1001,50	100,00	100,00	100,00			
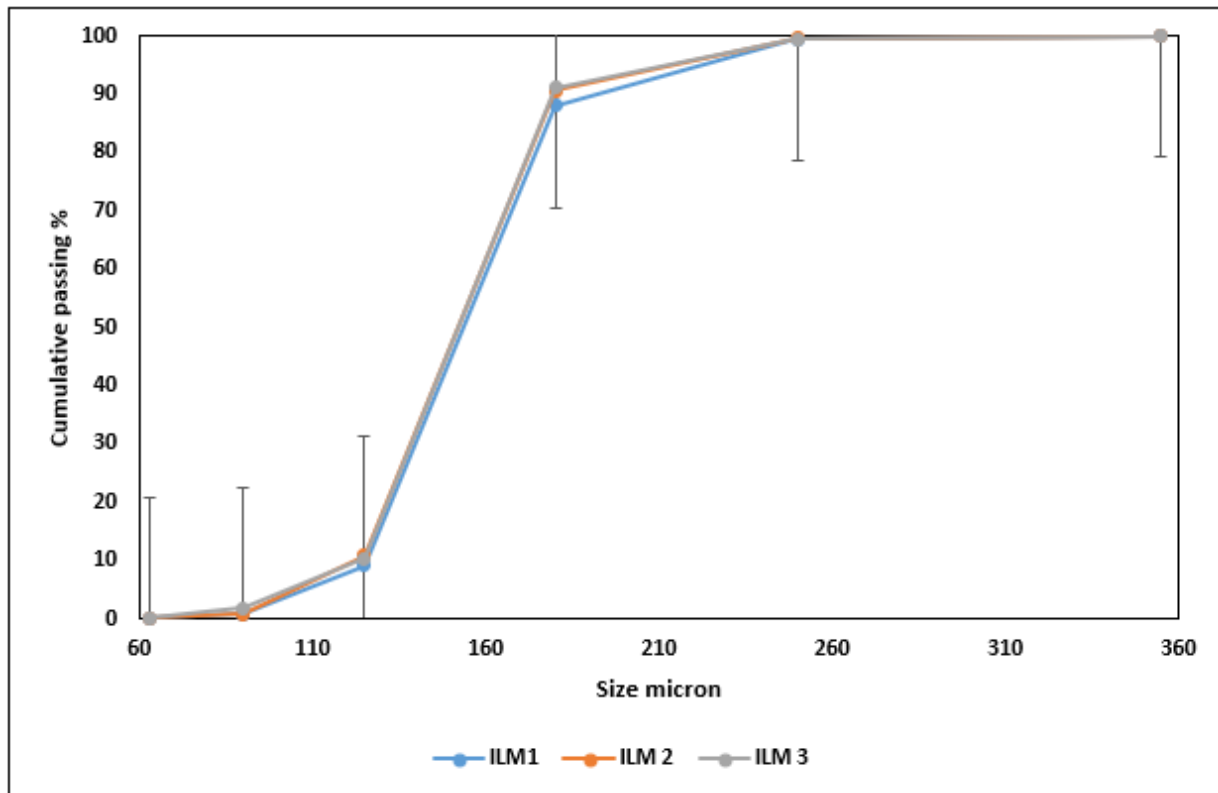
8.8 Appendix 8 Particle size distribution of ilmenite (Malvernsizer)

Log size	Sieve	Cumulative passing %
1,80	63	0,01
1,85	71	0,16
1,90	80	0,95
1,95	89	3,20
2,00	100	7,61
2,05	112	14,85
2,10	126	25,09
2,15	142	37,76
2,20	159	51,75
2,25	178	65,54
2,30	200	77,69
2,35	224	87,20
2,40	252	93,79
2,45	283	97,64
2,50	317	99,53
2,55	356	99,99
2,60	399	100,00
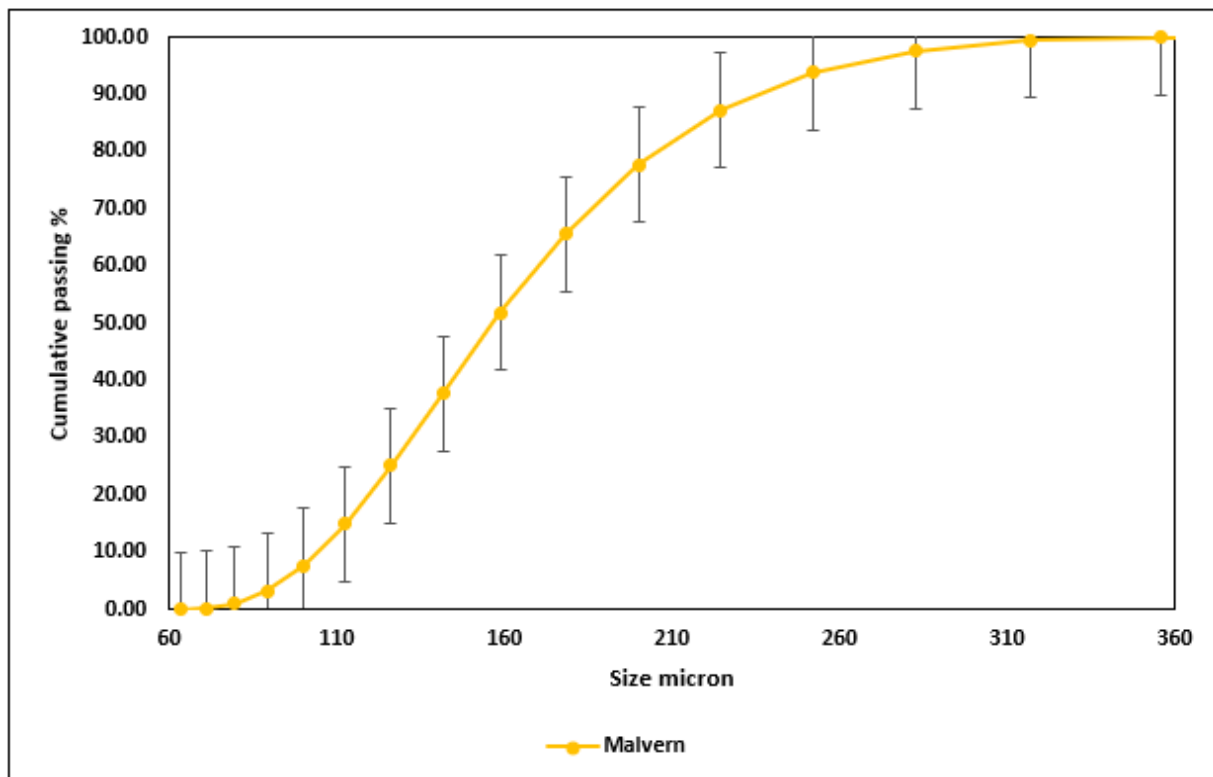
8.9   Appendix 9 Particle size distribution of fine coal

Sieve size in Micron	Log size	Mass (g)			Mass %			Cumulative Passing %		
		FC1	FC2	FC3	FC1	FC2	FC3	FC1	FC2	FC3
300	2,48							100	100	100
212	2,33	203,43	207,69	206,93	20,34	20,82	20,68	79,66	79,18	79,32
150	2,18	248,54	250,82	247,98	24,85	25,15	24,78	54,80	54,03	54,55
106	2,03	182,54	172,93	173,92	18,25	17,34	17,38	36,55	36,69	37,17
75	1,88	183,38	188,43	189,58	18,34	18,89	18,94	18,21	17,80	18,22
53	1,72	100,67	99,66	101,14	10,07	9,99	10,11	8,15	7,81	8,12
Pan		81,45	77,88	81,25	8,15	7,81	8,12			
	Total	1000,00	997,40	1000,80	100,00	100,00	100,00			
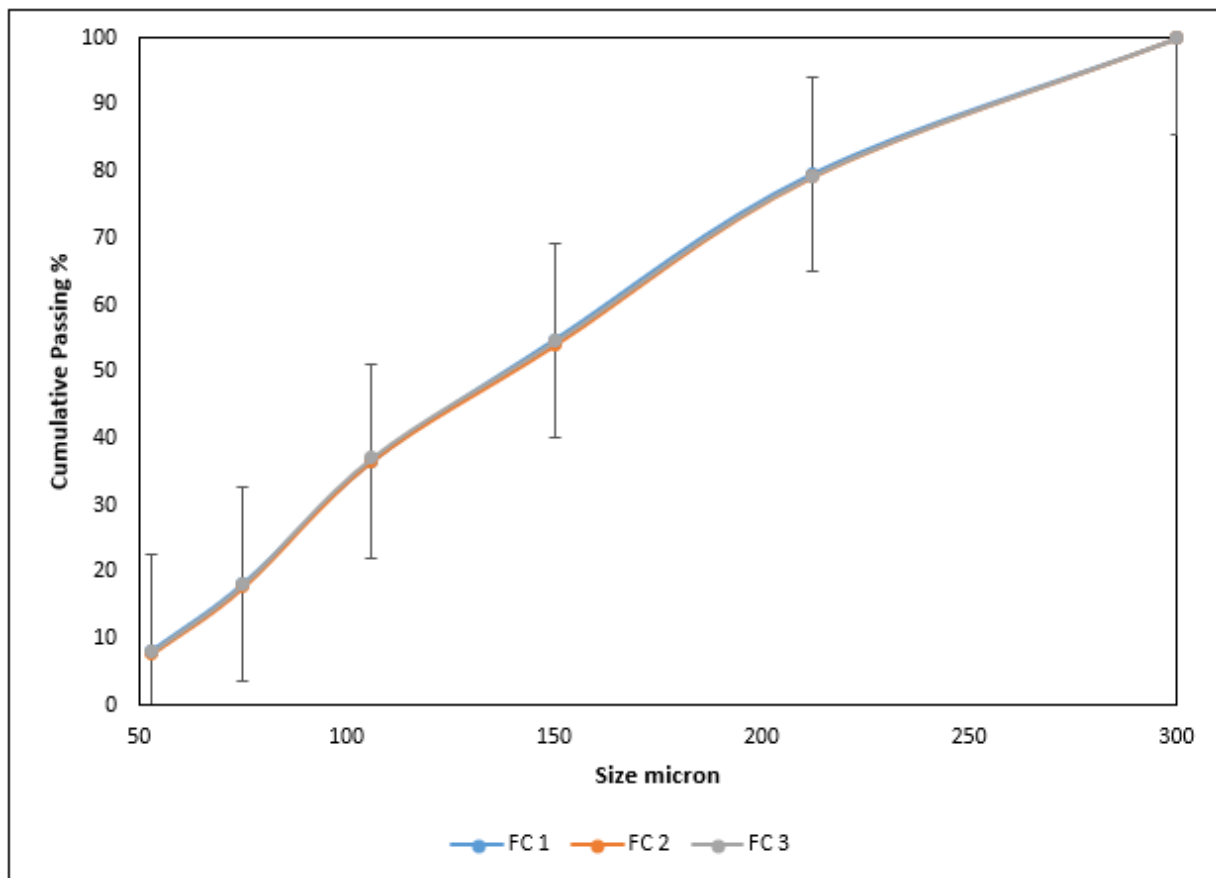
8.10 Appendix 10 Particle size distribution of sand

Sieve size in Micron	Log size	Mass (g)			Mass %			Cumulative Passing %		
		Sand 1	Sand 2	Sand 3	Sand 1	Sand 2	Sand 3	Sand 1	Sand 2	Sand 3
300	2,48							100	100	100
212	2,33	358,47	357,33	360,04	35,85	35,72	35,91	64,15	64,28	64,09
150	2,18	388,70	389,63	389,32	38,87	38,95	38,83	25,28	25,33	25,26
106	2,03	150,30	150,66	150,54	15,03	15,06	15,01	10,25	10,27	10,24
75	1,88	56,15	56,28	56,24	5,61	5,63	5,61	4,64	4,65	4,63
53	1,72	26,52	26,58	26,56	2,65	2,66	2,65	1,99	1,99	1,98
Pan		19,87	19,91	19,90	1,99	1,99	1,98			
Total		1000,00	1000,40	1002,60	100,00	100,00	100,00			
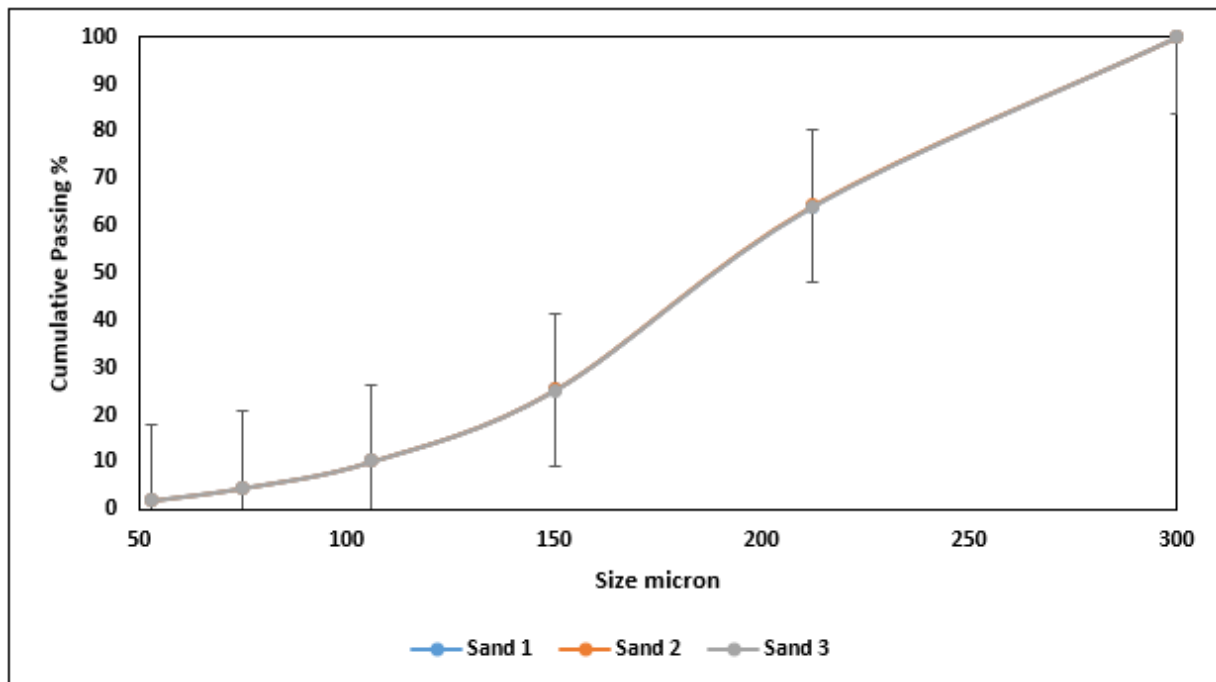
## 8.11 Appendix 11 Superficial gas velocity vs orifice pressure drop
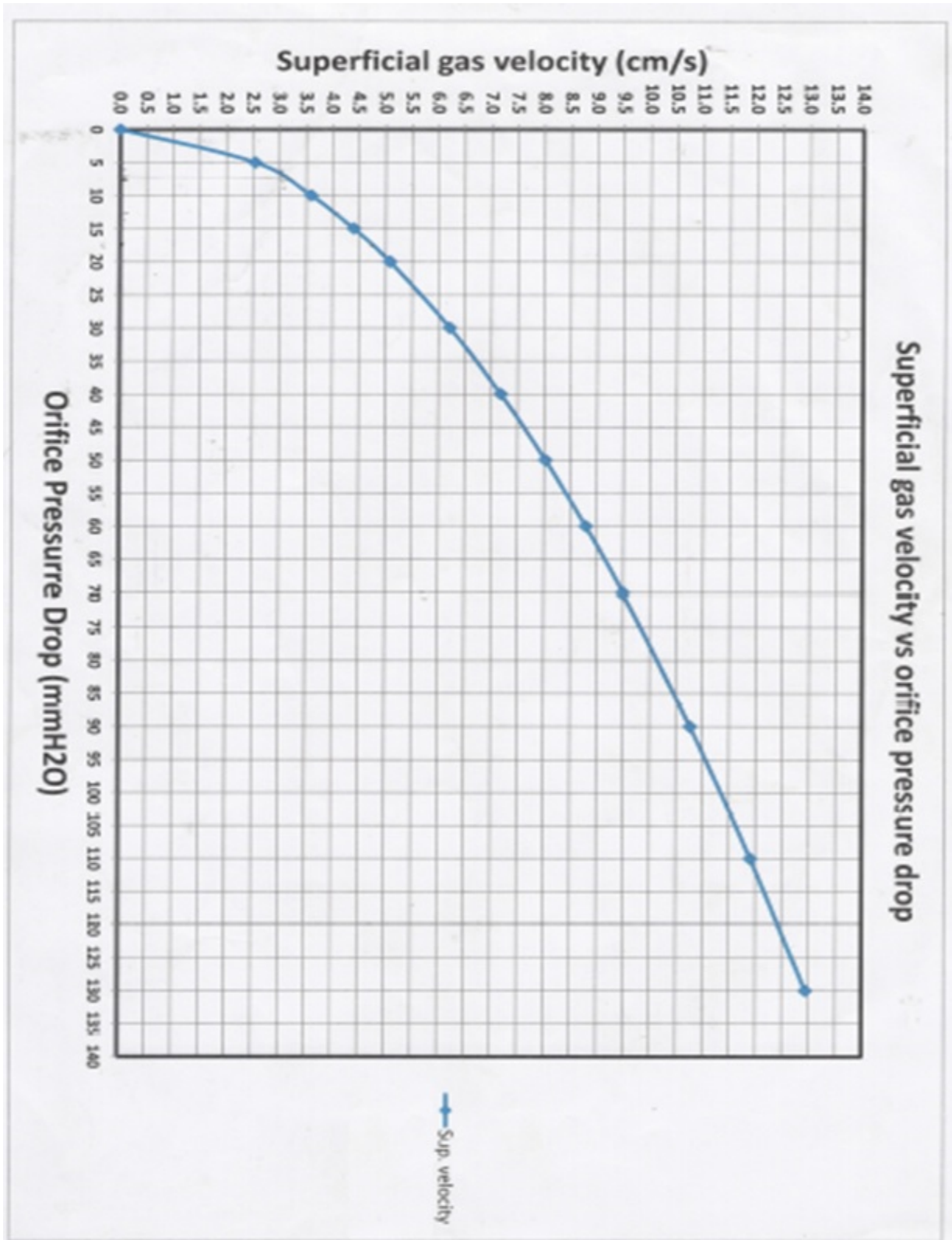
8.12 Appendix 12 Pressure drop as a function of superficial gas velocity of 100% ilmenite medium

Superficial velocity (m/s)	Pressure drop (mH2O)
0,010	0,245
0,015	0,250
0,020	0,255
0,027	0,265
0,030	0,260
0,035	0,260
0,041	0,260
0,046	0,260
0,052	0,260
0,058	0,260
0,068	0,260
0,079	0,260
0,083	0,260
0,092	0,260
0,106	0,260

8.13 Appendix 13 Pressure drop as a function of superficial gas velocity of 100% sand medium

| Superficial velocity (m/s)	Pressure drop (mH2O)
0,015	0,095
0,020	0,100
0,027	0,110
0,035	0,120
0,041	0,128
0,046	0,135
0,052	0,130
0,058	0,130
0,068	0,130
0,079	0,130
0,083	0,130
0,092	0,130
0,106	0,130

## 8.14 Appendix 14 Pressure drop vs minimum fluidization velocity of mixture 30% ilmenite and 70% sand medium

| Superficial velocity (m/s)	Pressure drop (mH2O)
0,027	0,145
0,035	0,155
0,041	0,165
0,046	0,170
0,052	0,170
0,058	0,170
0,068	0,170
0,079	0,170
0,083	0,170
0,092	0,170
0,106	0,170

8.15 Appendix 15 Position of tracers using ilmenite with sand medium in an air dense medium fluidized bed

Sand 20%

Sand 30%

Sand 40%

Sand 50%
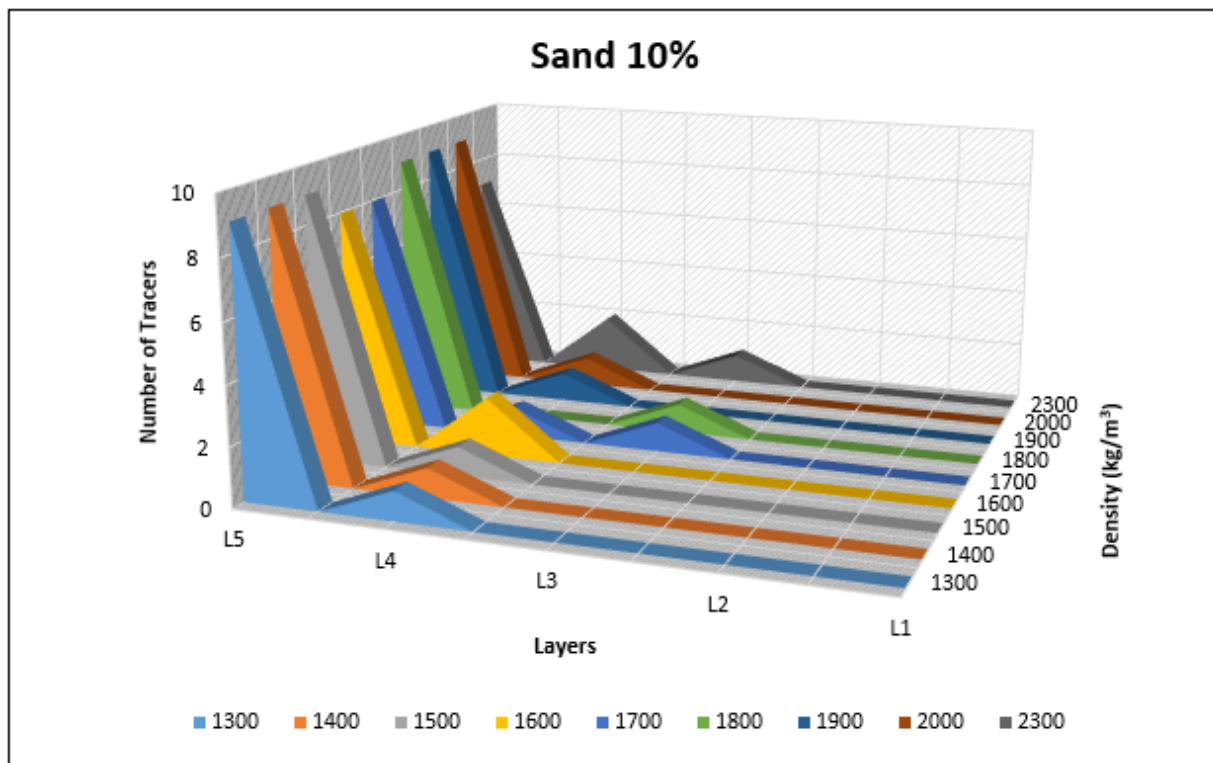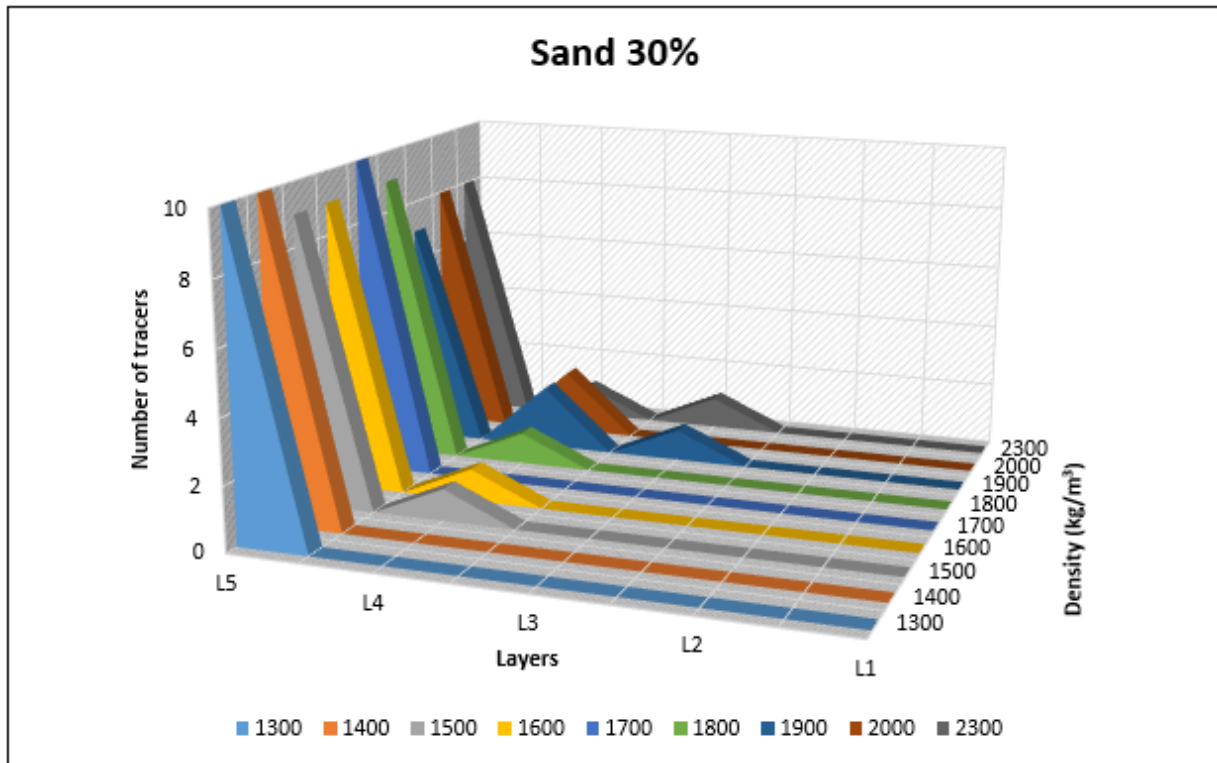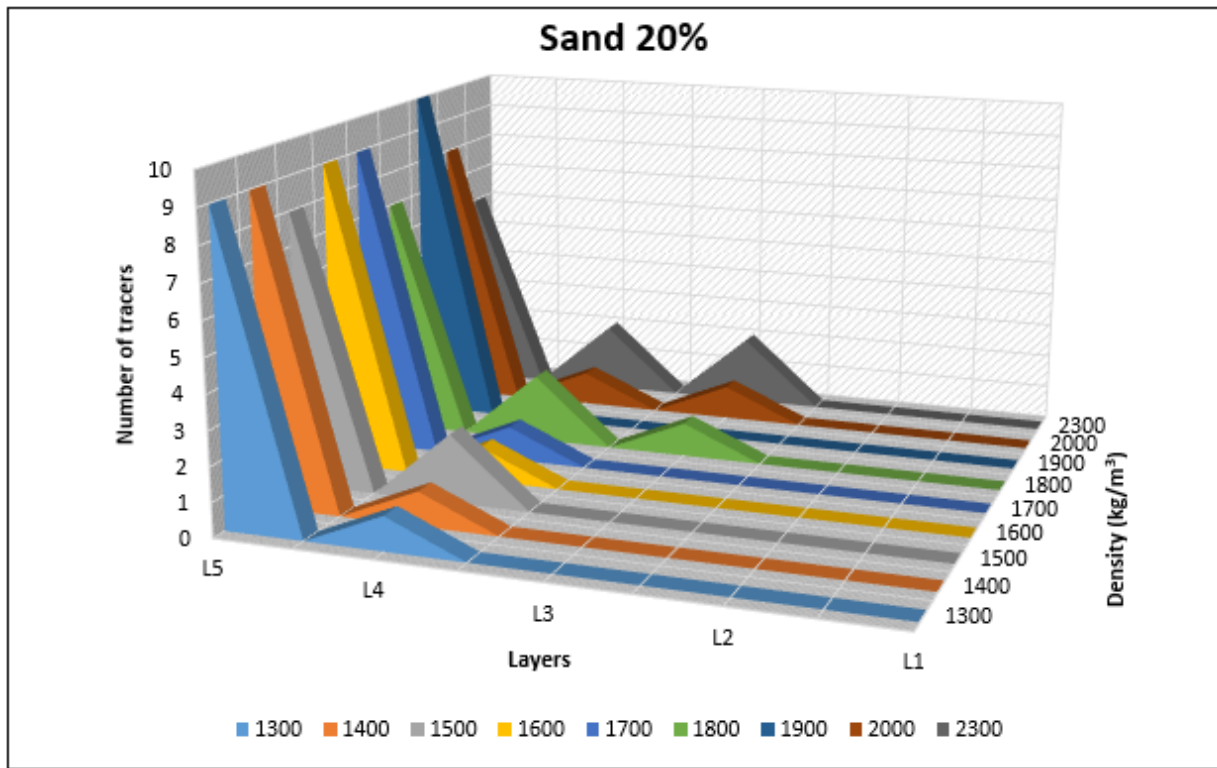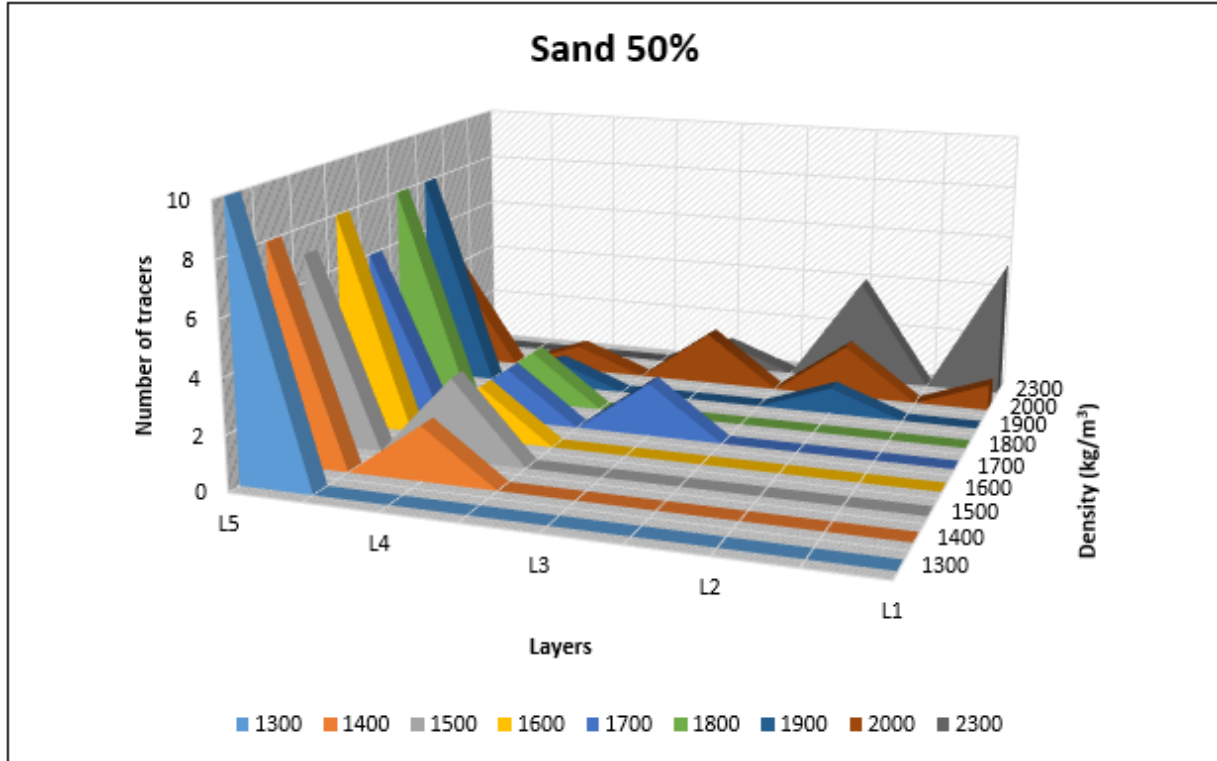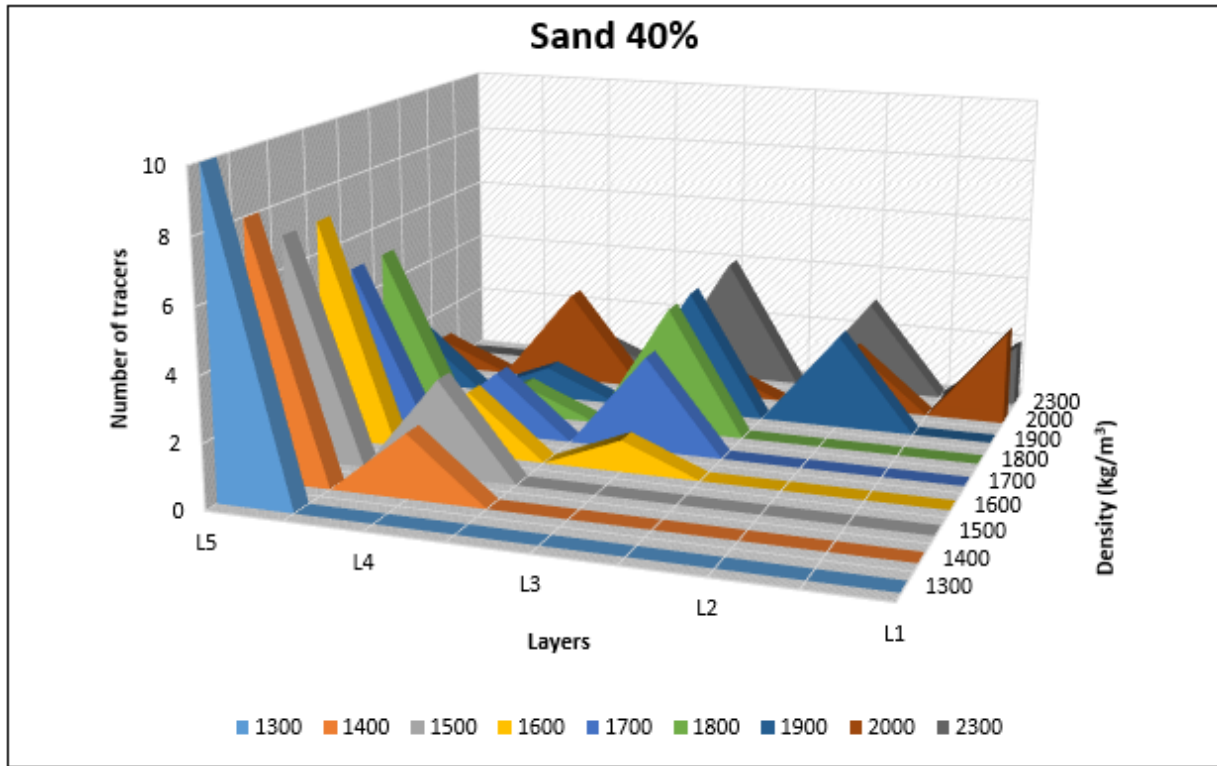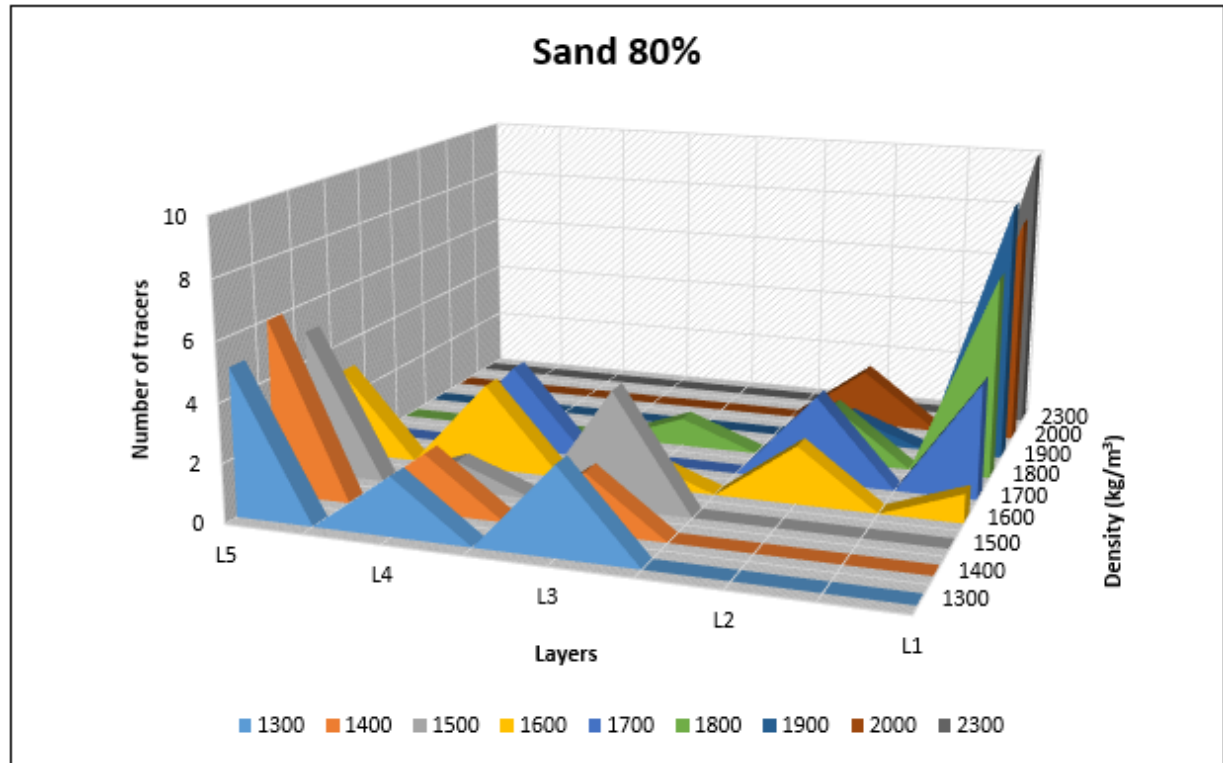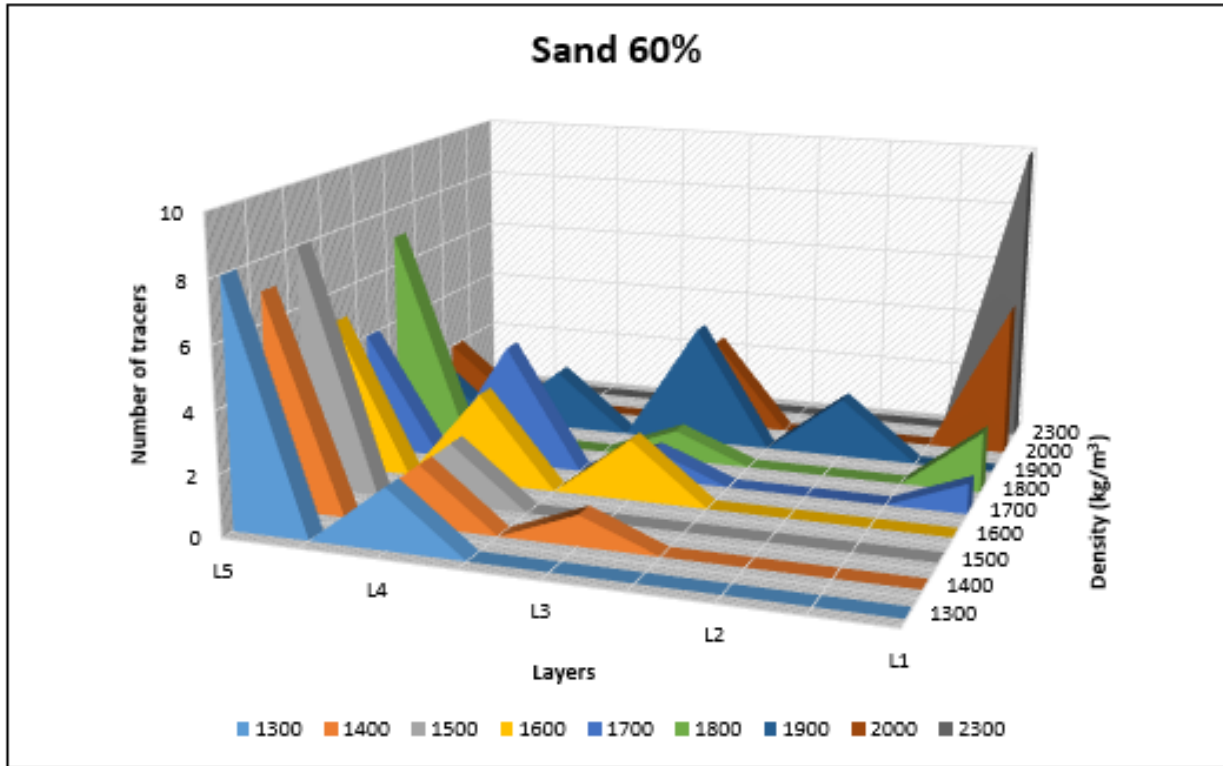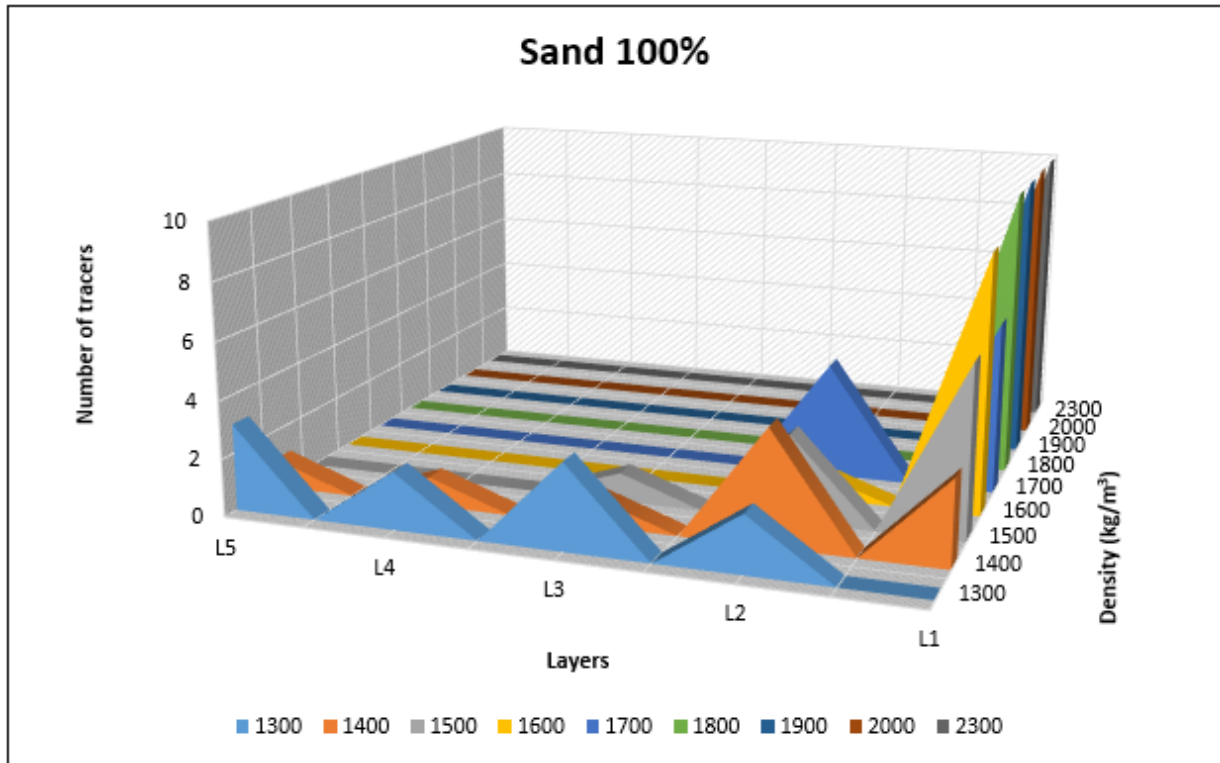
8.16 Appendix 16 Partition curve of mixture ilmenite with sand medium
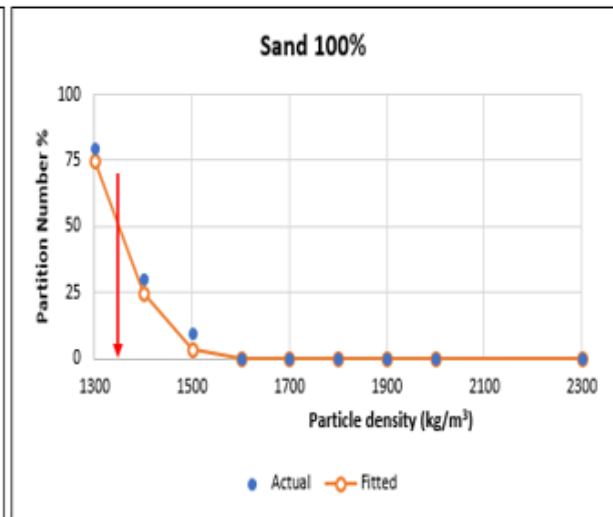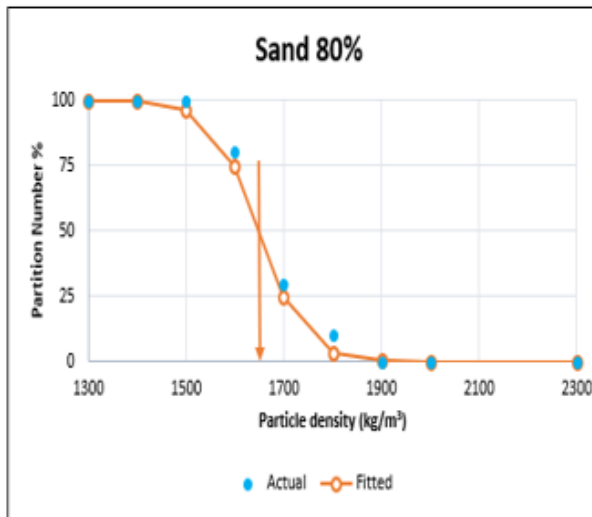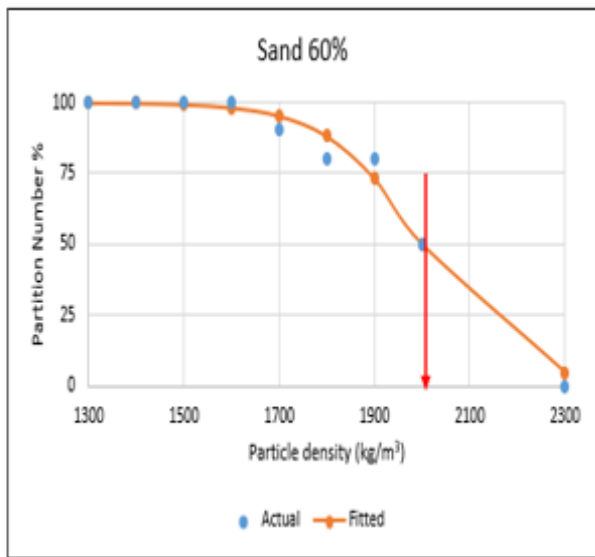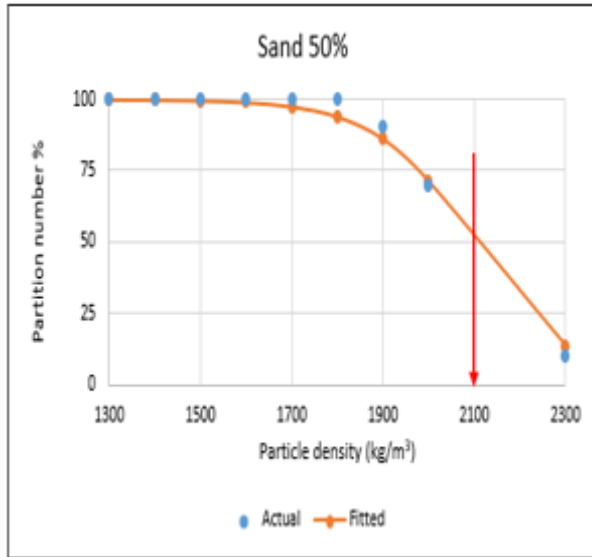
8.17 Appendix 17 Segregation of bed by size of mixture 30% ilmenite and 70% sand medium

| Sample ID					Segregation Ilmenite + Sand							
Total weight Sam		1322,8	1320,9	1095,7	1398	Mass %	Mass %	Mass %	Mass %	Cumul	Cumul	Cumul	Cumul
Sample loss		0,8	0,34	0,1	0,2	feed	Top	Middle	Bottom	Feed	top	Middle	bottom
Sieve	Log size	Feed	Top layer	Middle layer	Bottom layer								
300	2,48									100	100	100	100
212	2,33	240	241,9	202,2	254,3	18,2	18,3	18,5	18,2	81,8	81,7	81,5	81,8
150	2,18	304	304,1	244,2	303,6	23,0	23,0	22,3	21,7	58,9	58,7	59,3	60,1
106	2,03	290	288,6	230,5	307	21,9	21,9	21,0	22,0	36,9	36,8	38,2	38,1
75	1,88	380	380,8	327,6	421,5	28,7	28,8	29,9	30,2	8,2	8,0	8,3	8,0
53	1,72	100	97,1	84,2	101,9	7,6	7,4	7,7	7,3	0,6	0,6	0,6	0,7
pan		8	8,06	6,9	9,5	0,6	0,6	0,6	0,7	0,0	0,0	0,0	0,0
Total weight		1322	1320,56	1095,6	1397,8								
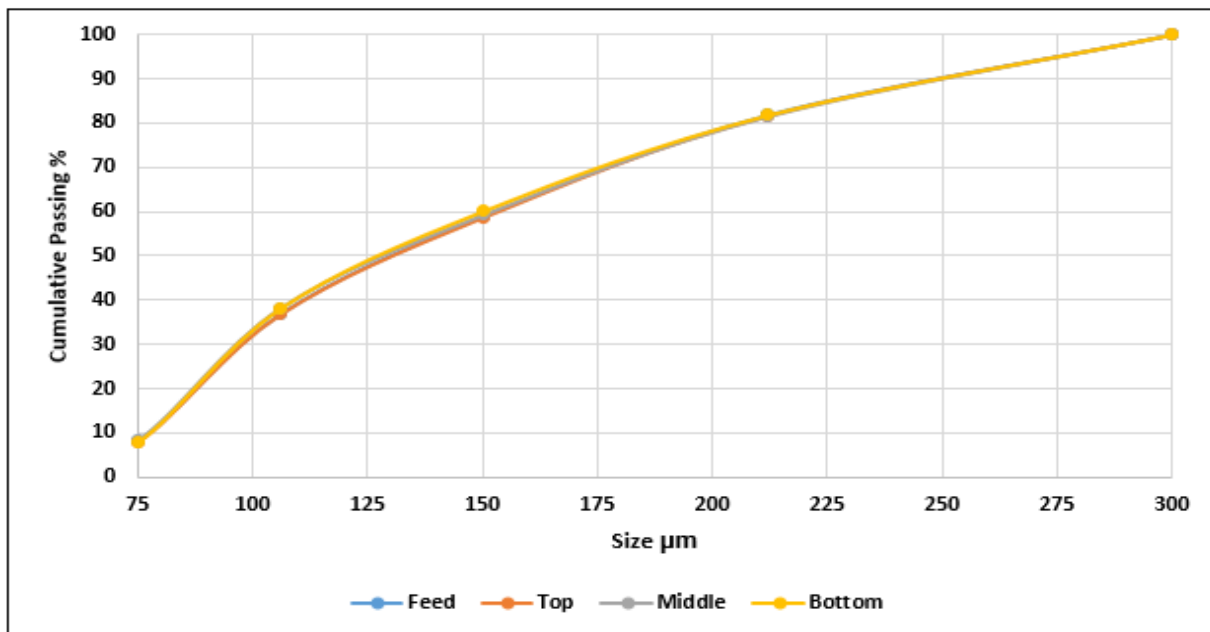
8.18 Appendix 18 Pressure drop as a function of superficial gas velocity of 100% fine coal medium

Superficial velocity (m/s)	Pressure drop (m H2O)
0,005	0,045
0,010	0,050
0,015	0,055
0,020	0,055
0,027	0,055
0,035	0,055
0,041	0,055
0,046	0,055
0,052	0,055
0,058	0,055
0,068	0,055

8.19 Appendix 19 Pressure drop vs minimum fluidization velocity of mixture 40% ilmenite and 60% fine coal medium

Superficial velocity (m/s)	Pressure drop (m H2O)
0,010	0,140
0,015	0,145
0,020	0,150
0,027	0,150
0,030	0,150
0,035	0,150
0,041	0,150
0,046	0,150
0,052	0,150
0,058	0,150
0,068	0,150

8.20 Appendix 20 Position of tracers using ilmenite with fine coal medium in an air dense medium fluidized bed

Fine coal 10%

Fine coal 20%

Fine coal 30%

Fine coal 40%

Fine coal 50%

Fine coal 70%

Fine coal 80%
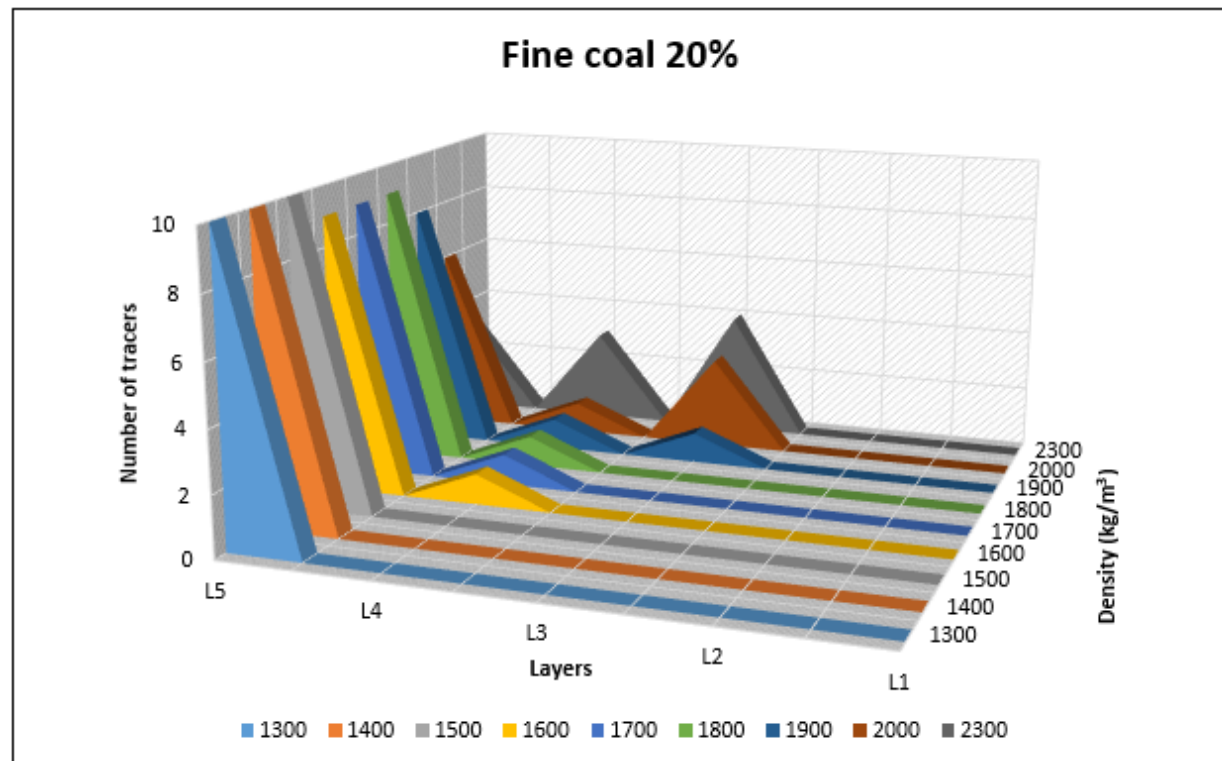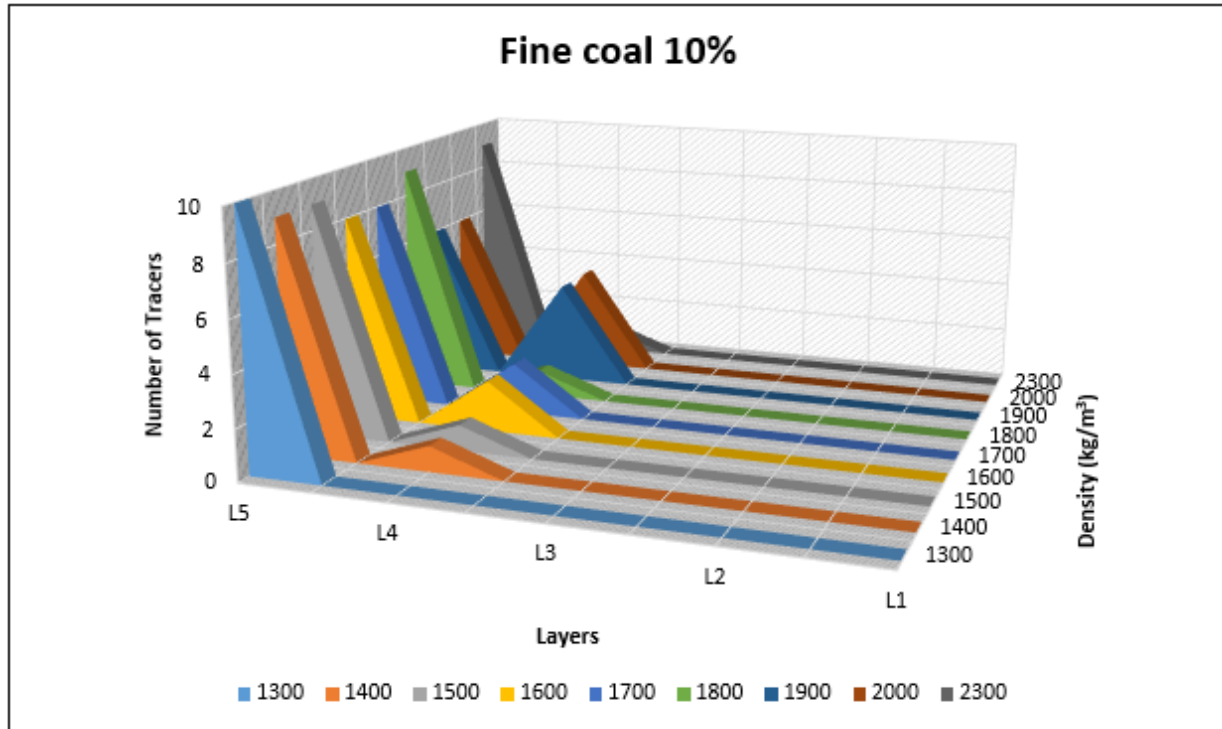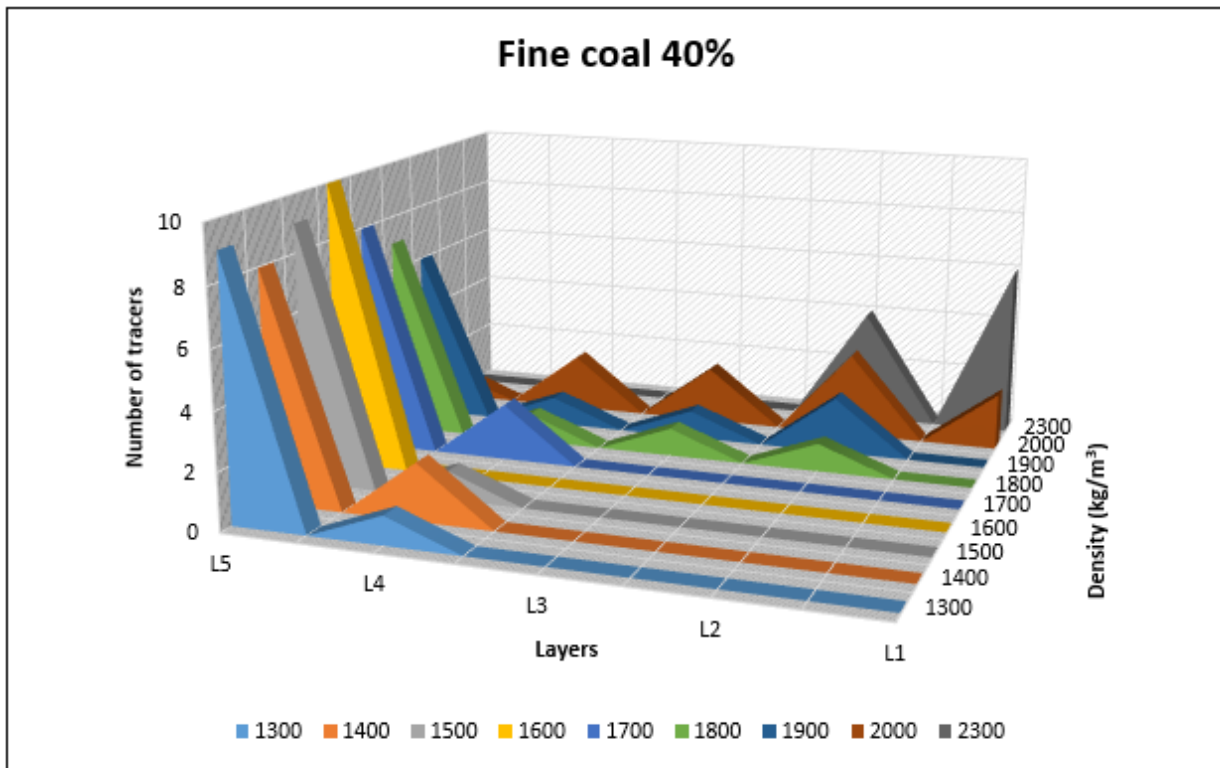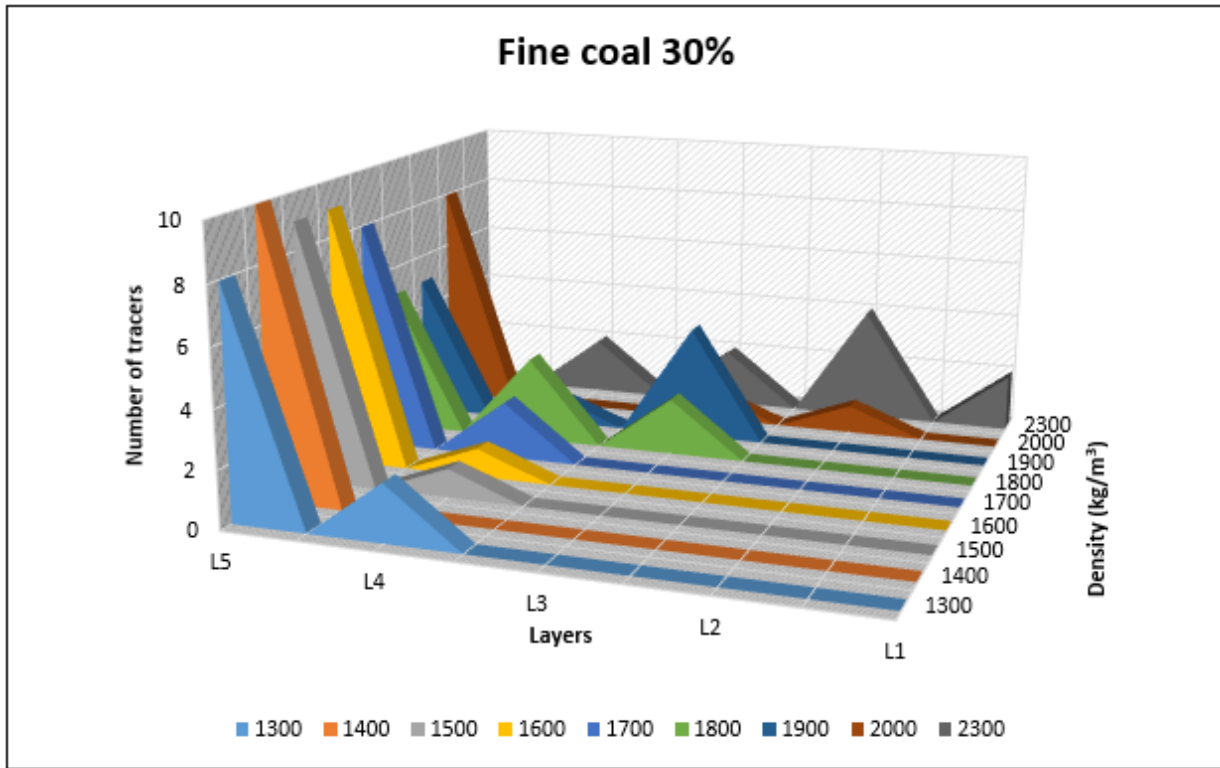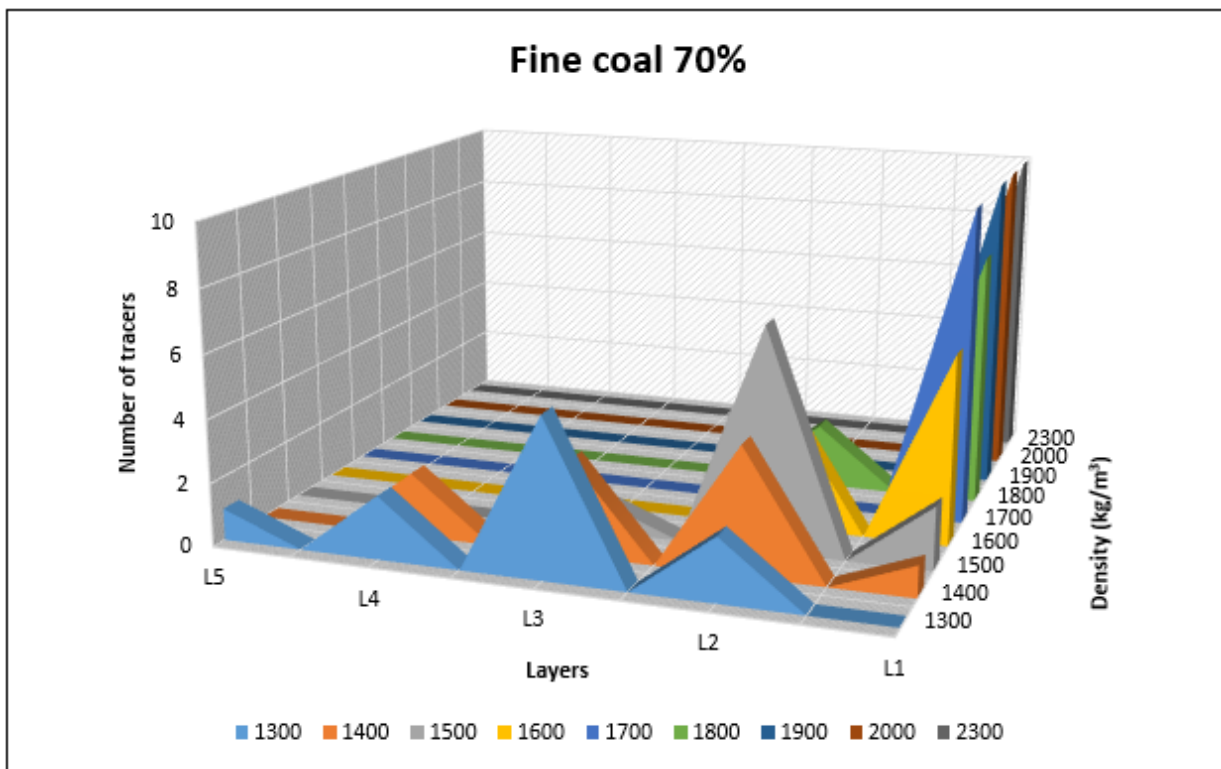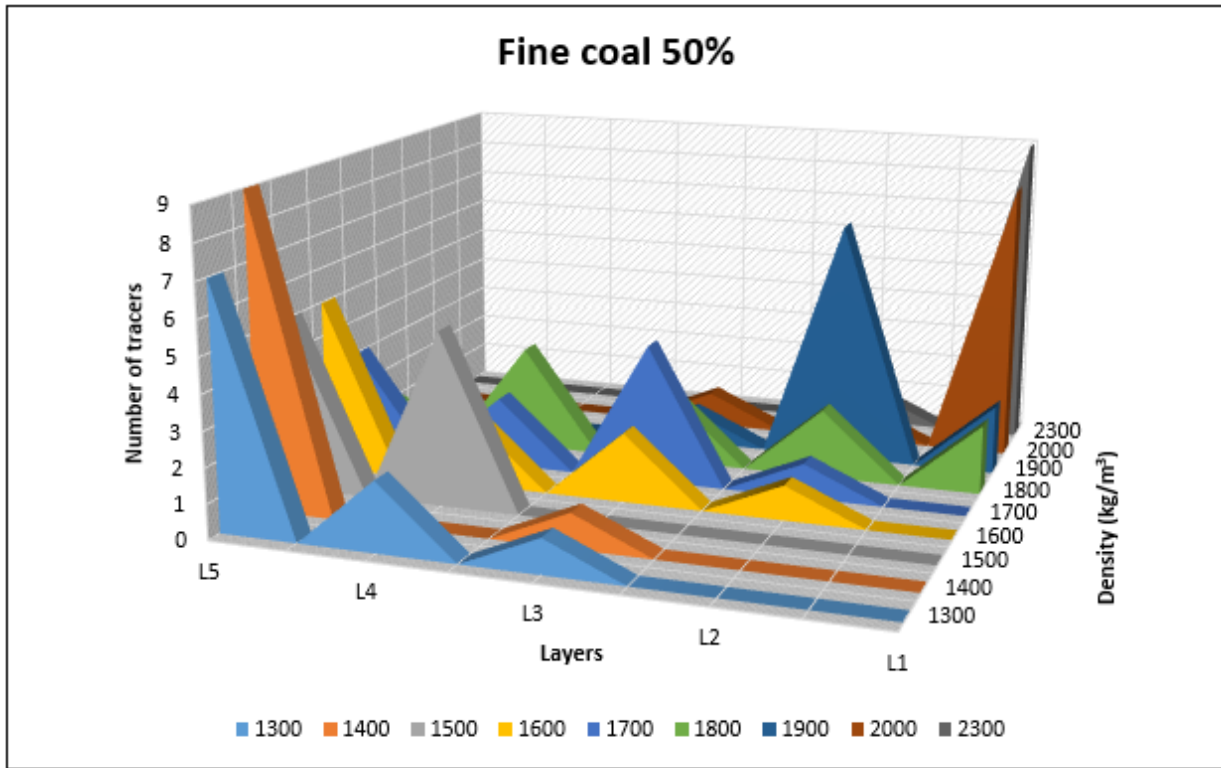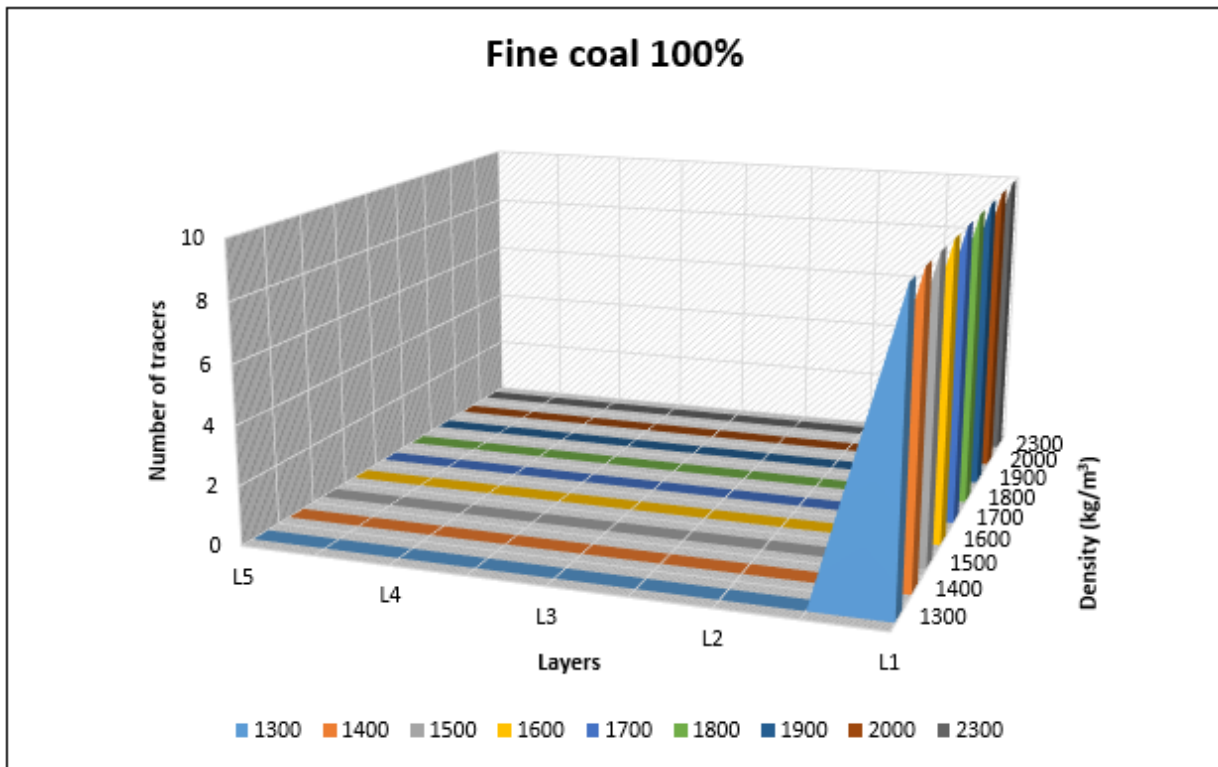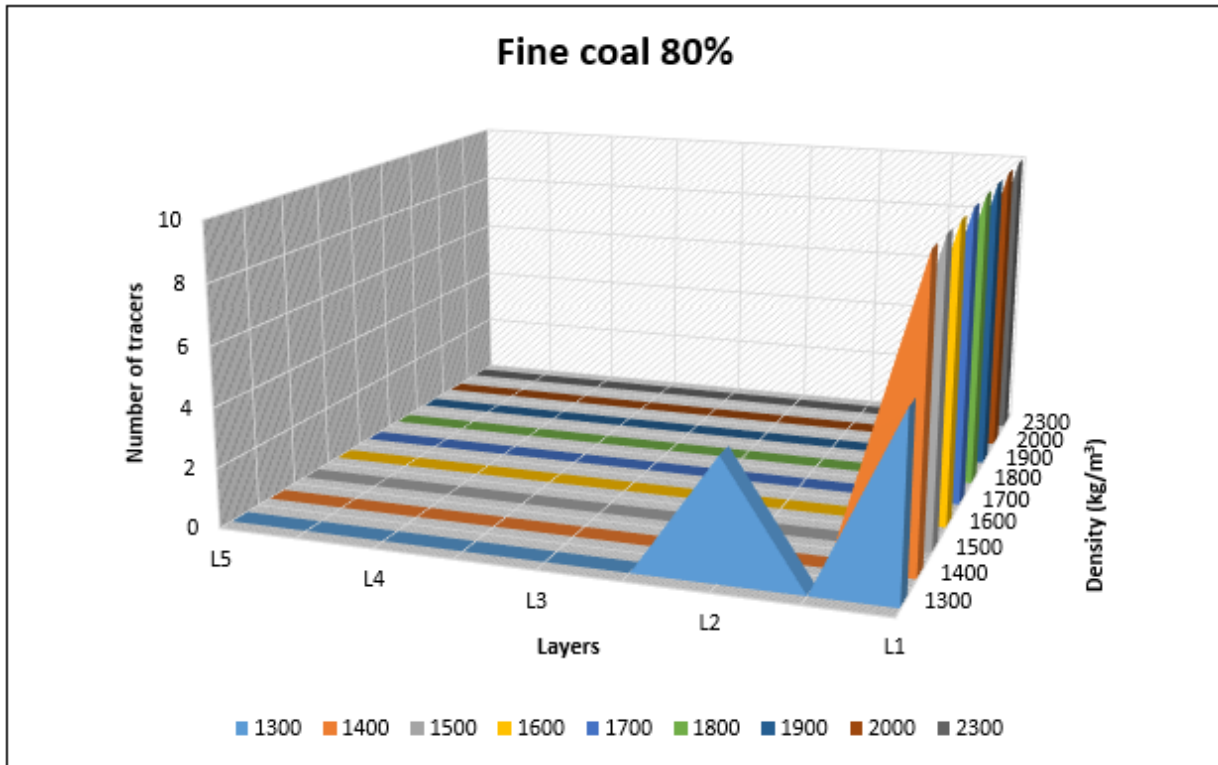
Fine coal 100%

8.21 Appendix 21 Partition curve of mixture ilmenite with sand medium
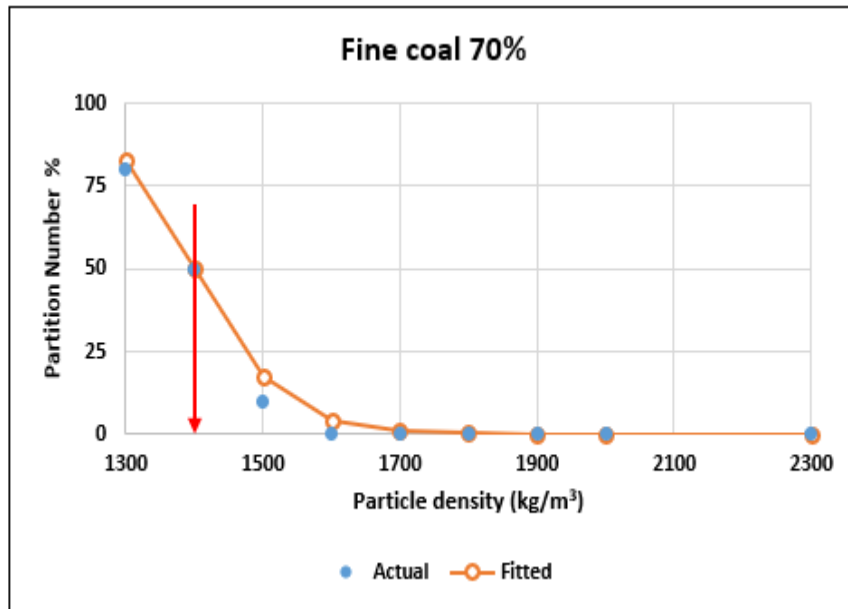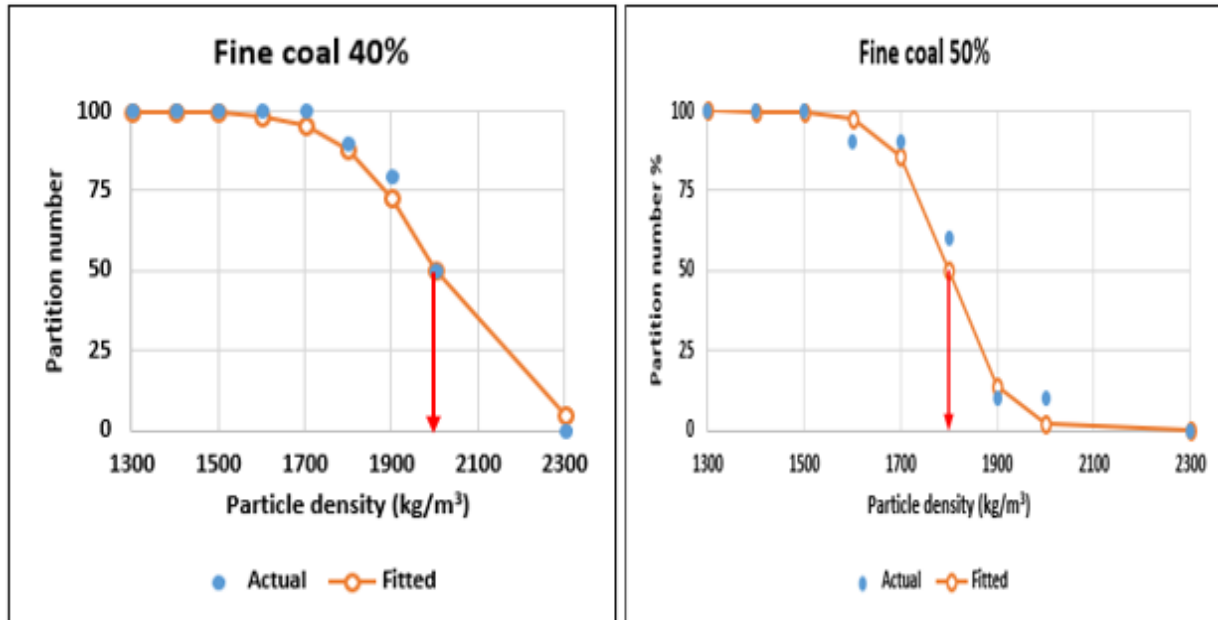
8.22 Appendix 22 Segregation of bed by size of mixture 40% ilmenite and 60% fine coal medium

| Sample ID		Segregation Fine coal 40% + Ilmenite 60%											
Total weight Sample (g)		748	1776,5	747,1	769,9	Mass % feed	Mass % Top	Mass % Middle	Mass % Bottom				
Sample loss	(g)	0,7	0,9	0,4	0,4					cumul feed	Cumul top	Cumul Middle	Cumul bottom
Sieve	Log size	Feed	Top layer	Middle layer	Bottom layer								
300	2,48									100	100	100	100
212	2,33	1,3	2,1	1,1	1,1	0,2	0,1	0,1	0,1	99,8	99,9	99,9	99,9
150	2,18	58,2	165	57,8	58,4	7,8	9,3	7,7	7,6	92,0	90,6	92,1	92,3
106	2,03	234	661	232,8	277	31,3	37,2	31,2	36,0	60,7	53,4	60,9	56,3
75	1,88	348,8	808,3	350	328,3	46,7	45,5	46,9	42,7	14,1	7,8	14,1	13,6
53	1,72	81,5	103,9	81,5	84,8	10,9	5,9	10,9	11,0	3,1	2,0	3,1	2,6
pan		23,5	35,3	23,5	19,9	3,1	2,0	3,1	2,6	0,0	0,0	0,0	0,0
Total weight		747,3	1775,6	746,7	769,5								
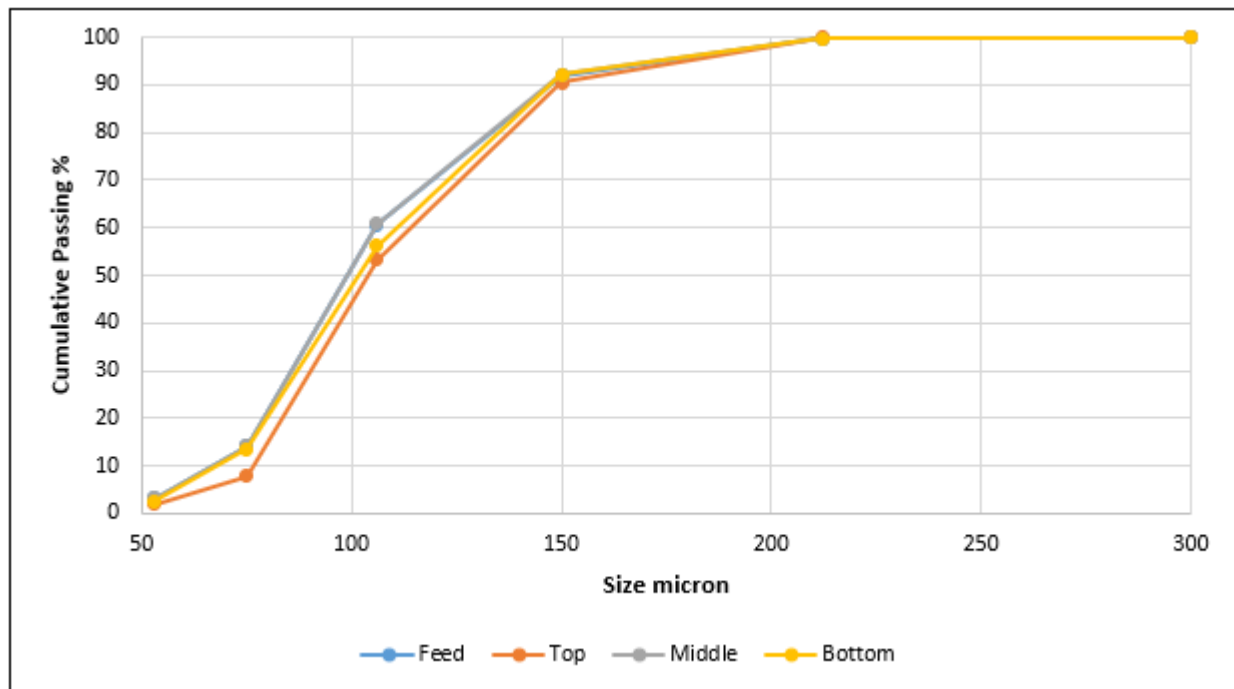
8.23 Appendix 23 Recovery of ilmenite from dry coal

Dry coal	Ilmenite (g)	Fine coal (g)	Magnetic (g)	Coal avg. (g)	Recovery %	Losses g/kg	Standard deviation
1 times	1223	445	1220,43		99,79	5,13	
	1223	445	1221,68	501,42	99,89	2,63	0,101799
	1223	445	1219,19		99,69	7,60	
Average	**1223**	**445**	**1220,43**		**99,79**	**5,12**	
4 times	1223	445	1215,65		99,40	14,64	
	1223	445	1216,97	501,91	99,51	12,01	0,118299
	1223	445	1214,08		99,27	17,77	
Average	**1223**	**445**	**1215,57**		**99,39**	**14,81**	
10 times	1223	445	1210,28		98,96	25,32	
	1223	445	1212,09	502,37	99,11	21,72	0,152103
	1223	445	1214		99,26	17,92	
Average	**1223**	**445**	**1212,12**		**99,11**	**21,65**	

8.24 Appendix 24 Recovery of ilmenite from wet coal

Dry coal	Ilmenite (g)	Fine coal (g)	Magnetic (g)	Coal avg. (g)	Mag. Sep. (g)	OS Losses (g)	Total Losses g/kg	Recovery %	Standard deviation
Wet coal 1%	1223	445	1219,88		3,12	0,00	6,09	99,74	
	1223	445	1220	512	3,00	0,00	5,86	99,75	0,012
	1223	445	1219,71		3,29	0,00	6,43	99,73	
Average	**1223**	**445**	**1219,86**		**3,14**	**0,00**	**6,13**	**99,74**	
Wet coal 2%	1223	445	1217,48		3,88	1,64	10,79	99,55	
	1223	445	1218,03	511,6	3,60	1,37	9,71	99,59	0,023
	1223	445	1217,67		3,53	1,80	10,42	99,56	
Average	**1223**	**445**	**1217,73**		**3,67**	**1,60**	**10,31**	**99,57**	
Wet coal 3%	1223	445	1214,2		6,01	2,79	17,09	99,28	
	1223	445	1215,08	515	5,56	2,36	15,38	99,35	0,036
	1223	445	1214,67		5,66	2,67	16,17	99,32	
Average	**1223**	**445**	**1214,65**		**5,74**	**2,61**	**16,21**	**99,32**	
Wet coal 4%	1223	445	1210,04		7,32	5,64	24,88	98,94	
	1223	445	1210,29	521	7,60	5,11	24,40	98,96	0,030
	1223	445	1210,77		6,98	5,25	23,47	99,00	
Average	**1223**	**445**	**1210,37**		**7,30**	**5,33**	**24,25**	**98,97**	

8.25 Appendix 25 Micro XRF analysis on ilmenite samples

Clean ilmenite sample	Used ilmenite sample

Co clean / Co used
Cr clean / Cr used
K clean / K used
V clean / V used
Sr clean / Sr used

Na clean

Na used

Ni clean

Ni used

P clean

P used

S clean

S used

Ilmenite clean

Ilmenite used